INVESTIGATIONS TO DEVELOP WIND TUNNEL TECHNIQUES

for

MEASURING ATMOSPHERIC GASEOUS DIFFUSION IN

MODEL VEGETATIVE SURFACES

by

E. J. Plate and J. E. Cermak

July 1963

CER63EJP-JEC28

INVESTIGATIONS TO DEVELOP WIND TUNNEL TECHNIQUES FOR MEASURING ATMOSPHERIC GASEOUS DIFFUSION IN MODEL VEGETATIVE SURFACES

by

E. J. Plate and J. E. Cermak

Final Report on Contract No. 12-14-100-4546(41)
with
U. S. Department of Agriculture
Agricultural Research Service
Soil and Water Conservation Research Division
Beltsville, Maryland

Civil Engineering Section
Fluid Dynamics and Diffusion Laboratory
Colorado State University
Fort Collins, Colorado

July 1963 CER63EJP-JEC28

ACKNOWLEDGEMENTS

Many persons have contributed directly or through their encouragement to the research summarized in this report.

Dr. M. Poreh and Dr. R. C. Malhotra, both former graduate students of Colorado State University, have contributed the most, the former through his efforts which led to Chapter 3, and the latter in developing the concentration instrumentation and through his cooperation during many phases of the research.

A dedicated group of graduate students, foremost of which are Messrs. A. A. Quraishi, H. Shokouh, and M. Susunai, have helped in taking experimental data.

Administrative support was given by Dr. A. R. Chamberlain, Vice President of Colorado State University and Mr. Milton E. Bender, Head, Department of Civil Engineering, Colorado State University.

The cooperation of the Western Plains Branch, Agricultural Research Service, U. S. Department of Agriculture, Fort Collins, especially that of Dr. C. E. Evans and Dr. H. R. Haise is gratefully acknowledged.

TABLE OF CONTENTS

TABLE OF CONTENTS--Cont'd

TABLE OF CONTENTS--Cont'd

LIST OF FIGURES

Chapter 2

Chapter 3

Chapter 4

Chapter 5

Figure

Chapter 6

Chapter 6

Figure

LIST OF TABLES

INVESTIGATIONS TO DEVELOP WIND TUNNEL TECHNIQUES FOR MEASURING ATMOSPHERIC GASEOUS DIFFUSION IN MODEL VEGETATIVE SURFACES

1. INTRODUCTION

Turbulent diffusion in vegetative covers has as yet not been studied extensively, even though its importance in transferring gases and water vapor is recognized. One reason for this lies in the difficulty in obtaining data which can be generalized because the continually varying climatic conditions and differences in topography lead to large variations of data. Therefore, a set of modeling laws are desired which will permit an indirect study of the natural situation in the controlled environment of a laboratory.

The present study constitutes a first attempt to investigate possible model laws for diffusion in vegetated areas by performing experiments designed to outline regions in which a simplification of the mathematical system of thermodynamic and aerodynamic equations governing the turbulent diffusion process is permissible. For this purpose, the problem was subdivided into four sub-problems.

The first problem which required solution was the establishment of diffusion characteristics for a standard or reference turbulent flow. It appeared advisable to express the diffusion characteristics of gas plumes in vegetated regions in terms of deviations from a standard reference case. In boundary layer studies, turbulent flow over a smooth boundary is most generally used as the reference for describing wall effects; therefore, the turbulent boundary layer along a smooth flat plate was chosen as the reference flow. For a diffusion source, a line source located at the floor was considered most fundamental, partly because it offers certain experimental and theoretical advantages, and partly because many diffusion phenomena in agriculture such as evaporation from area sources and dispersion of insecticides from aircraft are related to the line-source problem.

The results of this initial study have been reported in the first and second semi-annual reports. In the meantime, a paper(3-13) was prepared on this subject by M. Poreh and J. E. Cermak and submitted for publication. In it, the problem of diffusion from a line source into a turbulent boundary layer over a flat plane boundary has been discussed by using the concepts and tools commonly associated with the theory of boundary-layer development. While these concepts are quite adequate to describe gaseous diffusion in a phenomenological sense, they do not explicitly yield modeling parameters for practical field applications. The major contribution of this part of the study was a definition of zones of different diffusion behavior, which are useful for defining ranges of validity of model laws. This study is summarized in Chapter 3 of this report.

For practical modeling parameters, quantities are needed which can be measured or defined in the atmosphere as well as in the laboratory. This need constitutes the second problem. Recently this problem has yielded to analysis through the concept of "Lagrangian Similarity." J. E. Cermak extended this concept and applied it to, among other sets of data, the data for the study mentioned above. His paper (4-6) summarized the experimental efforts on diffusion studies in the Fluid Dynamics and Diffusion Laboratory of Colorado State University. His results for neutral boundaries are summarized in Chapter 4 of this report.

Successful as the modeling laws based on the hypothesis of Lagrangian similarity appear, they are nonetheless not easy to apply since they depend on some quantities which are well defined, but very difficult to measure in the atmospheric boundary layer. The most important of these parameters are the roughness height z_o and the friction velocity u_*. Both are parameters which also determine the mean-velocity profile, and are usually derived from it by assuming a given shape of the mean velocity distribution. It is well established that for both wind tunnel and field measurements the velocity distribution for neutral stability can be expressed, with a fair degree of approximation, by a logarithmic velocity-distribution law. This has been verified for smooth boundaries and also for rough boundaries where the roughness element height is small compared with the boundary layer, and comparable to the thickness of the viscous sublayer.

If, however, the roughness elements penetrate substantially into the boundary layer--like crops appear to do--the validity of a logarithmic velocity-distribution law cannot be taken for granted, and a thorough examination of the velocity distribution within and above the elements has to be performed before any conclusions can be drawn on the quantities z_o , and u_* . Furthermore, the significance of the ground-level shear becomes questionable, and the shear representative for the flow above the roughness level may be related to the ground shear in a complex manner. Also, the effective roughness height z_o , which for a rigid and dense assembly of roughness elements appears to depend on the roughness geometry only, will for flexible elements, like plants, become a function of velocity also and cannot be assumed a constant. This increases the difficulty of its definition.

In view of these features which are pertinent to most crops, the third problem was to find defining parameters for the aerodynamic behavior of and diffusion in simulated crops consisting of flexible plastic strips. Velocity profiles were measured, and mean concentration distributions within and outside the plant cover were determined by direct sampling. The results of this study will be analyzed in detail in a forthcoming Ph.D. Dissertation; but the most significant results will be presented in Chapter 5 of this report.

The fourth problem concerns the effect of the extent of the roughness. As fields of crops do not always extend far enough to permit establishment of fully developed turbulence conditions, and because single row-shelter belt type obstructions - may have profound effects on the diffusion processes on their lee side, a study was initiated on the diffusion into a boundary layer which is obstructed by a flat plate placed on the wall perpendicular to the flow direction. This program, outlined in the Third-Semi-Annual Report has been concluded and is described in Chapter 6.

2. EXPERIMENTAL EQUIPMENT AND PROCEDURES

The experiments were performed in two essentially different wind tunnels, with instruments which were improved during the course of the program. This chapter describes the features of the wind tunnels, the equipment, and its limitations.

2.1 The Wind Tunnel

At the beginning of the study, the available wind tunnel was of the open duct type, with the air taken from the inside of the building and discharged to the outside by means of a ventilation fan and a duct extending through a window of the building, as shown in Figure 2-1. The cross section of the test section in which the experiments were performed is approximately 6 x 6 ft, slightly increasing in width in the direction of the flow (1 in. per 8 ft) to provide zero pressure gradients at wind speeds of approximately 15 fps.

Preliminary studies showed a secondary circulation in the boundary layer. The secondary motion was eliminated by a honeycomb made of 24 in. long, 2 in. diameter paper tubes which were placed upstream of the test section and followed by a 50 x 50 mesh, 0.008 wire size stainless steel screen. The honeycomb and the screen produced a high level of turbulence of about 0.6% in the ambient air.

A turbulence stimulator consisting of a sawtooth strip and a 4 ft length of 1/4 in. closely packed gravel was placed immediately downstream of the screen. This helped to "trip" the flow, so that a stable turbulent boundary layer was obtained.

Air flow in the tunnel was produced by means of an electric fan driven by a 20 hp motor. Velocities from 6 to 17 ft/sec could be obtained by adjusting regulating vanes in the exhaust duct of the tunnel downstream of the blower.

In this wind tunnel, the experiments on the diffusion from a line source into the boundary layer on a smooth plate, and the diffusion studies for the boundary-layer flow obstructed by a plate perpendicular to the flow direction were performed.

The studies on the flexible roughness were conducted in the new U. S. Army Micrometeorological Wind Tunnel Facility which was completed in November 1962. This wind tunnel is described in detail in (2-1). The features which are pertinent to the present research are the low turbulence level (below 0.1%) and the fact that the pressure gradient can be adjusted to zero. The air speed is obtained by an aircraft propeller driven by a 250 hp DC-motor which permits, together with the pitch adjustment of the propeller continuous variation in speed from about 1 fps to 120 fps. The floor plan of the tunnel is shown in Figure 2-2.

The tunnel test section was equipped with an instrument carriage that permitted remote positioning of the instrument probes anywhere within the test section. This carriage is also described in (2-1).

2.2 Velocity Measuring Instrumentation

The instruments used for measuring mean-velocities were a mean velocity hot-wire anemometer with auxiliary instrumentation and a pitot-static tube in conjunction with a manometer. For measuring turbulent intensities, one channel of a two-channel, turbulence hot-wire anemometer was used.

2.21 Mean-velocity Measurement

The mean-velocity, hot-wire anemometer consists of a platinum wire 0.001 in. thick and about 1/2 in. long soldered across two needle prongs. The wire is kept at constant resistance by adjusting the heating current to the wire until a Wheatstone bridge, of which the hot-wire anemometer forms a branch, is balanced.

The pitot static tube is of standard design. It is used with a zero-type, sloping-arm manometer (Flow Corporation Type MM-2) which permits the manometer pressure to be read with an accuracy of about 0.0005 in. of H_2O.

2.22 Turbulent-velocity Measurement

A feedback controlled constant-temperature, turbulence hot-wire anemometer[1/] was used to measure turbulent quantities. This instrument uses platinum coated tungsten wire of about 0.00014 in. thickness and approximately 1/4 in. length. The system has a frequency response which is flat beyond 10,000 cycles per second it is thus adequate for all frequencies encountered in the low operating speed ranges used.

The AC component of the turbulence signal was fed into a Bruel and

1/ Manufactured by the Hubbard Instrument Company.

Kjaer type 2416 true rms (root mean square)-meter from which was read the rms value of the fluctuating signal, which is proportional to the rms value of the velocity fluctuations in the direction of mean flow. For some cases, the spectral distribution of this rms signal was determined by an automatic audio-frequency spectrometer (Type Bruel and Kjaer 2109 with Type 2306 level recorder) which has an adequate frequency response of 16 to 32,000 cps.

2.3 The Gas Feeding and Sampling System

The gas feeding was done from two different types of sources, a line source located at ground level, and an elevated line source. Two different systems were used for sampling.

The method of supplying, sampling and analyzing gas samples was gradually developed during a number of years of diffusion studies at Colorado State University's Fluid Dynamics and Diffusion Laboratory (Ref. 2-2 and 2-3). The gas was anhydrous ammonia (NH_3 99.99% pure) which was purchased in bottles.

2.31 Gas-feeding Equipment

The ammonia was emitted from a line source located within the boundary layer. The source at ground level consisted of a pipe counter sunk into the floor into which gas was passed at a constant rate--the rate was monitored by a Matheson Type 205 rota-meter. The pipe had a number of holes through which the gas escaped into an equalizing chamber and then through slots in the tunnel floor into the test section. The source is shown in Figure 2-4. The length of the source was 44 inches.

The elevated source consisted of an airfoil made from a 1/4 in. pipe with two circular sheet metal cords as shown in Figure 2-5. Plastic tubing was placed ten tubes wide between the sheet metal cords and each tube ending a distance of 1 in. away from the end of any other tubes. The other end of the tubing was inserted into a 1-1/2 in. diameter pipe into which the gas was fed from the ammonia bottle. The pipe served as a pressure equalization chamber. Each piece of tubing was of equal length, so that the discharge rate was constant along the line source. The length of the elevated source was 22 inches.

2.32 Sampling and Analysis

Downstream concentrations were measured by obtaining samples of the air-gas mixture and determining the amount of ammonia present by colorimetric analysis.

The sampling systems are schematically illustrated in Figures 2-5a and b. All connections between units consisted of polyethylene tubing which was selected because of its chemical inertness. The components of the source and sampling probes were made from stainless steel. The diffusing mixture of air and ammonia gas was drawn through the sampling system by inducing negative pressure with a vacuum pump. The sampling velocity was maintained below the local velocity expected near the boundary. Between successive samples, the sampling system was steadily purged by diverting the flow through an H_2SO_4-bath to absorb NH_3 . A dessicating flask containing silica gel eliminated moisture from the air entering the fine bore tube of the sampling-rate flowmeter.

The metered sample of air containing ammonia was passed through an absorption tube containing 25cc of diluted hydrochloric acid, which completely absorbed the ammonia from the sample. After sampling, the dilute HCl component of the sample was neutralized by adding 25cc of a dilute solution of NaOH which left NH_3 dissolved in a neutral solution. The neutralized sample containing NH_3 in solution was mixed with 2cc of Nessler's reagent, which gave a yellowish-brown coloration dependent on the concentration of NH_3 present in the sample. The absolute quantity of NH_3 was ascertained with the aid of an Evelyn Photoelectric Colorimeter which was calibrated by using a standardized solution containing 0.1, 0.075 and 0.025 mg of NH_3 in 1cc of this solution.

2.4 The Accuracy of the Measurements

A number of tests were performed in order to check the accuracy of the test results. The colorimetric method permits some scatter due to variation in the zeroing blank tube, and due to dilution errors in preparing the samples. In addition, fluctuations are caused by small variations in flow rates of sampling, feeding, and also in air speed in the wind tunnel. All these external effects were encountered in a test where the sampling probe was held at a fixed position, and samples were taken at time intervals of 5 minutes over a long period of time. The result of one of these tests is shown in Figure 2-6. The maximum deviation from the mean is about 10%.

The total effect of inaccuracies can best be judged from comparison of profiles taken under precisely the same conditions but on different days. Apart from those profiles which were retaken to duplicate a questionable one (where obviously something went wrong during the data acquisition of analysis), repeats showed variations in excess of 10%, especially in the regions of between 0 and 46%. The maximum error corresponds however to an error of only 15% if referred to C_{max} instead of c .

3. STUDY OF A DIFFUSION FROM A LINE SOURCE IN A TURBULENT BOUNDARY LAYER OVER A SMOOTH, FLAT PLATE--Poreh and Cermak (3-13).

3.1 Introduction

The ability to diffuse matter, heat and other contaminants is one of the basic characteristics of turbulent flow. Turbulent diffusion of matter and heat is of primary importance in several industrial and chemical processes as well as in agriculture, meteorology and atmospheric studies. Since the source of such contaminants is in many cases close to the solid boundaries, the study of diffusion in turbulent boundary-layer flows is of special interest.

The general problem in diffusion studies is to express the turbulent transport rate of transferable scalar quantities in terms of statistical functions of the turbulent motion and of the boundary conditions. A complete solution of the transport problem can be exprected only if there is a complete knowledge of the turbulent motion. G. I. Taylor (3-1) has demonstrated that the characteristics of transport processes are related to the Lagrangian statistical functions of the turbulent motion. He has formulated such a relation for the simple case of homogeneous turbulence. Measurement of the Lagrangian statistical quantities is difficult and a relation between the Lagrangian and Eulerian variables is available only for highly simplified models.

In view of these difficulties, phenomenological theories based on the concept of a "mixing length" or an "eddy diffusivity" were introduced and have been used in meteorological and engineering studies. Such theories have attempted to relate the mean flux of the contaminant by turbulent fluctuations to known variables of the turbulent field at the same point. The widely used Fickian treatment of atmospheric diffusion assumes that the flux $q_i = \overline{u_i'c'}$ is proportional to the gradient of the concentration $\frac{\partial c}{\partial x_i}$; thus, the flux normal to the stream becomes $q_y = \overline{v'c'} = \epsilon \frac{\partial c}{\partial y}$, where ϵ is called the coefficient of eddy diffusivity in analogy to the coefficient of molecular diffusivity. The existence of very large eddies comparable in size to the boundary-layer thickness itself does not justify such an analogy; however, a coefficient of eddy diffusivity can always be introduced as a mathematical operation, hoping that such a representation will simplify the problem. Such a construction was found successful in studies of free turbulence (3-2) where ϵ can be approximated by a constant. It was disappointing to find that in a boundary layer ϵ is not a constant (3-3). In view of the results found in the study of diffusion in homogeneous turbulence, there was some hope that ϵ could be related theoretically or experimentally to simple turbulent quantities like $\overline{v'^2}$ or $-\frac{\overline{u'v'}}{\frac{\partial u}{\partial y}}$ which corresponds to an eddy diffusivity for momentum transfer. The latter model was reported to be successful in a few cases of diffusion from an area source where a continuous flux of matter or heat, analogous to a wall shear stress, was emitted along the boundary (3-4). In general, universal relations between ϵ and the turbulent quantities were not obtained but the use of the mathematical model has been continued since no theoretical work has yielded methods adequate for use in practical problems. The theoretical difficulties to formulate a model of the diffusion pattern have encouraged much experimental work.

Field studies of atmospheric diffusion which suffer from the inherent disadvantages associated with an uncontrolled atmosphere did not remove these difficulties. An alternative experimental approach is a wind-tunnel investigation of diffusion within boundary layers. This chapter summarizes the work of Poreh (3-5) on diffusion from a ground-level line source and formulates and analyzes the diffusion pattern for short and large distances downstream of the source taking into consideration the non-homogeneity of the boundary layer. The experimental work of Wieghardt (3-6) for a line source of heat is compared with the mass-diffusion data.

3.2 The Experimental Data

Two series of experiments were conducted. In each series three ambient velocities were used--approximately 9, 12, and 16 ft/sec. In Series I, the source was located at the boundary at station 33.5 ft (Fig. 3-1). Measurements of the concentration were taken at 3, 5, 9, 15, and 21 feet downstream from the source. The mass flux of ammonia per unit width in Series I was $G = 0.66$ mg/cm-sec. In Series II the source was located at station 15.5 ft. Measurements were taken at 17, 23, 35.5 and 43.5 ft downstream from the source. The mass flux of ammonia per unit width in Series II was $G = 0.55$ mg/cm-sec.

The mean-velocity profiles within the test section shown in Figure 3-2 were approximately similar and the boundary-layer thickness δ varied from 5 to 11 inches (Fig. 3-3). The Reynolds number $U_{amb} \frac{\delta}{\nu}$ varied from 25,000 to 56,000. The limited turbulence measurements are plotted in Figure 3-4.

3.3 The Experimental Results

3.31 Introductory Remarks

A relative-rate parameter β is defined to assist in dividing the field downstream from the source into zones and in considering the effect of the non-homogeneity of the flow field on the diffusion pattern.

A characteristic length which gives an indication of the rate of change of growth of the boundary layer is

$$L_\delta = \frac{\delta}{\frac{d\delta}{dx}} \tag{3-1}$$

A similar length can be defined to express the diffusion process. If λ is a characteristic height of the region contaminated by tracer matter (hereafter referred to as the plume) then,

$$L_\lambda = \frac{\lambda}{\frac{d\lambda}{dx}} \tag{3-2}$$

The ratio:

$$\beta = \frac{L_\lambda}{L_\delta} \tag{3-3}$$

can be considered as a measure of the relative rates of growth of the plume and the momentum boundary layer. The value of β near the gas source is determined by the distance of the gas source from the origin of the boundary layer which is assumed to start upstream of the source; however, near the source β will always be small and it will increase with the distance downstream from the source. Whenever the plume and the boundary layer attain a similar rate of growth β becomes unity. Since the vertical-velocity component v is related to the rate of change of the boundary-layer thickness, β will indicate the relative importance of transfer by mean vertical velocity.

3.32 Description of the Diffusion Pattern

Examination of the experimental results indicates that the effect of the non-homogeneity of the field in the diffusion is not uniform and suggests a division of the field into a series of four zones. Other considerations which support such a division of the field will be mentioned later. A description of the diffusion pattern becomes clear and simple by using zones. Approximate limits of the various zones in terms of $\frac{x}{\delta_a}$ where δ_a is an average boundary-layer thickness as defined in Figure 3-7 are suggested.

(1) The Initial Zone

Very large velocity and concentration gradients made it impossible to obtain reliable data close to the source with the available equipment. It is, however, possible that the laminar sublayer and the large longitudinal gradients which are negligible further downstream will affect the diffusion process in this region. The similarity of the concentration profiles measured nearest to the source and the profiles downstream suggests that measurements in the initial zone were not made and consequently, that the upper limit $\frac{x}{\delta_a} = w$ for this zone was not determined. Moreover, one expects this limit to be related to some characteristic height of the laminar sublayer rather than to $\frac{x}{\delta_a}$ alone.

(2) The Intermediate Zone

The diffusing plume, within this zone, is submerged in the boundary layer; but, its thickness is large compared to that of the laminar sublayer. Longitudinal gradients are small compared to vertical gradients and the boundary-layer-type approximation becomes possible. The ratio β is small and the diffusion depends only slightly on the rate of the boundary-layer growth.

The mean-concentration profiles can be described by a dimensionless universal curve:

$$\frac{c}{C_{max}} = f(\xi) \tag{3-4}$$

where $\xi = \frac{y}{\lambda}$ and $f(1) = 0.5$

as shown in Figure 3-5. The function $f(\xi)$ appears to be independent of U_{amb} and δ in this zone and is described in Figure 3-6. Variation of λ initially is given by

$$\lambda = 0.076\, x^{0.8} \tag{3-5}$$

where x and λ are measured in cm. Slight deviation of the data from equation (3-5) when $U_{amb} = 59$ ft/sec is noted. The values of C_{max} appear to be inversely proportional to U_{amb}. The initial variation of $C_{max}\ U_{amb}$ (in c.g.s. units) can be approximated by

$$C_{max}\ U_{amb} = 17.3\ x^{-0.9} ,$$

or

$$C_{max} \ U_{amb} = 26.2 \ G \ x^{-0.9} \qquad (3\text{-}6)$$

The variation of β and $\frac{\lambda}{\delta}$ is given in Figure 3-7. A decrease in the rate of growth of $\frac{\lambda}{\delta}$ is noted beyond $\frac{x}{\delta_{ave}} = 18$ where $\frac{\lambda}{\delta}$ is about 0.39. At the same time, the shape of the concentration profiles changes from that described by $f(\xi)$ (see Fig. 3-11). The value of $\frac{x}{\delta_{ave}} = 18$, therefore, can be taken as an approximate upper limit of this zone.

(3) The Transition Zone

The effect of the mild mixing processes in the ambient air is to decrease the rate of growth of the diffusing plume and to gradually change the shape of the concentration profile.

Within the zone, $18 < \frac{x}{\delta_a} < 60$, β increases to unity. Downstream of $\frac{x}{\delta_a} = 60$, $\frac{\lambda}{\delta}$ remains constant at 0.64.

(4) The Final Zone

Diffusion of matter beyond the boundary layer into the ambient air is controlled by the molecular action and the turbulent fluctuations in the ambient air, similar to the control of the diffusion of momentum. The final zone starts at approximately $\frac{x}{\delta_a} = 60$. The limited length of the test section did not permit measurements in all the zones for the same position of the gas source. Measurements in the final zone were taken during different flow conditions--Series II--in which the source was moved upstream a distance of 18 ft as shown in Figure 3-1.

The concentration profiles within this zone can be described by

$$\frac{c}{C_{max}} = F\left(\frac{y}{\delta}\right) \ . \qquad (3\text{-}7)$$

In Figure 3-10, the empirically determined form of F is shown. The ground concentration C_{max} shown in Figure 3-9 can be approximated by

$$C_{max} \propto (U_{amb} \cdot \delta)^{-1} \ ,$$

or

$$C_{max} = \frac{\frac{G}{0.55}}{U_{amb}} \cdot \delta \tag{3-8}$$

when c.g.s. units are used.

3.4 The Analytic Formulation of the Problem

The conservation of mass for the two-dimensional case is expressed by the equation

$$u\frac{\partial c}{\partial x} + v\frac{\partial c}{\partial y} = \frac{\partial}{\partial y}\left(k\frac{\partial c}{\partial y} - \overline{v'c'}\right) + \frac{\partial}{\partial x}\left(k\frac{\partial c}{\partial x} - \overline{u'c'}\right). \tag{3-9}$$

Excepting near the source, boundary-layer-type approximation of the equation becomes possible which gives:

$$u\frac{\partial c}{\partial x} + v\frac{\partial c}{\partial y} = \frac{\partial}{\partial y}\left(k\frac{\partial c}{\partial y} - \overline{v'c'}\right). \tag{3-10}$$

Integration of equation (3-10) is possible using the distribution functions obtained in the experiments. The variation of $\overline{v'c'}$ and $\epsilon = -\frac{\overline{v'c'}}{\frac{\partial c}{\partial y}}$

can thus be examined.

3.41 The Intermediate Zone

Consider the following mean velocity and concentration fields (Figs. 3-2 and 3-5):

$$c = C_{max}\, f(\xi) \tag{3-4}$$

where $$\xi = \frac{y}{\lambda} \text{ and } f(1) = 0.5\ , \tag{3-11}$$

and $$u = U_{amb}\, \eta^{1/n}\ ,\ (n = \tfrac{1}{7})\ .$$

Since c vanishes as y becomes large

$$\int_0^\infty cu\, dy = G \tag{3-12}$$

where G is a constant of the diffusion field and is equal to the flux of the diffusing quantity per unit time and width. It follows that

$$C_{max} \cdot U_{amb}\, \lambda \left(\frac{\lambda}{\delta}\right)^{1/n} \int_0^\infty \xi^{1/n}\, f(\xi)\, d\xi = G$$

and according to equation (3-4)

$$c = \frac{G}{\int_0^{\infty} \xi^{1/n} f(\xi)\, d\xi} \; \frac{\delta^{1/n} f(\xi)}{\lambda^{\frac{n+1}{n}} U_{amb}} \qquad (3\text{-}13)$$

The value of $\int_0^{\infty} \xi^{1/n} f(\xi)\, d\xi$ was evaluated from the data with $n = 7$ and is approximately equal to 0.98. The mutual variation of the parameters $\delta^{1/n}$, λ and $C_{max} U_{amb}$ shown in Figure 3-6 is consistent with equation (3-13).

Equation (3-10) can be integrated using equations (3-11) and (3-12) and assuming for simplicity that $\delta^{1/n}$ is a constant within this zone (justification for this assumption is seen by the small change in $\delta^{1/n}$ shown in Figure 3-6. The integration gives:

$$k\frac{\partial c}{\partial y} - \overline{v'c'} = -\frac{G}{\lambda}\frac{d\lambda}{dx}\left[F_1(\xi) - \beta F_2(\xi)\right] = -\frac{G}{\lambda}\frac{d\lambda}{dx} S_\lambda(\xi, \beta) \qquad (3\text{-}14)$$

where

$$F_1(\xi) = \frac{\int_0^{\xi} \xi^{1/n}\left[\frac{n+1}{n} f(\xi) + \xi f'(\xi)\; d\xi\right]}{\int_0^{\infty} \xi^{1/n} f(\xi)\, d\xi},$$

$$F_2(\xi) = \frac{\int_0^{\xi} \frac{1}{n+1}\, \xi\, \frac{n+1}{n} f'(\xi)\, d\xi}{\int_0^{\infty} \xi^{1/n} f(\xi)\, d\xi}$$

and β is the ratio defined in equation (3-3). The term $\beta F_2(\xi)$ is the contribution to convective transfer by the mean vertical velocity. If $\overline{v'c'}$ is separated according to the Fickian model $\overline{v'c'} = -\epsilon\frac{\partial c}{\partial y}$ one obtains

$$k + \epsilon = -\lambda\frac{d\lambda}{dx} U_{amb}\left(\frac{\lambda}{\delta}\right)^{1/n} \frac{S_\lambda(\xi, \beta)}{f'(\xi)} \int_0^{\infty} \xi^{1/n} f(\xi)\, d\xi \qquad (3\text{-}15)$$

The function $f(\xi)$ can be estimated from Figure 3-5 however, the evaluation of $f'(\xi)$ from the same figure is not reliable. Using the experimentally determined $f(\xi)$, $S_\lambda(\xi, \beta)$ was determined by graphical methods and is plotted in Figure 3-12.

Although $f'(\xi)$ was not evaluated, one can estimate ϵ at the beginning of the intermediate zone by using the following values:

$$\lambda = 3 \text{ cm}, \frac{d\lambda}{dx} = 0.024, \int_0^\infty \xi^{1/n} f(\xi)\, d\xi = 0.98 ,$$

$$\left(\frac{\lambda}{\delta}\right)^{1/7} = 0.75, \; f'(\xi) = -0.6 \text{ (maximum)}, \; f(\xi) = 0.25 ,$$

$$U_{amb} = 260 \text{ cm/sec}, \quad k = 0.23 \text{ cm}^2/\text{sec}.$$

Substituting into equation (3-15) one gets

$$\epsilon \cong 5.5 \text{ cm}^2/\text{sec} \gg k .$$

Since ϵ increases with x, it seems justified to neglect k in the intermediate zone except near the boundary. Neglecting the molecular-diffusivity term one gets

$$\epsilon = -\lambda\frac{d\lambda}{dx}\left(\frac{\lambda}{\delta}\right)^{1/n} \frac{S_\lambda(\xi, \beta)}{f'(\xi)} \int_0^\infty \xi^{1/n} f(\xi)\, d\xi \qquad (3\text{-}16)$$

and

$$\overline{v'c'} = \frac{G}{\lambda}\frac{d\lambda}{dx} S_\lambda(\xi, \beta) . \qquad (3\text{-}17)$$

3.42 The Final Zone

Similar integration in the final zone is possible even without approximating the velocity profile in a power law. Using the distribution functions

$$\frac{c}{C_{max}} = F(\eta) \qquad (3\text{-}7)$$

and

$$\frac{u}{U_{amb}} = g(\eta) \qquad (3\text{-}18)$$

where

$$\eta = \frac{y}{\delta} \text{ and } g(1) = 0.99$$

in the integral equation of mass conservation, the following expression for C_{max} is found:

$$C_{max} = \frac{G}{\int_0^\infty g(\eta)\, F(\eta)\, d\eta} \quad \frac{}{U_{amb} \cdot \delta} \cdot \tag{3-19}$$

Integration of equation (3-10), neglecting the molecular term, gives:

$$\overline{v'c'} = \frac{G}{\delta} \frac{d\delta}{dx} \; S_\delta \; (\eta)$$

where

$$S_\delta \; (\eta) = \frac{F(\eta) \qquad \int_0^\eta g(z)\, dz}{\int_0^\infty F(\eta)\, g(\eta)\, d\eta} \tag{3-20}$$

and

$$\epsilon = U_{amb} \; \delta \frac{d\delta}{dx} \; E(\eta) \tag{3-21}$$

where

$$E(\eta) = \frac{F(\eta)}{F'(\eta)} \int_0^\eta g(\alpha)\, d\alpha \; .$$

It is instructive to derive similar expressions for $\overline{v'c'}$ and ϵ in the case of diffusion in homogeneous turbulence (3-7) where

$$c = \frac{G}{u \sqrt{\frac{\pi}{2}}\, \sigma} \; \exp - \left\{ \frac{y^2}{2\sigma^2} \right\}$$

and the mass-conservation equation is

$$u\frac{\partial c}{\partial x} = - \frac{\partial}{\partial y} \overline{v'c'} = \frac{\partial}{\partial y} \epsilon \frac{\partial c}{\partial y} \; .$$

Integrating the mass-conservation equation one gets

$$\overline{v'c'} = \frac{G}{\sigma} \frac{d\sigma}{dx} \; S_\sigma \left(\frac{y}{\sigma} \right) \tag{3-22}$$

where

$$S_\sigma(z) = z \exp -\frac{z^2}{2}$$

and

$$\epsilon = U_{amb}\,\sigma\frac{d\sigma}{dx} \quad . \qquad (3\text{-}23)$$

In general $\sigma\frac{d\sigma}{dx}$ is a function of x ; however, when x is very large and $\sigma \propto x^{1/2}$, ϵ becomes a constant--the limiting case in homogeneous turbulence. The structure of equations (3-16) (3-21) and (3-23) is similar but unfortunately within the boundary layer ϵ does not become independent of either the vertical or the horizontal coordinate. Comparing S_σ with S_λ and S_δ (Fig. 3-12) we find that the distribution of this dimensionless function is very similar except that the value of S_δ drops off faster as one approaches the edge of the plume. The decrease of S_δ together with the increase of $\frac{\partial c}{\partial y}$ (Fig. 3-11) is due to the reduction of the turbulent transport at the outer edge of the layer.

3.5 Discussion

3.51 The Intermediate Zone

Within the intermediate zone, where the diffusing plume is totally submerged in the boundary layer, the rate of growth of the vertical dimension of the plume is large compared to the rate of growth of the boundary layer itself and thus β is small (0.10 to 0.33). The diffusion pattern is affected little by the boundary-layer changes and the contribution of the vertical velocity fluctuations to the transfer is small as can be seen from the small contribution of the term in equation (3-14), and Figure 3-12.

Equation (3-5), determined from Figure 3-6, indicates that the vertical scale of the plume is independent of the ambient velocity. It implies that the agents of the flow which control the vertical diffusion within the boundary layer are proportional to the ambient velocity in such a way that the vertical transfer of the mass is approximately proportional to the convection of mass by the longitudinal velocity.

However, the formulation of the results in the form $\lambda = 0.076\, x^{0.8}$ and the above conclusion should be regarded as an approximation since they do not take into consideration the size of the boundary layer and the changes which take place in the velocity field. The small value of β in this region indicates that the rate of change of the boundary layer is not important, but the process of the diffusion at any section is definitely determined by the local thickness of the boundary layer. The deviation of the data obtained at the velocity $U_{amb} = 59$ ft/sec from the above formula is therefore, a result of the different rate of growth and thickness of the boundary layer near the source rather than experimental scatter.

The same arguments hold with regard to Wieghardt's formulation of his data. Wieghardt (3-6) approximated his findings by the expression

$$\frac{\theta}{\theta_{max}} = \exp\left\{ -\left[\frac{y}{F_1(x)} \right]^{\alpha} \right\}$$

where θ is the temperature increase, and found that $F_1(x)$, which can be regarded as a measure of the plume size similar to λ , varies as

$$F_1(x) = 0.55\, x \left(\frac{U_{amb}\, x}{\nu} \right)^{-1/5} = 0.55\, x^{0.8} \left(\frac{U_{amb}}{\nu} \right)^{-1/5} .$$

This formulation implies that the pattern of diffusion is completely independent of the thickness of the boundary layer and that the diffusion pattern will be the same if the source is placed close to or far away from the leading edge. In his attempts to formulate the data in this manner, Wieghardt found it necessary to vary α from 1.64 for $U_{amb} = 17.7$ ft/sec. to 2.0 for $U_{amb} =$ 59 ft/sec.

It appears that a more adequate formulation of the data is obtained in terms of the parameter $\frac{\lambda}{\delta}$ and $\frac{x}{\delta_{ave}}$ as shown in Figure 3-7. Such a formulation accounts for the non-homogeneity of the space and the thickness of the boundary layer at each section. One can see in Figure 3-7 that Wieghardt's data with $U_{amb} = 59$ ft/sec agrees better with the other data when formulated in this manner.

Equation (3-16) exhibits the shortcomings of the Fickian model and the concept of an eddy diffusivity. One hopes to find that ϵ is a function of the flow field and that its value at a point can be specified as a function independent of the position of the source. However, the form of equation (3-16) indicates that this cannot be so. Recalling that the intermediate zone can be regarded as an approximate model for atmospheric diffusion from a ground source in the absence of buoyancy forces, one concludes that a description of the ability of the atmosphere to diffuse matter in terms of an ϵ varying only with height is incomplete and misleading.

It should be remarked that an initial dependence of ϵ on the distance from the source is expected. As in the case of diffusion in homogeneous turbulence such a dependence would probably last for a distance of the order of the Lagrangian integral scale. Direct measurements of the Lagrangian integral scale are not available. It is shown, however, that a time delayed dimensionless velocity correlation can maintain large values for a longitudinal distance of four boundary-layer thicknesses (3-8). Measurements by Baldwin and Mickelsen (3-9) in a pipe flow show that the space-time correlation coefficients have a magnitude of about 0.2 at separation distances of 16 pipe radii. It is, therefore, possible to assume that the Lagrangian integral scale of the boundary layer will be of the order of 10 boundary-layer thicknesses.

Another interesting result is the similarity of the distribution of $\overline{v'c'}$ in the boundary layer and in homogeneous turbulence as shown by equations (3-17) and (3-22) and Figure 3-12. In both cases, $\overline{v'c'}$ is inversely proportional to the characteristic length scale of the diffusing plume and the dimensionless distribution is very similar.

3.52 The Final Zone

Some of the features of the diffusion, such as the dependence of $\overline{v'c'}$ and of c on $\frac{G}{U_{amb}}$ are the same throughout the diffusion field. The major difference between the intermediate zone and the final zone is that the characteristics of the diffusion field are independent of the position of the source in the final zone, as expressed by equations (3-7) and (3-8).

Once such relations are established, it is possible to relate parameters like $\overline{v'c'}$ and ϵ to the velocity field as shown in equations (3-19) and (3-20). It is also possible to relate ϵ to other parameters like $\epsilon_m = -\frac{\overline{u'v'}}{\frac{\partial u}{\partial y}}$; however, the various expressions are related and none of them express a true relation between the phenomena and its causes.

It should be realized that the developing boundary layer is not self preserving (3-10), which means that the characteristics of the diffusion will change together with the boundary layer and any similarity will be limited to a certain range of Reynolds numbers. The changes will be mild for large Reynolds numbers; however, the Reynolds number is undoubtedly a parameter to which the diffusion process is related.

The second parameter upon which the diffusion process depends as suggested by the dimensionless equations is the Schmidt number $\frac{\nu}{k}$. Although the importance of the molecular diffusivity in determining the spatial distribution of the diffusing scalar is fundamental, one realizes that it is mainly caused by the turbulence of the boundary layer. It is expected therefore, that even for large Schmidt numbers the matter will quickly diffuse and "fill" the turbulent boundary layer and that further growth of the plume will be similar to the growth of the boundary layer.

If the value of k is increased, it is clear that the diffusion rate of mass near the upper edge of the boundary layer will be amplified and that the plume size will increase more rapidly. It remains to be asked whether, for very small Schmidt numbers, the plume will increase indefinitely beyond the boundary layer and a similarity will not be established. That this is not likely to happen can be concluded from the exact solution of diffusion of matter and momentum in laminar flow (3-11), which indicates that the corresponding ratio of $\frac{\lambda}{\delta}$, which is a function of the Schmidt number, does not depend on x . Since the growth of the turbulent boundary layer is faster than that of the laminar layer, it is unlikely that the diffusing plume will continue to grow faster than the boundary layer. It is important to note that beside the Schmidt number, the turbulent structure of the ambient air will be an important parameter in the final zone.

Similarity of scalar and momentum diffusion has been found in heated jets. Corrsin et.al. (3-12) introduced a concept of an "effective Prandtl number" by comparing the relative diffusion of heat and momentum in laminar and turbulent jets. He found that the effective Prandtl number in the turbulent jet is the same as the (laminar) Prandtl number. This suggests a comparison of the relative diffusion of the plume within the boundary layer for the laminar and turbulent cases. Figure 3-13 compares the results of these experiments $\frac{\nu}{k} = 0.72$ with the laminar case. The similarity of the structure suggests that the effect of the Schmidt number on diffusion in laminar and turbulent boundary layers is similar.

3.6 Nomenclature

Unless otherwise stated instantaneous values of any fluctuating variable p will be written as $p + p'$, where p is the mean value and p' is the fluctuating component. Time averages will be denoted by $(\overline{})$, for example $\overline{p + p'} = p$.

Symbol	Definition
C_{max} ,	maximum value of concentration profile, ground level concentration;
c ,	concentration of the diffusing matter;
$F(\eta)$,	universal concentration function in the final zone, defined in equation (3-7);
$F_1(\xi)$,	defined in equation (3-14);
$F_2(\xi)$,	defined in equation (3-14);
$f(\xi)$,	universal concentration function in the intermediate zone, defined in equation (3-4);
G ,	flux of the diffusing matter per unit time for a unit width;
$g(\eta)$,	universal velocity function in the test section, equation (3-18);
k ,	molecular diffusivity;

Symbol	Definition
$S_\lambda, S_\delta, S_\sigma$,	dimensionless functions associated with the description of $\overline{v'c'}$, defined in equations (3-14), (3-20), and (3-22);
U_{amb} ,	velocity of the ambient air stream;
u ,	velocity in the x-direction;
v ,	velocity in the y-direction;
x ,	distance downstream from the source;
x' ,	distance downstream from origin of turbulent boundary layer;
y ,	height above the boundary;
β ,	defined in equation (3-3);
δ ,	boundary-layer thickness, $\frac{u}{U_{amb}}(\delta) = 0.99$;
δ_{ave} ,	defined in Fig. 8;
ϵ	coefficient of eddy diffusivity, $= -\dfrac{\overline{v'c'}}{\frac{\partial c}{\partial y}}$;
η ,	dimensionless height $\frac{y}{\delta}$;
λ ,	characteristic height of the diffusing plume, $\frac{c(\lambda)}{C_{max}} = 0.5$;
ν ,	kinematic viscosity;
ξ ,	dimensionless height $\frac{y}{\lambda}$;
σ ,	the variance of the concentration profile for homogeneous turbulence.

4. LAGRANGIAN SIMILARITY HYPOTHESIS AS APPLIED TO TURBULENT SHEAR FLOW--Cermak (4-6)

4.1 Introduction

Although the analytic formulation presented in the last chapter correlated the data for the smooth, flat plate case quite satisfactorily it lacks the essentials for atmospheric modeling. The entire correlation of Chapter 3 is based on δ, the boundary-layer thickness. This parameter has essentially no meaning in the atmosphere. A satisfactory modeling criteria must be based on parameters that are measurable in both the wind tunnel and the atmosphere.

The most striking features of the diffusion problem in Chapter 3 were the different diffusion behaviors in different flow zones. It can be said that a diffusion plume which reaches the edge of the atmospheric boundary layer will in general be very rare, or at least of minor importance. Therefore, the modeling laws for atmospheric diffusion depend only on the lower regions of the velocity field, in which the boundary shear τ_o and the roughness of the ground are the determining factors in the development of the mean and turbulent velocity field. In the terminology of Chapter 3, this means that experimental data can be used for the atmosphere only if they are measured in the intermediate or initial zone.

Although no model exists for the turbulent motion in shear flow from which a detailed theory of turbulent diffusion may be constructed, gross characteristics of the concentration field may be predicted through use of similarity arguments. Batchelor (4-2) demonstrated the power of similarity reasoning when he applied the hypothesis that turbulent motions of particles in steady, self-preserving, free shear flows possess similarity in the Lagrangian sense. Based on this hypothesis he was able to predict that dispersion and maximum mean concentrations are proportional to certain powers of x for single particle release and continuous particle release. The application of Lagrangian similarity arguments to a turbulent shear flow produced by flow along a solid boundary (boundary layer flow) in the region where mean velocity varies as the logarithm of wall distance y was suggested by Batchelor (4-3). For this case where the Eulerian properties of the flow depend only upon the shear velocity u_* and the roughness length z_o , Batchelor (4-4) and Ellison (4-9) determined the power of x at large distances with which maximum mean concentration decays at ground level. The results were calculated for a continuous point or line source of passive particles released at ground level.

The basic formulation of Batchelor and Ellison is used to predict the way in which gross characteristics of the concentration field for continuous point and line sources vary with x when the source height is arbitrary and x is not necessarily large. This extended formulation of Cermak (4-6) presented here permits use of data from both atmospheric and laboratory diffusion experiments in checking theoretical predictions based on the Lagrangian similarity hypothesis. Laboratory data are provided by a group of studies conducted in a wind tunnel where a tracer gas was diffused (Davar 4-8, Poreh 4-16, Malhotra 4-12) and where heat was diffused (Wieghardt 4-18). Atmospheric diffusion data within a neutral surface layer are available from the studies at Porton (Pasquill 4-15) and, for approximately neutral conditions, from Project Prairie Grass (Barad C-1).

4.2 Basic Theory

Foundations for the basic theory involved in applying the Lagrangian similarity hypothesis to diffusion in turbulent boundary layers is given by Batchelor (4-4) and Ellison (4-9). For clarity in extending the basic results and in the interpretation of experimental data, a review of the basic theory is presented. The formulations needed for treating the experimental data are then developed.

4.21 Review of Basic Theory

Only motion of a marked fluid particle or some conserved scalar entity which is carried with the fluid without affecting the fluid motion is considered. The flow considered is a region of the boundary layer where the velocity u_* , excepting for the roughness length z_o which is a measure of the scale of turbulence where the mean velocity vanishes; i.e., a region where

$$u = u_* f(y/z_o) \tag{4-1}$$

For such a region of flow the hypothesis may be expressed as follows:

> "The statistical properties of particle motion at time t depend only upon u_* and $t - t_v$ when $t \geq O(h/u_*)$. A virtual-time origin with magnitude of order h/u_* is represented by t_v and h is the value of y when the particle is marked at $t = 0$."

A direct result of the hypothesis is that relative to the mean position ($\overline{x}$, 0, $\overline{y}$), the distribution of particle-displacement probability density for an ensemble of single-particle releases P_{sp} will be similar in shape for $t \geq O(h/u_*)$; thus,

$$P_{sp} = \psi \left(\frac{x - \overline{x}}{\overline{y}}, \frac{y - \overline{y}}{\overline{y}}, \frac{z}{\overline{y}}\right) . \tag{4-2}$$

This form follows from dimensional reasoning since the only length arising from variables in the hypothesis is $u_*(t - t_v)$ which is shown in the next paragraph to be proportional to $\overline{y}$.

For particles released from $y = h$ at $t = 0$, a relationship can be obtained between the mean longitudinal position $\overline{x}$ and the mean vertical position $\overline{y}$ at any time $t > O(h/u_*)$. As a consequence of the hypothesis three equations may be written --

$$\frac{d^2\overline{y}}{dt^2} \propto \frac{u_*}{t - t_v} , \tag{4-3}$$

$$\frac{d^2\overline{x}}{dt^2} \propto \frac{u_*}{t - t_v} \tag{4-4}$$

and

$$\frac{d^2\overline{z}}{dt^2} \propto \frac{u_*}{t - t_v} . \tag{4-5}$$

Equation 4-5 is trival since the assumed mean flow does not vary in the z-direction; therefore, because of symmetry $\frac{d^2\bar{z}}{dt^2} = \frac{d\bar{z}}{dt} = 0$ and $\bar{z} = 0$ by proper selection of the origin of coordinates. If $\frac{d\bar{y}}{dt}$ is to be finite for all finite time, the constant of proportionality for equation 3 must be zero and the equation for $\bar{y}$ becomes

$$\frac{d\bar{y}}{dt} = bu_* \quad . \tag{4-6}$$

subject to the condition that $\bar{y} = h$ at $t = 0$, the mean vertical displacement of a particle at time t is given by

$$\bar{y} - h = bu_* t \quad . \tag{4-7}$$

An integration of equation 4-4 gives the longitudinal velocity of the mean longitudinal position of a particle as a function of time. However, neglecting longitudinal diffusion, the velocity $\frac{d\bar{x}}{dt}$ may be given with reasonable exactness by the mean fluid velocity at height $y = \bar{y}$ corresponding to $x = \bar{x}$; therefore,

$$\frac{d\bar{x}}{dt} = u_* \, f(\bar{y}/z_o) \quad . \tag{4-8}$$

Time t may be replaced with the variable $\bar{y}$ by virtue of equation (4-7) to give

$$\frac{d\bar{x}}{d\bar{y}} = \frac{1}{b} f(\bar{y}/z_o) \quad . \tag{4-9}$$

Thus, the mean longitudinal position

$$\bar{x} = \frac{1}{b}\int f(\bar{y}/z_o)\, d\bar{y} + \text{constant} \tag{4-10}$$

may be obtained from a knowledge of the mean-velocity function f .

The hypothesis is used to obtain information on the concentration field by employing the probability density function in the form given by equation 4-2. When Q particles are released from a point instantaneously the concentration χ at (x, y, z) is proportional to the probability density at the same point; therefore,

$$\chi_{(\text{instantaneous point source})} = \frac{Q}{\bar{y}^3}\,\psi\left(\frac{x - \bar{x}}{\bar{y}}, \frac{y - \bar{y}}{\bar{y}}, \frac{z}{\bar{y}}\right) . \quad (4\text{-}11)$$

For the continuous point source the mean concentration χ_{cp} is then obtained by integration over all time to give

$$\chi_{cp} = Q_{cp} \int_0^\infty \frac{\psi}{\bar{y}^3}\, dt \quad (4\text{-}12)$$

Since the function ψ is expected to have a sharp maximum at $x = \bar{x}$, an approximate expression may be obtained for χ_{cp} by changing the variable of integration to $(x - \bar{x})\,\bar{y}$ and considering that the contribution at $x = \bar{x}$ dominates the integral. Effecting the change of variable through equation (4-7) and (4-8) gives

$$\chi_{cp} = \frac{Q_{cp}}{bu_*} \int_0^\infty \frac{\psi}{\bar{y}^2\left[\frac{x - \bar{x}}{\bar{y}} - \frac{1}{b}\, f(\bar{y}/z_o)\right]}\, d\left(\frac{x - \bar{x}}{\bar{y}}\right) \quad (4\text{-}13)$$

and the maximum ground-level concentration is

$$\chi_{cp}\left(\frac{x - \bar{x}}{\bar{y}}, 0, 1\right) = \frac{Q_{cp}}{bu_*} \int_0^\infty \frac{\psi\left(\frac{x - \bar{x}}{y}, 0, 1\right)}{\bar{y}^2\left[\frac{x - \bar{x}}{\bar{y}} - \frac{1}{b}\, f(\bar{y}/z_o)\right]}\, d\left(\frac{x - \bar{x}}{\bar{y}}\right) \quad (4\text{-}14)$$

Thus, when ψ has a sharp peak at $x = \bar{x}$,

$$\chi_{cp}(0, 0, 1) \propto \frac{Q_{cp}}{u_*}\, \frac{1}{\bar{y}^2(x)\, f(\bar{y}/z_o)} \quad (4\text{-}15)$$

where $\bar{x}$ and $\bar{y}(x)$ are related by equation (4-10).

The fundamental equations resulting from the Lagrangian similarity hypothesis are equations (4-10) and (4-13) while equation (4-15) permits calculation of the way in which χ_{cp} varies with distance downstream from the source.

4.22 Equations for Neutral Boundary Layers--Logarithmic Velocity Distribution

In this case, expressions for maximum ground-level-concentration dependence on x are presented for continuous point and line sources and an expression for plume-width growth with x is given for a continuous point source. The mean velocity distribution is given by

$$u = \frac{u_*}{k} \log (y/z_o) \tag{4-16}$$

where k is the Karman constant. The mean trajectory defined by equation (4-10) with the approximate condition that $\bar{x} = u(h)\,(h/u_*)$ at $\bar{y} = h$ becomes

$$bk\,\frac{\bar{x}}{z_o} = \frac{\bar{y}}{z_o} \log \frac{y}{z_o} - \left(\frac{\bar{y}-h}{z_o}\right) + (b-1)\,\frac{h}{z_o} \log \frac{h}{z_o} \tag{4-17}$$

or, introducing dimensionless variables

$$\xi = \frac{\bar{x}}{z_o}\ ,\ \zeta = \frac{\bar{y}}{z_o}$$

and

$$H = \frac{h}{z_o}$$

$$bk\xi = \zeta \log \zeta - (\zeta - H) + (b-1)\,H \log H \tag{4-18}$$

A "relaxation period" of order h/u_* during which similarity of the mean concentration distribution is attained is provided by the condition on $\bar{x}$ for $\bar{y} = h$. The maximum ground-level concentration given by equation 15 for a continuous point source takes on the form

$$\chi_{cp}\ (0,\ 0,\ 1) \propto \frac{Q_{cp}\ k}{u_*\ z_o^{\,2}}\ \frac{1}{\zeta^2 \log \zeta} \tag{4-19}$$

and the corresponding expression for the continuous line source is

$$\chi_{cl}\ (0,\ 0,\ 1) \propto \frac{Q_{cl}k}{u_*\ z_o}\ \frac{1}{\zeta \log \zeta} \tag{4-20}$$

All of the experimental data reported in the literature have been used to determine the power m in an expression of the form $\chi \propto x^m$. Therefore, in comparing theory and experiment, an expression for m must be obtained from equation (4-18, 4-19, 4-26). Since m represents the slope of a tangent to points on the curve where log χ is a function of log ξ , the required relationships are

$$m_{cp} = \frac{d(\log \chi_{cp})}{d(\log \xi)} = - (kb\ \xi) \left(\frac{1+2 \log \zeta}{\zeta \log^2 \zeta}\right) \tag{4-21}$$

and

$$m_{cl} = \frac{d(\log \chi_{cl})}{d(\log \xi)} = (kb\ \xi) \left(\frac{1+\log \zeta}{\zeta \log^2 \zeta}\right) \tag{4-22}$$

If the probability density function does exhibit similarity as expressed by equation (2), it follows that any measure of the plume width will vary with x as does $\bar{y}$ (this is true also for any measure of the plume height). Let the relationship for plume width Y be

$$Y \propto x^n . \tag{4-23}$$

Equation (4-18) gives, for the continous point source,

$$n_{cp} = \frac{d(\log \zeta)}{d(\log \xi)} = \frac{bk\ \xi}{\zeta \log \zeta} \tag{4-24}$$

4.3 Diffusion Data from Experimental Studies

Brief descriptions will be presented of the experimental studies in the laboratory and in the atmosphere in which data required to test one or more of the equations for m_{cp}, m_{cl}, or n_{cp} were obtained. The essential data from these experiments are tabulated in Table I. All experimental values of n_{cp} were obtained from information on plume width.

The data of Davar (4-8) and Malhotra (4-12) were obtained by diffusing ammonia gas in a turbulent boundary layer formed on the smooth floor of a wind tunnel test section which was 6 x 6 ft square and 24 ft long. By using roughness elements at the beginning of the test section a boundary layer about 3 in. thick was created at the location of the source when the ambient velocity was in the range 6-25 ft/sec. Ammonia gas was introduced through a tube 0.1 in. in diameter penetrating the floor and turned through 90° to emit gas in the direction of mean flow at a maximum elevation of about 1/8 in. Poreh (4-16) diffused ammonia gas from a line source made from a porous strip 3/16 in. wide placed flush in a smooth floor and orientated at right angles to the mean-flow direction.

Experiment	x (ft)	z_o (ft)	h (ft)	L	kbξ	H	α	$-m_{cp}$	$-m_{cl}$	n_{cp}
1. Laboratory-- point source										
Davar (C-8)	1.5	9.9×10^{-5}	9.38×10^{-3}	∞	621	95	0	1.20	--	--
	4.5	10.5 "	9.38 "	"	1750	89	"	1.47	--	--
Malhotra (C-12)	4.5	2.4 "	5.20 "	"	7380	208	"	1.47	--	--
	2.5	2.5 "	5.20 "	"	4100	208	"	----	--	0.60
	2.5	10.5 "	9.38 "	"	975	80	"	----	--	0.60
Wieghardt (C-18)	1.03	3.7 "	--	"	1140	--	"	1.42	--	0.67
	1.03	2.0	--	"	2130	--	"	1.42	--	0.67
2. Laboratory-- line source										
Malhotra (C-12)	4.5	2.5×10^{-5}	5.20×10^{-3}	∞	7380	208	0	----	0.80	--
Poreh (C-16)	7.5	6.2 "	--	"	4350	--	"	----	0.90	--
	7.5	4.8 "	--	"	6400	--	"	----	0.90	--
	7.5	3.5 "	--	"	8700	--	"	----	0.90	--
Wieghardt (C-18)	1.23	3.8 "	--	"	1320	--	"	----	0.90	--
	1.23	2.04 "	--	"	2470	--	"	----	0.90	--
3. Field-- point source										
Porton (Pasquill C-15)	1640	2.85×10^{-2}	$5^* \times 10^{-1}$	∞	685	5	0	1.76	--	--
	656	9.85 "	5 "	"	273	5	"	----	--	0.74
Prairie Grass (Cramer C-7)	1976	3.28 "	9.85 "	"	2460	30	"	1.8	--	0.80
4. Field-- line source										
Porton (Pasquill C-15)	1640	9.85×10^{-2}	$5^* \times 10^{-1}$	∞	685	5	0	----	0.9 - 1.0	--

*Estimated with the assistance of Dr. Pasquill

Table I. Data on diffusion in neutral boundary layers -- Cermak (4-6)

The work of Poreh (4-16) was accomplished in a wind tunnel test section 6 x 6 ft square by 80 ft long with an ambient air-speed range of 9-17 ft/sec (discussed in Ch. 3 of this report). At the source the boundary-layer thickness ranged from 5 to 7 in. Wieghardt (4-18) diffused heat created by an electrically heated coil 3 mm in diameter placed in a slot cut into an otherwise smooth floor. To produce the point source, a 1-1/4 in. long slot with axis in the flow direction was used while the line source was created by a slot cut across the entire width of the tunnel. Dimensions of the tunnel used by Wieghardt were 4-1/2 ft wide, 1.3 ft increasing to 2 ft high and 20 ft long. The mean air-speed range was 17 to 100 ft/sec.

The exponents given for the field data obtained at Porton (4-15) represent the mean values of several separate experiments. In each case smoke was diffused into a nearly neutral atmosphere from smoke candles or other smoke generators placed on the ground. The site for the Portion studies was flat grassland. Although no exactly neutral conditions were encountered during the experiments of Project Prairie Grass (Barad 4-1), Cramer (4-7) estimates the exponents for a point source from the near neutral data. These experiments were realized by releasing sulfur dioxide into the atmosphere from a point source at a height of 30 cm. As at the Portion site, the terrain was flat grassland.

4.4 Calculation of Parameters

For all the laboratory experiments, in which the boundaries were all smooth, the value of z_o was estimated by using the mean velocity function $u/u_* = \frac{1}{k} \log \frac{u_* y}{u} + 4.9$. This gives the result $z_o = 0.141 \left(\frac{\nu}{u_*}\right)$. The value of the shear velocity u_* was taken as the mean value over the distance x up to where the exponent of x was measured and was calculated either by differentiation of the momentum thickness θ , or by using the Schultz-Grunow drag formula $\left(\frac{2}{C_f}\right)^{1/2} = 6.30 \log \frac{u_{amb}\theta}{\nu} + 2.40$.

In all cases the exponents m_{cp}, m_{cl}, and n_{cp} were obtained by measuring the slope of a tangent drawn to curves constructed by plotting the logarithm of the appropriate variable as a function of log x . In all cases x was restricted so that $\frac{\lambda}{\delta} \leq 0.40$. In this ratio δ is the boundary-layer thickness and λ is a characteristic length of the concentration field--the height y where the mean concentration is one-half the maximum. As shown in Ch. 3, for a line source the concentration profiles are similar for $\frac{\lambda}{\delta} \leq 0.40$, but then gradually changed form until $\frac{\lambda}{\delta} = 0.64$, when a new similarity profile is attained. Since the similarity hypothesis is formulated only for the inner part of the boundary layer, only the first similarity region is strictly within the restrictions of the analysis.

In numerical calculations, the value of Karman's constant k has been taken as 0.41 and the value of b (Batchelor's constant), has been taken as 0.1. The value of 0.1 for b gives good agreement with the data but should be considered only as a rough approximation until more precise data are available to determine the true value. Batchelor (4-4) estimated b to be about 0.1 or 0.2. A rough estimate of Batchelor's constant may be obtained by multiplying the approximate maximum vertical plume velocity of $0.75u_*$ reported by Monin (4-14) by the ratio of elevation at mean concentration to elevation at 0.01 of maximum concentration (outer edge of plume). Using the exponential function for the vertical concentration distribution given by Calder (4-5), this ratio of elevations is 4.82 which gives a value of b of 0.15. Ellison (4-9) concluded that $b = k = 0.4$ on the assumption that the turbulent diffusion coefficients for mass and momentum in the vertical are the same; however, since the boundary conditions for mass and momentum are entirely different--point or line source for mass and area sink for momentum--the assumption has little justification.

4.5 Discussion

Data given in Table 1 obtained from the studies briefly described in the preceding section may be used to determine the validity of results obtained from the hypothesis of Lagrangian similarity. Figures 4-1 to 4-3 show both the experimental data and selected theoretical curves to facilitate comparison. For an aerodynamically smooth surface the curve where $H = 75$ corresponds to h equal to the laminar sublayer thickness and $H = 225$ corresponds to an h where transition to the logarithmic profile has been completed. The curves for H equal to 30 and 100 correspond closely with the value of H for the Prairie Grass data and certain wind-tunnel data respectively. The degree of agreement between theory and data is sufficiently good to justify use of the Lagrangian similarity hypothesis as the basis of diffusion modelling in the atmospheric surface layer.

4.51 Comparison of Theory and Experiments

In Figure 4-1 all the values of m_{cp} for aerodynamically smooth boundaries (wind tunnel experiments) correspond to theoretical values of $H > 75$. Where the value of H is known from the experimental conditions, the exponent m_{cp} from experiment is within 10 percent of the corresponding theoretical value. For the data of Wieghardt in which H is not explicitly known, the relationship between the experimental points and the theoretical curves indicate that the apparent source height for a source embedded in a smooth boundary is between the height of the laminar sublayer and the height corresponding to where the logarithmic velocity distribution is attained. The mean Porton and Prairie Grass data for neutral conditions shown in Figure 4-1 are within about 2 percent of the corresponding theoretical values. Project Prairie Grass data for mildly non-neutral surface layers are also shown in Figure 4-1 to emphasize the importance of the parameter H in the present theory. As is evident, the mild lapse and mild inversion produce values of m_{cp} which diverge with increasing distance above and below respectively from the neutral curve for $H = 30$.

Figure 4-2 gives the available experimental data and theoretical curves for attenuation of maximum ground-level concentration for a continuous line source in neutral boundary layers in terms of m_{cl}. The wind-tunnel data of known H due to Malhotra was obtained by integration of his point-source concentrations and is about 5 percent lower than the corresponding theoretical value. Wind tunnel-data of Poreh with gas emitted from a smooth porous line source is consistent with the idea of the effective source height parameter for such sources being in the range $75 < H < 225$. The progression of points from left to right represent increasing mean ambient velocity and consequently decreasing values of z_o. Since the data of Wieghardt correspond to values of $H < 75$ for this case, it is concluded that the transverse boundary slot containing the source produced a large scale disturbance making the effective z_o (local turbulence scale) larger than that calculated by considering the boundary to be smooth. Field data obtained at Porton give a range of m_{cl} with a mean value very near the predicted value of about -0.95. The scatter of m_{cl} at this site can easily be accounted for through varying roughness and small departures from neutral conditions.

Both average values of n_{cp} giving the rate of plume-width growth for Porton and Prairie Grass data under neutral conditions are in good agreement with the theoretical values shown in Figure 4-3. Values of n_{cp} for the neutral wind tunnel data and the corresponding theoretical values are also in satisfactory agreement.

4.6 Significance of Findings for Modeling

The basic formulation presented here for the neutral boundary layer has been extended to include the diabatic case (thermally stratified flow) with arbitrary source height. Gifford (1-10) also extended the analysis to diabatic flows but without including the parameter $H = \frac{h}{z_o}$. There was, once again, satisfactory agreement between theory and experiments. From this extended analysis it is seen that diffusion in the boundary layer of a wind-tunnel model of the atmospheric surface layer will be similar to the prototype if the parameter $H = \frac{h}{z_o}$ and $\alpha = \frac{z_o}{L}$ is the same for both. Here L is the Obukhov stability length which is equal to ∞ for the neutral case (thus $\alpha = 0$ for neutral flows). Hence, similarity seems assured if H is the same for model and prototype for neutral flows. This can be seen by examining equations (4-18, 4-21, 4-22 and 4-24).

Inoue (4-11) reached the same conclusion by requiring that the angle of diffusion and a dimensionless diffusion length $\frac{U\tau}{h}$ (τ is the Lagrangian time scale for motion in the direction of mean velocity U) be the same for both model and prototype. Of course, the modeling can be accomplished only if the wind tunnel boundary layer is sufficiently thick to ensure that $\frac{\lambda}{\delta} \leq 0.4$ over the ranges of ζ covering the model.

An even more important consequence of the agreement between results of the Lagrangian similarity hypothesis and data from field and laboratory is the implied similarity of the turbulence structures. This means that in properly designed laboratory experiments measurements of turbulence structure for controlled stability and roughness will yield information applicable to the atmospheric surface layer.

4.7 Conclusions

Examination of the data and analytical results presented by Cermak (4-6) support the Lagrangian similarity hypothesis. Therefore, this simple but powerful concept affords a rational basis for describing the gross characteristics of a diffusion field within a turbulent boundary layer. The use of z_o as a reference scale of turbulence successfully accounts for differences in diffusion rates when diffusion takes place on scales varying from those encountered in the laboratory to those existing in the atmospheric surface layer. Further study of diffusion rates for a wide range of z_o and H, such as can be accomplished in a wind tunnel using boundaries with fixed or flexible roughness elements accompanied by heating or cooling of the boundary would be particularly illuminating. In applying the existing formulation of the Lagrangian similarity hypothesis to diffusion in wind tunnel boundary layers the plume of diffusing mass or heat should be well within the boundary layer--(i.e. $\frac{\lambda}{\delta} \leq 0.40$). On the other hand, the foregoing analytical results do not apply immediately downstream from the source for distances of order $u(h)\ (h/u_*)$.

The analysis states that two fields of diffusion within the inner region of a turbulent boundary layer will be similar if H and α for one field are equal to H and α respectively for the other field. This not only gives a basis for modeling practical cases of diffusion in the atmospheric surface layer but also provides a means by which laboratory measurements of basic turbulence structure may be applied to the atmosphere.

4.8 Nomenclature

Symbol	Definition
b ,	Batchelor's constant;
C_f ,	drag coefficient;
$f(\frac{z}{z_o})$,	universal velocity distribution function;
h ,	source height
H ,	non-dimensional source height, $\frac{h}{z_o}$;
k ,	von Kármán constant;

Symbol	Definition
L ,	Obukhov stability length
M_{cp} ,	slope of the ground concentration attenuation with x for a point source;
M_{cl} ,	slope of the ground concentration attenuation with x for a line source;
N_{cp} ,	slope of the width of plume growth with x for a point source;
P_{sp}, ψ ,	particle - displacement probability density for an ensemble of single-particle releases;
Q ,	strength of the instantaneous point source;
Q_{cp} ,	strength of the continuous point source;
t ,	time measured from release;
t_v ,	virtual time origin, $\frac{h}{U_*}$;
U ,	mean longitudinal velocity;
U_* ,	shear velocity;
U_{amb} ,	mean ambient velocity;
x, y, z ,	instantaneous position of particles with origin at source;
$\bar{x}, \bar{y}, \bar{z}$,	mean position of particles;
y	width of plume;
$\bar{x}_v$,	relaxation distance $U(h)\,\frac{h}{U_*}$;
z_o ,	roughness height;
α ,	z_o/L;
δ ,	boundary layer thickness;

Symbol	Definition
ρ ,	non-dimensional height, z/z_o ;
θ ,	momentum thickness;
λ ,	$\dfrac{\chi_{cl}(x, \lambda)}{\chi_{cl}(x, 0)} = 0.5$;
ν ,	kinematic viscosity;
ξ ,	non-dimensional distance, $\overline{x}/z_o$;
τ ,	Lagrangian time scale;
χ_{ips} ,	instantaneous point source mean concentration;
χ_{cp} ,	continuous point source mean concentration;
χ_{cl} ,	continuous line source mean concentration.

5. DIFFUSION IN AND ABOVE SIMULATED PLANT COVERS

An experimental program on modeling vegetative cover faces a problem in that every crop might have entirely different characteristics regarding its interaction with the wind blowing over it. This then is reflected in the behavior of the diffusion cloud above it or inside the cover. Fortunately, experience has shown that most diffusion patterns over rough or smooth boundaries tend to reach similarity profiles at some distance downstream from the source, with the type of roughness cover, wind speed and geometry of boundary affecting only the similarity parameters.

Since there was some hope that a similarity of the velocity distributions at some distance from the upstream edge of the plant cover might be found, an analysis could be based upon the similarity profiles for mean velocity and concentration. Results of such an analysis would have more than local significance. The problem then became one of defining regions of validity for a similarity assumption for a trial crop cover which exhibits the characteristics of a natural crop, preferably wheat or corn. For these regions, the appropriate form of the Lagrangian similarity hypothesis was to be applied, and the results of the calculations compared with the results of the experiments.

5.1 Roughness Elements

Since it was the task of the present study to define modeling parameters for modeling diffusion in and above crops, the model roughness cover to be decided on for the experiments should have been determined experimentally. However, the type of model roughness had to be selected without benefit of prior experimental information.

A first step in deciding on the types of flexible boundaries to be used, consisted in studying the literature on field data in order to obtain some information on the properties which such a roughness should have. However, the references are very scarce indeed. The only data found was taken during the 1930's and reported on by Paeschke (as reported by Geiger reference 1) on wind profiles over different crops, some data on wind profiles in tree stands (Geiger, Ref. 5-1), data reported by Lemon (5-2) and (5-4) and data taken by Lemon as reported by Tan (5-3). All these data were presented in raw form. Only the last of the quoted references (5-3) contains an attempt at an analytical description. This approach, however, merely resulted in a number of different empirical coefficients which appeared to be valid only for the particular crop (corn or wheat) and velocity of air considered. The data in (5-3), however, showed that a well-defined crop characteristic appears to be the distribution of the velocity within the crop. This distribution can be represented in dimensionless form, in a rather elementary manner by using the crop height, or a length dimension proportional to the crop height as reference length, and by using the mean air velocity at the reference height as a measure of the velocity parameter. Both these parameters are easily determined in the wind tunnel and in nature. The plot made of the field data is shown in Figure 5-1. It is very interesting to note that the data for wheat agree quite well for data taken under as different conditions as the one of Paeschke (5-1) in Germany and Lemon (5-2) in New York State.

It was therefore decided to use a crop, chosen according to availability of material and convenience in manufacture, which exhibits a similar velocity distribution law within the crop as was found for wheat or corn in (5-3). After trying a number of other ideas, roughness elements were chosen which consist of strips of plastic, flexible material fastened to lumber strips as shown in Figure 5-2. The present data were obtained with plastic strips 0.25" wide, 0.01" thick, and of a height h_o of 4". In one case they were arranged to face the direction of the wind with their broad side (Arrangement 1) with a transverse spacing of one element per 2 linear inch, and a spacing in the direction of flow of one row every 2 inches. A second arrangement was used in which the flexible elements were turned 90^o, so that the wind struck the thin side (Arrangement 2). The setup is shown in Figure 5-3.

An initial experiment was performed in order to determine the geometry of the roughness elements under the action of wind. At no wind speeds, the elements were of curved shape, all elements being deformed approximately by equal amounts, but deflected randomly either to the upwind or the downwind direction. With gradual increase of the wind velocity, the former of the elements would first be straightened somewhat and then deflected downwind, so that at a wind speed of approximately 20 fps almost all elements lean somewhat in the downstream direction. For higher speeds the deflection of the elements by wind becomes more noticeable, the elements become bent down and the height of the roughness cover z_o decreases. This is shown in Figure 5-4.

5.2 Velocity Measurements

Velocity profiles were taken over the model crop for three different velocities of 10, 20 and 40 fps, at various stations downstream from the roughness cover's leading edge. The velocity profiles are shown in Figures 5-5 to 5-8, and the pertinent profile parameters are listed in Table 5-1*.

An analysis of the velocity distribution along the lines commonly used for turbulent boundary layers - i.e. by using a logarithmic distribution law - cannot be used directly. This is mainly due to the unusual shear situation in the canopy. The friction losses in the canopy are obviously not caused by friction on the ground alone but also by the drag of the plant cover. This rules out a determination of the shear from the gradient of velocity profile at the ground.

There is considerable activity going on in different quarters to circumvent this difficulty. The writers are aware of efforts being made by the staff of the micrometeorological group of the Meteorology Department, U.S. Army Proving Ground, Fort Huachuca, to analytically determine canopy flow profiles; the efforts of Tan et. al. (5-1) were already mentioned, and Lemon (5-4) gives a number of references which are to be published soon. Since all these analyses depend on experimental data for their empirical constants, it seems sufficient at the present time to determine parameters which correlate the wind-tunnel data. The main objective is therefore to find similarity parameters for the velocity profiles, and define regions in which the similarity profiles are valid.

5.21 Similarity Profiles

For this purpose, the data were analyzed in an entirely empirical manner. All data were initially plotted in dimensionless form obtained by dividing y by the local boundary-layer thickness δ and u by the ambient velocity u_a. The results are shown in Figures 5-9 to 5-12. The figures show that the velocity

---

*The velocity profiles have been taken with partial financial support by the Army Micrometeorology Department, Fort Huachuca, under a grant for the investigation of boundary-layer roughness.

follows an approximate similarity law, at least from a station which has a distance of about 10 ft downstream from the leading edge of the canopy. A closer inspection shows, however, that similarity profiles are no where exactly reached; for there is a small increase of the convexness of the distribution noticeable for all velocities. A correlation was obtained for the profiles inside the canopy by defining arbitrarily a velocity u_h which is equal to $0.4\ u_\delta$. This is the "theoretical" velocity at the canopy top, which may actually occur slightly above or below $y = h$. The level h then will be a function of the wind speed and the crop geometry, with the values for the present geometry and those velocities of 10, 20 and 40 fps listed in Table 5-2. For the velocities of 20 and 40 fps, comparison with Figure 5-4 shows that $\frac{h}{h_o}$ is about 1.2. If this result could be generalized, it would mean that the effect of wind bending on the canopy flow finds its expression in the fact that the reference height should be related to the deflected canopy and not to the original. With this reference velocity u_h and h, the velocity profiles become similar in the canopy for all velocities and stations (Fig. 5-13) larger than 10 ft from the edge of the canopy. The result indicates that, for a given arrangement of crops, the wind profile in the canopy would depend only on the drag coefficient of the plant, on the density of the plant spacing, and on the deflected plant height, but would be independent of the velocity. Contrary to the behavior of flexible elements chosen for this study, for actual plants the drag coefficient might change with velocity. The field data of Figure 5-1 indicate, however, that if this effect exists it is small indeed - as long as the plants are in the same stadium of growth. For wheat, the change might not be too significant, as indicated by the agreement of the data taken by different observers at different locations. For crops which grow seed heads, however, the effect can be quite large.

The average curve of the data points is indicated in Figure 5-1. According to this curve, apparently the arrangement chosen offers somewhat less obstruction to the air flow than either corn or wheat, but the conclusions drawn from these data are, in the light of the foregoing discussion, just as valid.

The profiles above the canopy are markedly improved in similarity if the velocity ratio is plotted versus the non-dimensional ratio $(y-h)/(\delta-h)$. The profile obtained can be represented with good accuracy by a power law of the form

$$\frac{u}{u_\delta} = \left(\frac{y-h}{\delta-h}\right)^{1/3} \qquad (5\text{-}1)$$

which holds for the upper 80 percent of the profile, but deviates (as it must) in the lower portion. The profile has been sketched into Figure 5-14 together with the experimental data. It can be noted that the velocity data for Sta. 6 and for the velocity of 10 fps show the largest deviation from the average curve. The deviations of the 10 fps data are undoubtedly mainly due to calibration errors of the hot wire, since the manometer for velocities smaller than 10 fps gives unreliable readings. The deviations for Sta. 6 are systematic, indicating that similarity was not yet obtained.

The similarity parameter δ depends on the station downstream from the leading edge of the crop as well as of the boundary layer. It is shown, for the experimental data, in Figure 5-15.

5.22 Calculations of Boundary Shear

In principle, three different methods commonly used in wind-tunnel experiments could be used for determining the boundary shear. The first one starts from the assumption, that the logarithmic velocity distribution law holds for the distribution over a crop. This proposition, used by Tan et. al (5-3) is of doubtful value; as is shown in 5.21, the profile is more adequately described by a power law with large exponent (a log-law can be approximated generally by a power law with small exponent). The second method is to use the friction coefficient as defined by the equation of Ludwieg and Tillmann (see equation 6-8). Again, for a canopy, this is a dubious procedure since the lower portion of the profile contributes highly to the shape factor $\frac{\delta^*}{\theta}$ while certainly in it the drag is not governed by the boundary.

Both these shortcomings do not apply to the third method; that of the application of Karman's momentum principle. According to this the shear per unit area τ_o is given by

$$\tau_o = \rho\, u_a^2 \frac{d\theta}{dx} \quad \text{where } \theta \text{ is the momentum thickness,}$$

provided that no pressure gradient exists in the x direction, and provided that the contributions by the turbulence can be ignored. The results of these calculations gave shear values of

$$\bar{\tau}_o = 2.24\ 10^{-3}\ \text{lb/ft}^2 \text{ for } u_a = 10 \text{ fps}$$
$$\bar{\tau}_o = 5.20\ 10^{-3}\ \text{lb/ft}^2 \text{ for } u_a = 20 \text{ fps}$$
$$\bar{\tau}_o = 6.14\ 10^{-3}\ \text{lb/ft}^2 \text{ for } u_a = 40 \text{ fps}$$

as an average value for all stations from 10 to 20 ft.

5.3 Diffusion in the Region of Flexible Roughness

The results obtained for the velocity profiles in and above the canopy suggest the use of h as a meaningful value for separating the flow and diffusion field into an upper and a lower layer. This separation should lead to an entirely different approach for the inside of the canopy as above it, with the flow above the canopy expressed as the flow along a flat plate, located at some distance h away from the true boundary.

This concept governed the analysis of the diffusion data which were taken for this part of the study. The diffusion profiles are shown in Figures 5-16 to 5-23. They were taken with the 44" long ground-level line source 2 ft upstream from the canopy, and with the elevated 22" long line source located inside the canopy at x' ft from the canopy beginning. The elevated source was placed at 4 different elevations: $H = 0"$ (ground level) $H = 2"$ (about half the cover height) $H = 4"$ and $H = 8"$. For the roughness arrangement 2 (across the rows), only two sets of data were taken, with the elevated line source at 8 ft distance from the cover edge, and source elevations of $H = 0"$ and $H = 4"$. In order to note the development of the profiles inside the canopy, the profiles were taken, for this case, somewhat closer together.

The elevated line source was not entirely satisfactory. As was found during the experiment, the source lost its 2-dimensional character at a relatively short distance downstream from its location. This became apparent by taking transverse profiles at a fixed elevation, and is mostly noticeable in the total amount of gas discharge found by integrating the product of velocity and concentration over the vertical, as shown in Figure 5-24. This three-dimensional effect will influence the maximum concentration and to a lesser extent also the rate of spread. For the present, however, it is ignored.

5.31 Concentration Profiles Inside Canopy

The most remarkable trend of the concentration profiles inside the canopy is the tendency to reach a constant vertical concentration within the plant cover. The shear generated on the flexible plants produces a large amount of turbulence, which in turn causes a rapid spreading of matter inside the canopy. Outside the canopy the turbulence level, and therefore, the spreading of the gas is somewhat slower, so that the turbulence underneath can eliminate all concentration gradients. This tendency lends support to considering the canopy diffusion as a problem essentially unrelated to the boundary-layer diffusion above, with only the boundary conditions for both layers relating them. This means that the maximum concentration outside the canopy will be affected by the spreading into the canopy, while the concentration profile above the canopy has a shape which is independent of the canopy. Also, the other similarity parameter, the spread λ-h, is independent of the canopy region, so that the diffusion outside behaves like a diffusion cloud on a smooth flat plate. It should be noted that the case of the instantaneous source would require an entirely different and more involved treatment than the one which can thus be given for the continuous source.

Another observation pertinent to the diffusion in the canopy can be made if attention is given to the concentration profile obtained for the case of flow across the row, line source elevated to H = 4, Sta. 9' 8" and Sta. 11' 4". These profiles look approximately symmetrical with respect to a horizontal line through the source height. This result is again not unexpected. The turbulence level inside the canopy is due to the effect of the roughness element and is very nearly homogeneous. Since the spreading is done by the turbulence, a homogeneity should be reflected in the spreading of the gas by producing a plume with symmetry about a horizontal plane.

No attempts have been made to follow the spread of the diffusion cloud inside the canopy in detail; these considerations will have to be made when turbulence measurements are available.

5.32 Concentration Profiles Outside the Canopy

As was stated before, the concentration profile above the canopy shall essentially display the features of a flat plate displaced by the height h. Therefore, the profiles were made dimensionless not by dividing the elevation by λ, but by dividing y-h by λ-h, as shown in Figure 5-25. The result is of great interest. The profiles are essentially separated into three different categories, which should, in the notation and concepts of Chapter 3, correspond to the intermediate, transition, and final zone. If this is the case, then the results of Chapter 3 concerning the limits of these zones should hold also. Therefore, the values of $\frac{\lambda-h}{\delta-h}$ have been plotted for the three zones in Figure 5-26. The result indeed shows that the same criteria apply for the canopy covered boundary as for the smooth flat plate.

No attempt was made to define a parameter β for the canopy. It was found that the concept developed in Chapter 3 did not apply for this case.

A length parameter defining the distance from the edge at which each one of the zones begins was not well defined. The first puzzling fact was that the 8" elevated source reached the final zone earlier than any of the others. This can be explained by the same considerations used for the flow inside the canopy, except that here the low turbulence of the ambient air outside of the boundary layer prevents a spreading to the outside. For the sources which were located well within the boundary layer, the final zone was reached at Station 16, that is 8 ft downstream from the source location. For the ground source located in front of the cover the final zone was reached at Station 10, or about 12 ft downstream from the source. All other data for these sources fell into the transition zone, and no attempts were made to investigate the initial zone, since this should essentially reflect mainly the local effects; i.e. source geometry, feed velocity, etc.

The other parameters defining the profiles are the spread $\lambda - h$ and the maximum concentration c_{max} . These quantities will vary with distance, with the trends shown for λ in Figure 5-24 and for c_{max} in Figure 5-28. In the latter, the ground concentration rather than the maximum concentration is given. This corresponds to the maximum concentration only in the zone of transition and in the final zone.

The data are plotted without regard for the parameter h , and some improvement could no doubt be obtained by considering it. The data show, however, that at large distances downstream the ground concentration are the same for all source elevations, for the same velocity. The deviation of the 10 fps data are caused by the deviations of the velocities. The reason is that for a constant feed rate, the concentrations are related to the velocity, since for similar velocity profiles, the product $u_a\ c_{max}$ must be equal.

The trends in the values of λ are not easily explained. It appears that by suitable choice of coordinate origin the data for 20 fps, arrangement one, can be brought into agreement, but the justification for this has not yet been found.

5.33 Lagrangian Similarity Hypothesis

The attenuation of the ground concentration can be determined by using the graphs of Figures 4-1, 4-2. It is seen in Figure 5-27 that the exponent of decay is given for source heights $H = 0$ by 0.95 for the ground source. The parameters to be computed are

$$kb\xi = \left(0.41\right)\cdot\left(0.1\right)\frac{x}{z_o}$$

where $z_o \approx h$. For 20 fps, $h = 4.6"$ so that for an average x of $\backsim 15$ ft $\xi = \frac{15\cdot 12}{4.6} = 39$ and $kb\xi = 1.6$. As can be seen from Figure 4-2 this is in reasonable agreement for a value of H of less than one for a continuous point source. However, the agreement is partially fortuitous, since the velocity profile for the case considered is not very similar to a logarithmic profile, as required by the equation 4-22. Therefore, it is not surprising that no reasonable agreement can be found for the data on elevated sources especially since the elevated source has a behavior intermediate between the infinitely long line source and the point source.

It will be one objective of the Ph.D. dissertation based on this work to develop a suitable set of parameters which will bring the well-defined results of the present study into agreement with the findings of the Lagrangian similarity hypothesis.

5.4 Conclusions

5.41 Velocity Distributions

By searching for similarity parameters, it was found that the velocity profiles exhibited true similarity outside of the canopy, with the boundary-layer thickness δ and the ambient velocity u_a as similarity parameters, if the height h was subtracted from y and δ. The height h is defined as the height where $u(h) = 0.4\,u_a$ and was found to be dependent on the roughness type and ambient velocity. Most of the dependence upon ambient velocity is accounted for by relating h to the height of the deflected roughness elements h_o. The approximate relationship is that $h \doteq 1.2\ h_o$.

However, in order to reach similarity profiles, the air flow had to travel a length from the leading edge of the crop of approximately 20 to 30 times the crop height.

Within the canopy, it was found that the profile $\frac{u}{u_h}$ vs $\frac{z}{h}$ exhibited similarity for all stations downstream from Station 6. These results together with the field results demonstrated in Figure 5-1, are indicative of the possibility that each crop has its own "characteristic wind profile" within the canopy. This conclusion should be tested in the field for many different crops, at different stages of growth.

5.42 Concentration Distribution

The conclusions of different zones of diffusion are, at least for ground level sources, well confirmed also for diffusion above a canopy. The intermediate zone and the final zone are well defined both in the ratio of boundary layer thickness to plume width and in the profile shape. However, the height h had to be subtracted from all vertical heights before formation of parameters, which is in agreement with the velocity behavior.

The trend of the similarity parameters is, due to the influence of both the undisturbed and the canopy disturbed portions of the boundary layer and to distance from source, not well defined, and considerable work needs to be done to separate the influences of all pertinent variables.

Inside the canopy, the concentration assumes a value which is approximately constant with height.

5.5 Nomenclature

Symbols	Definition
y ,	vertical elevation;
δ ,	local boundary layer thickness;
u_h ,	ambient velocity at $y = h$;
u ,	velocity at y;
u_a ,	ambient velocity;
δ ,	boundary layer thickness;
δ^* ,	displacement thickness;
τ_o ,	shear at wall;
h ,	height representing reference height of crop (defined by $U(h) = 0.4 U_a$);
z ,	h_o height of wind deflected roughness elements;
H ,	source elevation;
λ ,	spread of diffusing plume, y at which $c = 1/2\ C_{max}$;
x ,	station from source;
$kb\xi$,	see Chapter 4;
ξ ,	coefficient $= \frac{x}{z_o}$;
$z_o = h$,	roughness height.

6. DIFFUSION DOWNSTREAM FROM A TWO-DIMENSIONAL WALL

The cases treated in the foregoing chapter are quite idealized compared to actual natural conditions, and two problems are seen at once in attempting to apply the results to other than very similar geometrical situations. The one concerns the fact that rarely is the "fetch" or the distance of approach before the crop equal to a smooth flat plate with a correspondingly developed boundary layer. Rather, the boundary layer of approach is a distorted and twisted flow field reflecting influences of topography, plant cover, and temperature variations which have occurred long distances upstream of the considered crop cover.

The other problem arises because of the finite length of any field. As was noted before, a certain length of crop cover is required before a kind of equilibrium of flow and concentration field is obtained.

In an attempt to find some indications on how serious both these problems are, the effect of a flat sharp edged wall, placed perpendicular to the direction of flow, and in contact with the floor, on the concentration field caused by a line source located upstream from the wall was studied. The natural situation which might be simulated by this arrangement is the diffusion field which is distorted by a shelter belt of great length and high density, or of a dense and long zone of long crops of little downstream extent or of a mountain range, all in essentially neutrally stratified flow. The results are extreme values in the sense that no other non-active obstacle can generate more profound disturbances.

The case of the diffusion in a boundary layer disturbed by a wall was studied in some detail. Concentration measurements were made for four wall heights of $h = 1/2"$, $1"$, $1\text{-}1/2"$ and $2"$. The case of $h = 1"$ was considered the reference case, and for it velocities were varied ($U_a = 5$, 9 and 14 fps for diffusion measurement, $V_a = 14$ and 20 fps for measuring velocities) and the effect of varying the distance between the source and the plate was studied.

6.1 Experimental Set-up

The source for the gas was the ground level-line source described in Chapter 2. The plates consisted of 1/4" steel plates of appropriate height with the edge facing the wind sharpened to a width of less than 1/64". The 1/2" plate consisted of a piece of angle iron which was screwed to the tunnel floor; the other three plates were screwed to the 1/2" plate.

The velocities were measured with a mean velocity hot-wire anemometer calibrated against a pitot-static tube. In addition to mean velocities, turbulent intensities in the flow direction and their spectra were determined as described in Chapter 2.

The concentrations were measured in the open-circuit tunnel with one set of velocity data. The data on velocities taken proved to be somewhat erratic, so that another set of velocity profiles, this time at a higher ambient velocity, was taken in the closed-circuit tunnel.

6.2 The Velocity Field

6.21 Flow Zones

The flow around a flat plate in contact with the wind-tunnel floor can be subdivided into four zones, as shown in Figure 6-1. Zone 1 is the region upstream from the plate in which the plate effect is not yet felt; the boundary layer behaves like the boundary layer along a smooth flat plate with zero pressure gradient. Directly upstream from the plate the flow is retarded, the pressure is increased, reaching a maximum at the upper part of the plate. The flow field separates at the sharp edge of the plate, and zone 2 contains the fixed eddy zone behind the plate. The fixed eddy region is separated from the somewhat accelerated outer flow through the separation stream line, along which the pressure, after a sudden drop at the separation point first decreases and then slowly increases again, reaching the undisturbed ambient pressure again downstream from the location of the stagnation point at which the separation streamline reattaches to the wall. The pressure measurements for U_a = 20 fps and U_a = 14 fps for all plate heights shown in Figure 6-2 reveal that this pressure is approximately similar for all plate heights, but the point where the pressure comes back to the value of the undisturbed flow is not well defined.

The pressure measurements were made with the static holes of the pitot static tube. Since the velocity and also the turbulence level in the fixed eddy region is very low, and since according to experimental results by Arie and Rouse (6-1) the pressure in the standing eddy region is constant in every vertical sections, the pitot tube was placed at a distance of 1/4" away from the floor. The accuracy is questionable due to the small pressures involved.

It was found by Nagabhushanaiah (6-2) on the basis of an extensive series of experiments with velocities of 9 and 12 fps, and plate heights ranging from 0.5 to 12 in., that the downstream stagnation point is located at a distance of 12.5 h downstream from the plate.

The point L = 12.5 h marks the beginning of the third zone, that is the transition from the standing eddy zone to the re-established boundary layer. Clearly, the boundary layer at the end of this zone must obey the classical distribution laws found valid for the boundary layer on a smooth flat plate by many experimentors. However, the flow inside zone 3 is not conveniently defined by similarity laws, and only qualitative information will be given which may lead to a better understanding on how to treat this type of flow.

6.22 Sandborn's Criterium

The stagnation point of the separation streamline at the point of reattachment exhibits all the geometric features of the point of inception of separation. Therefore, similar flow conditions should exist downstream from the reattachment point as exist in the flow before separation, and the same methods should apply for both situations. Of all the numerous analyses of separation -- as summarized for example by Schlichting (6-3) none appears to hold for more than some restricted cases. However, recently Sandborn (6-4) and Sandborn and Kline (6-5) have developed and applied a criterium - on purely empirical grounds - which appears to be applicable to a wide variety of separation cases. The basic idea behind the criterium is an attempt to extend the well-known power law velocity distribution to the two-layer model for the turbulent boundary layer which has become accepted as a valid concept through the efforts of Hama (6-6), Clauser (6-7) and Townsend (6-8). The velocity distribution law of Sandborn (6-4) is written

$$\frac{U}{U_a} = A + B\,(1 - \frac{y}{\delta})^m + C\,(1 - \frac{y}{\delta})^{2n}$$

where U_a and δ have their usual meaning, while A, B, C, m and n are disposable constants. Because of this large number of disposable constants the profile was found to fit practically all known distributions, including the one for laminar boundary layers. For the case of separation Sandborn obtained

$$2n = \infty,\ A = 1, \text{ and } B = -1, \text{ leading to}$$

$$\frac{U}{U_a} = 1 - (1 - \frac{y}{\delta})^m \qquad (6\text{-}1)$$

By introducing the profile parameters

$$\delta^* = \int_o^\infty (1 - \frac{U}{U_a})\,dy \qquad (6\text{-}2)$$

(displacement thickness),

$$\theta = \int_o^\infty (1 - \frac{U}{U_a})\,\frac{U}{U_a}\,dy \qquad (6\text{-}3)$$

(momentum thickness)

and the form parameter $H = \frac{\delta^*}{\theta}$, the exponent m can be eliminated to yield the Sandborn criterium for separating flows:

$$H = 1 + \frac{1}{1 - \frac{\delta^*}{\delta}} \quad .$$

In order to apply this criterium, a special series of experiments was performed at the distance of 12.5 h downstream from the plates. Velocity profiles were taken and the parameters δ , θ , δ^* and H were computed. The results are shown in Figure 6-3 together with all other data points taken during the program on the distorted boundary layer. Two observations stand out clearly:

a. no other data points but the ones taken at $x = 12.5$ h fall anywhere near the curve denoted by the criterium.

b. the data points taken at $x = 12.5$ h fall with surprising accuracy on the curve defining the criterium.

In view of these results, it appears quite obvious that the criterium might serve as a starting point for defining the profile at the downstream stagnation point, and also, the data results prove that Sandborn's distribution law equation (6-1) can be applied to the present data.

The application of equation (6-1) requires the knowledge of two parameters, namely m and δ . They can most conveniently be calculated from the bottom shear τ_o and the momentum thickness θ through the relations

$$\tau_o = \mu \frac{du}{dy} \quad \text{at} \quad y = 0 = \mu \frac{U_a m}{\delta} \qquad (6\text{-}5)$$

and

$$\theta = \delta \frac{m}{(m+1)(2m+1)} \qquad (6\text{-}6)$$

6.23 Calculation of Local Shear Stress

The local shear τ_o has to be found from an empirical relation. It is known that, if the profile parameters are known, then the local shear coefficient

$$C_f = \frac{2 \tau_o}{\rho U_a^2} \qquad (6\text{-}7)$$

can with reasonable accuracy be computed from the Ludwieg-Tillmann formula (see Sandborn and Kline (6-5))

$$C_f = 0.246 \cdot 10^{-0.678H} (Re_\theta)^{-0.268} \qquad (6\text{-}8)$$

when Re_θ = the momentum-thickness Reynolds number $\frac{\theta U_a}{\gamma}$.

The calculated values of C_f from the data of the present study have been plotted against $\frac{x}{h}$ in Figure 6-4. The results indicate that, at least for the sharp-edged plate, the friction coefficient can be approximated by a single curve. Whether the deviation for the 20 fps data from the curve through the 14 fps data is significant remains to be determined. There is good reason to believe that the momentum-thickness Reynolds number might enter as a third variable, in accordance with the law of resistance for the flat plate. (Schlichting (6-3) (p. 540)).

6.24 Calculation of Momentum Thickness

For determining the momentum thickness, use can be made of momentum considerations for the simplified case of two dimensional flow with zero pressure gradient.

It has been shown before that excluding a region extending slightly beyond the fixed eddy behind the plate, the pressure along the floor is essentially constant. For the case where the turbulence does not contribute any significant amount to the momentum flux and the pressure is constant at the vertical sections which denoted the control volume (see Fig. 6-1), the drag difference D between the two vertical sections is given by

$$\rho U_a^2 (\theta_2 - \theta_1) = D \qquad (6\text{-}9)$$

where θ_1 and θ_2 are the momentum thicknesses at the upstream and downstream vertical control surfaces respectively (Schlichting (6-3) (p. 161)). The drag between the two vertical sections is given by the drag on the plate and the drag on the floor.

In the standing eddy zone, a floor drag exists in the opposite direction of the floor drag in the boundary layer. It is canceled out to some extent by the drag in the redeveloping boundary layer. The distance at which these two portions are equal can be found by the use of equation (6-9), assuming a floor drag of zero. Then equation (6-9) becomes, after division by ρU_a^2

$$\theta_2 - \frac{1}{2} C_D h = \theta_{10} \tag{6-10}$$

where θ_2 is the measured momentum thickness, C_D is the drag coefficient of the wall (as determined experimentally by integrating the pressure over the whole wall and dividing by $\frac{1}{2} \rho U_a^2$), and θ_{10} is the momentum thickness of the undisturbed boundary layer at the location of the wall. The data are plotted in Figure 6-5, and it is clear that equation (6-10) is satisfied for all plate heights at about $\frac{x}{h} = 30$.

To find the momentum thickness at other stations, the wall drag has to be considered so that

$$\theta_2 - \frac{1}{2} C_D h = \theta_{10} + \int_{x_1}^{x_2 \text{ at } \frac{x}{h} = 30} C_f \, d_x \tag{6-11}$$

For C_f , Figure 6-4 should be used for $\frac{x}{h} < 50$, while for $\frac{x}{h} > 50$ the wall friction for the undisturbed boundary layer can be used. The result should be a θ_2 curve which, for each h , lies parallel to the curve for $h = 0$ downstream from $\frac{x}{h} = 50$. There is however, too much scatter of the data to show this trend in Figure 6-5. But there exists no doubt that the momentum thickness can be calculated from equation (6-11). However, the momentum thickness at the reattachment point can only be calculated if the pressure also is known, and for the present, this is not the case.

If the momentum thickness can be predicted, then another profile parameter, the displacement thickness δ^* can also be computed, for as shown in Figure 6-6, a unique relationship appears to exist, for the given plate heights, between the shape parameter H and the non-dimensional distance from the disturbing plate $\frac{x}{h}$.

6.25 Velocity Profiles Downstream from the Point of Reattachment

In the absence of a general theory on reattached flows, a search was made of similarity parameters for the velocity-distribution laws. The non-dimensionalized profiles for all plate heights have been plotted in Figures 6-7, 6-8, 6-9 and 6-10. Semi-logarithmic paper was used in order to facilitate detection of a logarithmic distribution law.

The outstanding observation is that the profile does appear to exhibit similarity in the upper portion for all stations. The similarity profile for this portion can be expressed by a form of the defect law:

$$\frac{u - u_a}{u_a} = A \log \frac{y}{\delta}$$

where A does not appear to be constant but rather depends on the plate. A correlation was empirically found for A as function of $\frac{h}{\delta}$, as shown in Figure 6-11.

The profiles in the lower portion are, over the observed region, curves of about constant slope for all data, but with an intercept depending on the distance from the plate. No conclusions could be reached on the functional form of the intercepts.

6.26 Turbulence Downstream from Stagnation Point

The large gradients in velocity near the leading edge of the disturbing plate generate a high intensity of local turbulence which is spread out downstream and tends to decrease the difference between lower and upper layer of the boundary layer. The result is that the transition between the two layers becomes more gradual with increasing distance downstream from the disturbing wall. Measurements of turbulent intensity have been made in order to demonstrate this process. The results of the measurements of intensity profiles are shown in Figures 6-12 to 6-15. These profiles have a number of interesting features. They show that a large intensity turbulence remains from the plate distortion even at large distances downstream. In fact, integration of the intensity over the whole profile has shown that this integral which represents an essential part of the total turbulent energy in the boundary layer, does not change with distance in a noticeable way - indicating that the decay of the turbulence generated by the plate is very slow indeed.

Another observation of interest is the fact that the turbulent intensity has a tendency to become uniform - and a study of the data by Arie and Rouse (6-1) indicate that this might be true also for the fluctuations in the vertical direction. Thus, over a substantial part of the turbulent boundary layer the turbulence field can be approximated by a field of homogeneous turbulence with a velocity gradient.

The spread of the zone of homogeneous turbulence was determined by defining the upper edge of the spread to be where the turbulence intensity has dropped to 90 percent of its maximum value in the homogeneous zone. (The turbulence very near the wall was thereby not considered, since this represents the effect of the boundary on the turbulence). The spread was found to be essentially linear with distance as shown in Figure 6-16.

The contribution of the turbulence to the momentum thickness is given by the integral

$$\theta_{turb} = \int_0^{\delta} \frac{\overline{u'^2} - \overline{v'^2}}{u_a^2} \, dy \qquad (6\text{-}13)$$

This quantity could not be determined since only $\overline{u'^2}$ was measured. However, since $\overline{v'^2}$ can only be positive, ignoring it will make θ_{turb} too large than actual. It was found that the ratio θ_{turb}/θ was at most of the order of 5 percent, so that no large errors were introduced in ignoring it in calculating the momentum thickness.

For a number of points on each vertical profile the spectrum of intensity was taken, for which an example is given in Figure 6-17. It appeared that the spectra were similar for all points within the region of constant intensity, while they deviated noticeably in other parts of the vertical profile.

6.3 The Diffusion Far Downstream From the Disturbing Plate

The concentration measurements for this part of the study were performed in the open-circuit wind tunnel. They were correlated in an entirely empirical manner by attempting to express the concentration profiles through suitable similarity profiles. This "search for similarity profiles" was guided by the findings of Chapter 3, according to which it can be expected well that the data might obey the laws for the transition and final zones.

The similarity parameters are the plume width λ and the ground concentration C_{max}.

6.31 The Plume Width

The plume width λ is equal to the distance from the wall of the point where the concentration c has dropped to half the maximum. It was plotted in Figure 6-18 as function of the distance from the source, with the wall height h as third variable. This double logarithmic plot indicates the following:

a. The rate of spread follows approximately the same law for all plates, including $h = 0$, over the distances considered. A region immediately downstream from the plate has to be excluded where λ varies at a smaller rate than further downstream. To a first approximation the limit between the two zones is given by $x/h \approx 50$. For the region downstream from $\frac{x}{h} = 50$ the value of λ increases with $x^{0.63}$.

b. The spacing of the lines of the decrease of λ show a systematic trend. It is clear that, at least within the distances considered, parallel lines imply much faster mixing for the high plate than for the low plate, which can be attributed to the higher turbulence level generated at the edge of the large plate. Therefore, attempts were made to relate the spread λ to a length parameter depending on the turbulence. Since this parameter should be of an average nature rather than of local significance, the length

$$\theta_{u'} = \int_0^{\delta} \frac{\overline{u'^2}}{u_a^2}\, dy$$

where the length $\theta_{u'}$ denotes the contribution of the turbulent fluctuations in the flow direction to the turbulent portion of the momentum thickness. The ratio

$$\frac{\theta_{u'}}{\theta_{u'_o}} = \overline{\theta}$$

was plotted versus the ratio $\lambda/\lambda_o = \overline{\lambda}$ where the subscript o refers to the case of the <u>smooth</u> <u>flat</u> plate without disturbance. The results are shown in Figure 6-19, from which can be seen that $\overline{\lambda}$ is equal to $\overline{\theta}$. This indicates that in a distorted boundary layer the diffusion depends mostly on the existing turbulence. In general it is suggested that the spread of the diffusion cloud can be expressed by an equation of the form

$$\lambda = C \cdot x^s$$

where s is the exponent determined by the Lagrangian similarity hypothesis according to Chapter 4 (which has to be modified to account for the different velocity distribution of this case), and C is a coefficient depending on the turbulence.

A critical experiment for the validity of these conclusions might consist of a diffusion experiment using a ground source discharging into a boundary layer with a high and controlled turbulence level superimposed.

The results found in Chapter 3 for the intermediate and for the final zone are compared with the data of this phase of the study. The ratio λ/δ , with δ being taken from the open-circuit wind tunnel data, has been written at each data point of Figure 6-18. It is seen that the final zone is reached with $\lambda/\delta \approx 0.64$, as in Chapter 3, while all other data fall into the intermediate zone. No value λ/δ exceeds the value of 0.67 significantly, thus confirming the consistency of λ/δ in the final zone of Chapter 3 for this phase also.

6.32 The Maximum Concentration

The maximum ground concentration represents the second similarity parameter for the concentration profiles. However, instead of c_{max} the product $c_{max} \cdot u_a$ has been plotted in Figure 6-20. This should be, for a given source strength, G , a well defined parameter, as explained in 3.32. The results for the open circuit where the velocity was varied but the source strength was kept constant, is shown in Figure 6-20 and does in fact confirm the uniqueness of the relationship for $u_a = 5$ and 9 fps.

For variation of source - wall distance, an effective source location can be defined as located at the position of the wall; for the given velocity of 9 fps the results are shown in Figure 6-20. With the exception of the distance of 4.5 ft, all data plot well on a common curve. The deviation of the data for 4.5 ft might be due to the fact, that the profile was already well established upstream of the wall, so that only the lower portion of the concentration profile was affected by the wall disturbance.

No attempts were made to check out the Lagrangian similarity hypothesis for these data, as presented in Chapter 4, since the velocity distribution is quite different from a similarity law of logarithmic form as was used in Chapter 4.

6.33 The Profile Shape

The concentration profiles obtained during this part of the study are shown in Figures 6-21 to 6-30. They all can be represented in the form

$$\frac{c}{c_{max}} = e^{-\ln 2 \left(\frac{y}{\lambda}\right)^{\alpha}}$$

where α is an exponent to be determined, λ is the elevation at which $c = 1/2\, c_{max}$, and c_{max} is the maximum concentration.

In order to determine profile parameters, the profiles were calculated by using Equation 6-14 and, by assuming c_{max} as given by the data, the best fitting curve was obtained with the parameters λ and α disposable. The best fit was obtained through taking the double logarithm of both sides and minimizing the square of the logarithmic deviations by means of a digital computer. The final results require careful interpretation since the logarithmic deviation places uneven emphasis on different parts of the curve.

The results of the computations are shown in Table 6-1 . The values of α , while fluctuating very strongly, nevertheless decrease quite noticeably with distance from the plate. A plot of x versus α is given in Figure 6-31 . It appears that the value of $\alpha = 1.4$ to 1.6 represents an asymptotic limit to the distribution, while it is quite likely that near the plate the value α is approximately 1.8 to 2.0, in agreement with the values found for the smooth flat plate (see Ch. 3).

The dimensionless concentration profiles for the intermediate zone are shown in Figure 6-32 , the profiles for the final zone in Figure 6-33 . The plots show that a similarity profile exists for each zone.

6.4 Conclusions

For a flat-plate boundary layer which is disturbed by a sharp edged, two-dimensional wall a flow field exists downstream from the wall which is largely governed by the drag coefficient of the wall. It is found that approximate similarity profiles of the mean velocity field is obtained at a distance of about $\frac{x}{h} \approx 50$ downstream from the wall with a profile, however, which appears to be different from the profiles in the undisturbed boundary layer. Within the distances considered, the integrated turbulent energy did not markedly decay; instead, the local maxima were reduced with distance but were accompanied by a wider spread of the high-intensity field.

The high-turbulence level causes a much faster spread of a diffusing cloud originating from a two-dimensional line source at ground level. The ratio of the spread of the diffusion plume for the wall cases to the spread of the plume for the smooth-plate boundary layer is equal to the ratio of the respective turbulent contributions to the momentum thickness.

The similarity parameters and concentration distribution laws appear to obey the laws for the different zones of Chapter 3, however, the Lagrangian Similarity Hypothesis as used in Chapter 4 is not directly applicable.

6.5 Nomenclature

Symbols	Definition
h ,	height of plate vertical above datum plane;
u_a ,	velocity of ambient air;
u ,	local velocity;
x ,	distance from source;
δ ,	boundary-layer thickness;
A ,	disposable constants in Sandborn's velocity distribution law;
B ,	disposable constants in Sandborn's velocity distribution law;
C ,	disposable constants in Sandborn's velocity distribution law;
m ,	disposable constants in Sandborn's velocity distribution law;
n ,	disposable constants in Sandborn's velocity distribution law;
δ^* ,	displacement thickness;
θ ,	momentum thickness;
H ,	form parameter $= \frac{\delta^*}{\theta}$;
τ_o ,	boundary shear;
μ ,	dynamic viscosity;
C_f ,	local shear coefficient;
ρ ,	density of air;
$\frac{u_a\theta}{\nu}$,	momentum thickness Reynolds number;
D ,	drag difference;
C_D ,	drag coefficient;
D_f ,	floor drag;

Symbols	Definition
x_1 ,	station of the stagnation point;
$\theta_{u'}$,	contribution of the longitudinal velocity fluctuations to the momentum thickness;
α ,	exponent in similarity law of concentration;
λ ,	elevation at which $c = 1/2\ c_{max}$;
c_{max},	maximum concentration;
c ,	local concentration;

7. SUMMARY AND CONCLUSIONS

The report is concerned with four different aspects of the diffusion problem and their applications to field use.

The first problem is presented and analyzed in Chapter 3. It concerns the diffusion from a ground level line source into the turbulent boundary layer along a smooth flat plate - or along a smooth portion of the earth's surface. Since a theoretical solution for the concentration distribution was not obtainable, experimental results were used throughout to draw conclusions.

For a detailed investigation of the concentration field the field was divided into four zones, according to the predominance of terms in the diffusion equation. The zone near the source was excluded from the study, and for the other regions the diffusion equation becomes

$$u \frac{\partial c}{\partial x} + v \frac{\partial c}{\partial y} = \frac{\partial}{\partial y} \left(k \frac{\partial c}{\partial y} - \overline{v'c'}\right)$$

where generally the molecular diffusion term $k\frac{\partial c}{\partial y}$ can be ignored. By assuming appropriate similarity laws for both the distributions of velocity and concentrations - which had to be found experimentally - the distributions of $\overline{v'c'}$ could be determined. For the parameters describing the diffusion cloud it was found that in the intermediate zone, where the rate of change of the plume spread is much larger than that of the boundary layer, the spread of the diffusion cloud depended on the distance from the source only and not on the boundary-layer characteristics. This zone corresponds most closely to the atmospheric surface layer for a ground-level source.

In the final zone, the rate of spread of the diffusion cloud becomes independent of the distance from the source and is governed by the growth of the boundary layer alone, with the plume spread λ proportional to δ ($\lambda = 0.64\ \delta$). The coefficient of proportionality and the shape of the distribution function for the concentration probably depends to some extent on the molecular diffusivity of the tracer gas; however, this dependency is of little significance for practical applications.

The second problem, analyzed in Chapter 4, was concerned with the application of wind-tunnel experiments to field needs. The concept of "Lagrangian Similarity" was expounded. This concept presumes that, in the absence of vertical temperature gradients, a significant length (z_o = roughness height) and a significant velocity (u_* = friction velocity) suffice to describe the whole velocity field, and thus the diffusion process.

With these assumptions it was possible to predict the rate of decay, and also the magnitude, of the ground concentrations. However, in order to compare field and experimental results, it is necessary that the wind-tunnel results be restricted to a ratio of $\lambda/\delta < 0.64$, in agreement with the findings of Chapter 3.

In Chapter 5, data are presented and analyzed, on the diffusion characteristics for flow in and above a model vegetative cover. It was found that a vegetative cover could be modelled, and a distribution function for the velocities inside a crop is given by $\frac{u}{u_h} = f\left(\frac{y}{h}\right)$ where h is a significant crop height and u_h is the velocity at $y = h$. The shape of the function depends on the type of crop. Experimentally, u_h was found to be related to the velocity u_a in the ambient air by $u_h = 0.4\ u_a$. The velocity distribution outside the cover can be represented by a power law of the form

$$\frac{u}{u_a} = \left(\frac{y - h}{\delta - h}\right)^{1/3}$$

in agreement with power-law representations for mean velocities in turbulent boundary layers over rigid rough boundaries. However, similarity of the mean velocity profiles was established only at a distance of between 24h to 30h from the beginning of the crop.

For the concentration distributions the separation into a layer above and a layer inside the canopy was found useful. Inside the canopy, the concentration becomes constant with height at some distance downstream from the source. Outside the cover, the behavior of the concentration distribution in the form

$$\frac{c}{c_{max}} = F\left(\frac{y - h}{\lambda - h}\right)$$

closely followed the same laws as for a smooth boundary (Chapter 3) except for the maximum concentration, which naturally reflected also the concentration change inside the vegetative cover.

The most important conclusions drawn from this part of the study for applications to field problems are the following:

1. There exists a region having a length of 30h from the upwind crop edge in which the velocity cannot be represented by a similarity law. This indicates that in this zone the boundary layer not only responds to the crop below but also to the ground cover upstream from the crop being considered.

2. The vertical spread of the concentration plume is larger in a dense crop than in a sparsely planted crop. Therefore, if it is desired to obtain high concentrations near the ground, the gas or diffusing material should be applied at low wind speeds in the direction where the crops offer low resistance to the flow. It if is desired to spread the gas uniformly over the whole plant height, then it is more advantageous to apply the gas at wind in the direction where the crop offers the largest resistance to flow.

Chapter 6 gives an investigation of the fourth problem, <u>diffusion-field perturbations caused when the boundary layer is distorted by a simple two-dimensional roughness element such as a hedge or solid fence</u>. The flow associated with this problem is a separation flow with reattachment downstream from a standing eddy zone behing the wall. It was found that Sandborn's criterium for separation held reasonably well also at the point of reattachment which was located at a distance of 12.5 times the element height downstream from the wall. The data showed that at a distance of about 50 times the wall height from the wall the ground shear stress and the form parameter H approached again that of the undisturbed boundary layer, while the velocity profile shape never returned to its original form over the distances considered. The main effect of the disturbance was a large increase in turbulent intensities.

For the diffusion in the region downstream from the disturbance it was found that the rate of spread remained constant for all heights of the disturbance, but the magnitude of the spread increased with height of the wall. This was closely related to the turbulence intensity, the non-dimensional ratio of $\overline{\lambda}$ to the non-dimensional turbulence integral length $\overline{\theta}$ remained constant. A proposed expression for the spread λ is of the form

$$\lambda = Cx^{s}$$

where s is an exponent to be determined by the Lagrangian similarity hypothesis, and the coefficient C depends on the turbulence.

For practical applications, the following observations are important. A two-dimensional wall introduces a turbulence level into the flow which persists for very long distances beyond the point at 50h where approximate similarity of the velocity distributions is obtained. This affects the initial spread of the diffusion cloud, but not the rate of spread. The shape of the cloud behaves similar to the cloud formed over a smooth boundary excepting near the disturbance.

APPENDIX A : TABLES

TABLE 5-1. Profile Parameters for Velocity Profiles

$u_a = 10$ fps									
Station**	-4	0	2	6	10	12	14	16	18
δ^*(in.)	1.865	2.301	5.521	7.296	7.252	6.625	7.960	7.993	8.461
θ(in.)	1.320	1.815	1.068	1.874	2.181	2.471	2.700	3.119	3.339
$H = \frac{\delta^*}{\theta}$	1.342	1.317	5.17	3.89	3.33	2.68	2.95	2.56	2.53
u_a(fps)	10.1	10.5	10.0	10.0	10.1	10.2	10.1	10.2	10.0
$u_a = 20$ fps									
Staion**									
δ^*	1.664	.972	4.216	5.468	5.798	6.284	6.808	7.045	7.389
θ	1.304	.814	1.104	1.633	2.107	2.429	2.602	2.346	3.012
H	1.276	1.193	3.91	3.35	2.51	2.59	2.34	2.47	2.44
u	2.5	20.2	20.0	20.2	20.2	20.4	20.2	20.0	20.5
$u_a = 40$ fps									
Station**									
δ^*	1.176	1.352	3.446	4.862	5.256	5.297	5.860	6.270	6.546
θ	.924	1.152	1.395	1.417	2.017	2.167	2.380	2.604	2.644
H	1.273	1.173	2.18	3.29	2.61	2.49	2.46	2.41	2.47
u	40.4	41.0	40.0	40.0	40.4	40.0	40.0	40.4	40.0

** Station in ft from the upstream edge of the plant cover.

TABLE 5-2. Similarity Parameter

(Along the row.)

Sta.	δ	h	h_{av}	H = 0 C_{max}	λ	H = 2 C_{max}	λ	H = 4 C_{max}	λ	H = 8 C_{max}	λ	G. S. C_{max}	λ
				Velocity 10 ft/sec.									
18'	21.5"	6.2"						280	17.0				
16'	20.1"	4.7"	Av.					360	15.0				
14'	18.7"	6.3"	5.70"					370	12.3				
12'	17.3"	5.8						660	11.1				
10'	16.0"	5.5						900	8.4				
6'	13.2"	6.3"											
2'	10.7"	5.2"											
0'	10.2"	0.1"											
				Velocity 20 ft/sec.									
18'	20.3"	4.6"		120	16.0	115	16.4	110	16.3	133	17.6	50	17.00
16'	18.6"	4.7"	Av.	170	14.6	155	14.5	165	14.7	170	15.2	70	14.00
14'	17.3"	4.8"	4.56"	240	11.4	220	11.8	250	11.6	225	13.9	70	12.40
12'	16.0"	4.5"		410	9.1	370	9.6	350	10.5	290	12.1	80	11.70
10'	14.6"	4.2"		840	6.6	740	7.0	640	7.4	450	10.0	90	11.2
6'	12.0"	5.3										150	8.25
2'	9.2"	4.3"										430	3.55
0'	8.0"	0											
				Velocity 40 ft/sec.									
18'	17.9"	4.0"											
16'	16.7"	4.3"	Av.										
14'	15.6"	3.9"	3.92										
12'	14.3"	3.6"											
10'	13.3"	3.8"											
6'	10.8"	4.2											
2'	8.7"	2.3											
0'	8.2"	0											

(Across the row.)

Sta.	δ	h	h_{av}	H = 0 C_{max}	λ	H = 2 C_{max}	λ	H = 4 C_{max}	λ	H = 8 C_{max}	λ	G. S. C_{max}	λ
				Velocity 20 ft/sec.									
16'4"	16.0	2.0		700	3.8"			340	7.7"				
14'8"	15.0	2.05		830	3.1"			370	7.2"				
13'0"				1080	2.9"			450	7.1"				
11'4"				1575	2.8"			570	5.3"				
9'8"				3200	1.8"			640	6.8"				

TABLE 6-1

h	D.S.	U	X	Code	λ	α	C_{max}	UC_{max}	X-DS
1/2"	1.5'	9	3	1222	1.43	1.80	657	5910	
		9	4.5	1232	2.04	1.75	532	4790	
		9	6	1242	2.36	1.75	346	3120	
		9	9	1252	2.47	1.53	309	2780	
		8.7	12	1262	3.64	1.85	263	2290	
		9.2	15	1272	4.15	1.13	229	2110	
1"	1.5	9.5	4.5	2232	2.46	1.40	350	3330	3
		9.4	6	2242	2.95	1.54	290	2730	4.5
					3.18	1.49			
		9	9	52	3.84	1.54	245	2210	7.5
		9.2	12	62	5.11	1.42	178	1640	10.5
		9.4	15	72	4.77	1.29	153	1440	13.5
1-1/2"	1.5	9.7	3	3222	3.36	2.15	518	4510	1.5
		9	4.5	3232	3.34	1.79	357	3220	3
		9	6	3234	4.18	2.11	281	2530	4.5
		9	9	3252	4.62	1.28	224	2020	7.5
		8,8	12	3262	6.00	1.56	179	1580	10.5
2"	1.5	9.0	3	4222	5.08	1.30	458	4120	
		9.4	4.5	4232	5.15	2.03	242	2280	
		8.8	6	4242	5.50	1.40	219	1930	
		8.9	9	4252	6.00	1.18	153	1360	
					6.50	1.44			
		8.9	12	4262	7.85	1.34	123	1100	
		8.9	15	4272	8.64	1.16	120	1070	
1"	9"	9.2	1.5	2211	2.52	4.10	696	6400	0.75
		9	3	2221	2.62	1.74	356	3200	2.25
		9.2	4.5	2231	3.16	1.05	325	2990	3.75
					2.98	0.94			
		9.2	6	2241	3.54	1.25	274	2520	5.25
		9.2	9	2251	4.97	1.55	198	1820	8.25
					4.91	1.30			
1"	2-1/4'	9.0	1.5	2213	0.63	1.9	1282	11620	
		9.0	4.5	2233	2.69	2.00	421	3790	2.25
					2.53	1.74			
		9.0	6	2243	3.20	1.51	316	2840	3.75
		9.0	9	2253	3.98	1.41	240	2160	6.75
		9.2	12	2263	4.43	1.53	191	1760	9.75
		9.2	15	2273	5.46	1.48	145	1340	12.75
1"	4.5'	9.0	9	2254	374	1.40	228	2050	4.5
		9.0	12	2264	4.33	1.48	179	1610	7.5

Table 6-1 continued

h	D.S.	U	X	Code	λ	α	C_{max}	UC_{max}	X-DS
1"	1.5'	5.2	3	2122	2.56	2.65	730	3800	1.5
					3.17	1.65			
		5.3	4.5	2132	2.97	1.30	616	3260	3.0
		5	6	2142	3.48	2.16	502	2510	4.5
		5	9	2152	4.39	1.67	439	2190	7.5
		5.2	12	2162	4.81	1.61	360	1870	10.5
		5.2	15	2172	5.00	1.704	282	1470	13.5
					4.19	1.29			
1"	1.5'	14	3	2322	2.51	2.16	393	5600	1.5
		14	4.5	32	2.92	1.57	306	4270	3.0
		13.8	6	42	2.60	1.28	215	2960	4.5
		13.8	9	52	3.64	1.42	190	2620	7.5
		13.8	12	62	4.68	1.40	133	1830	10.5

APPENDIX B : FIGURES

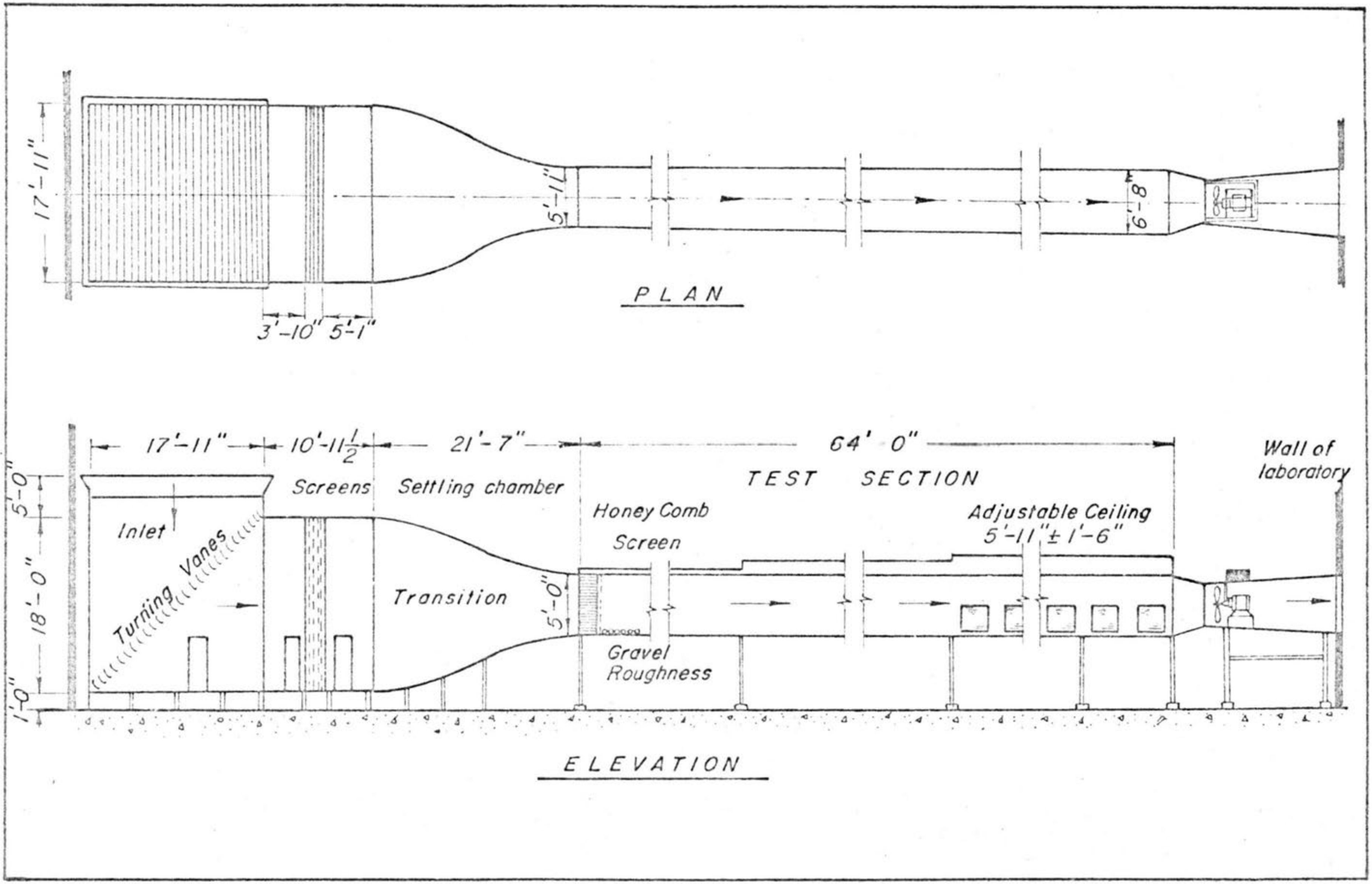

FIG. 2-1 OPEN CIRCUIT TUNNEL

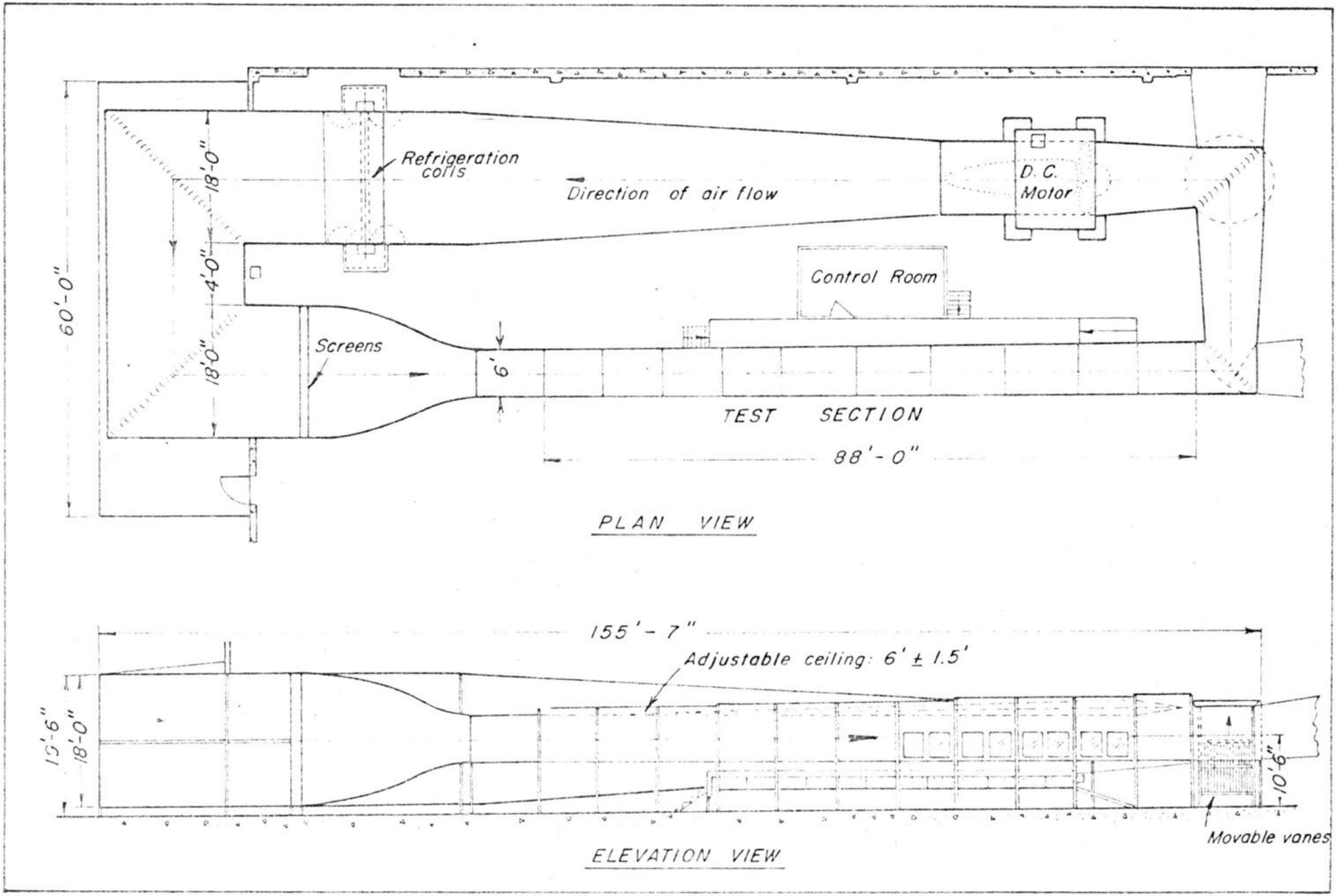

FIG. 2-2 LARGE WIND TUNNEL

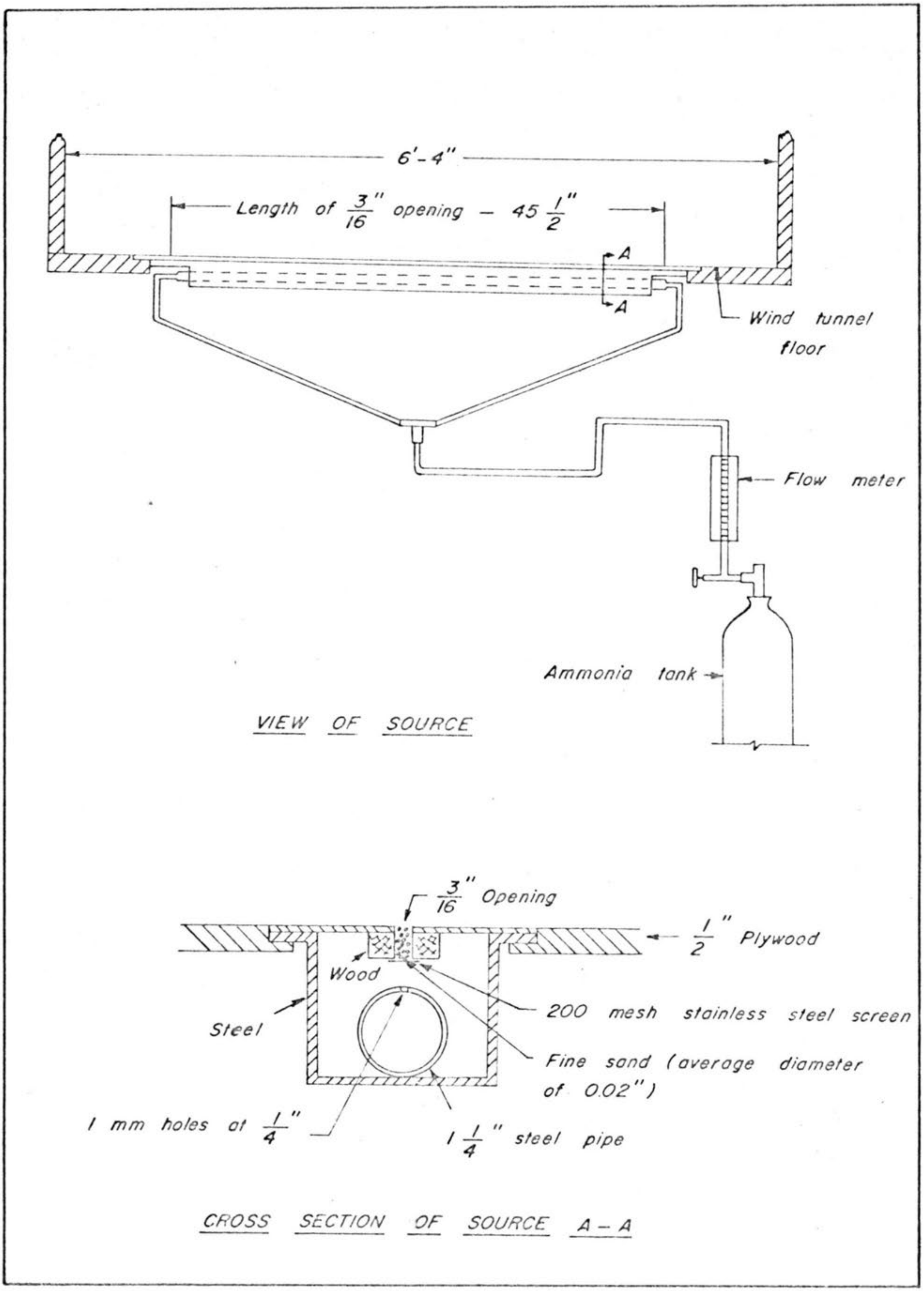

FIG. 2-3 GROUND SOURCE

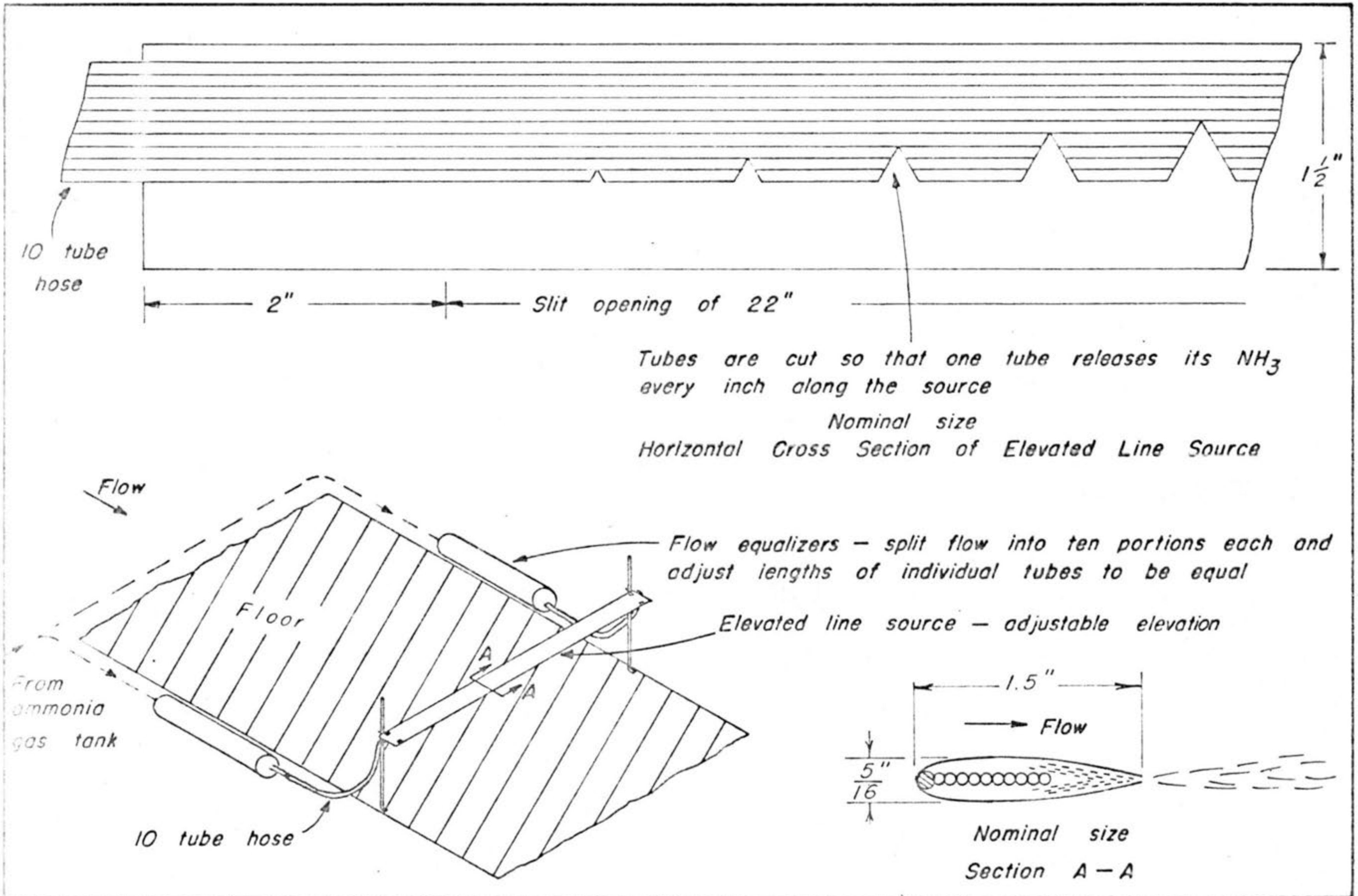

FIG. 2-4 · ELEVATED SOURCE

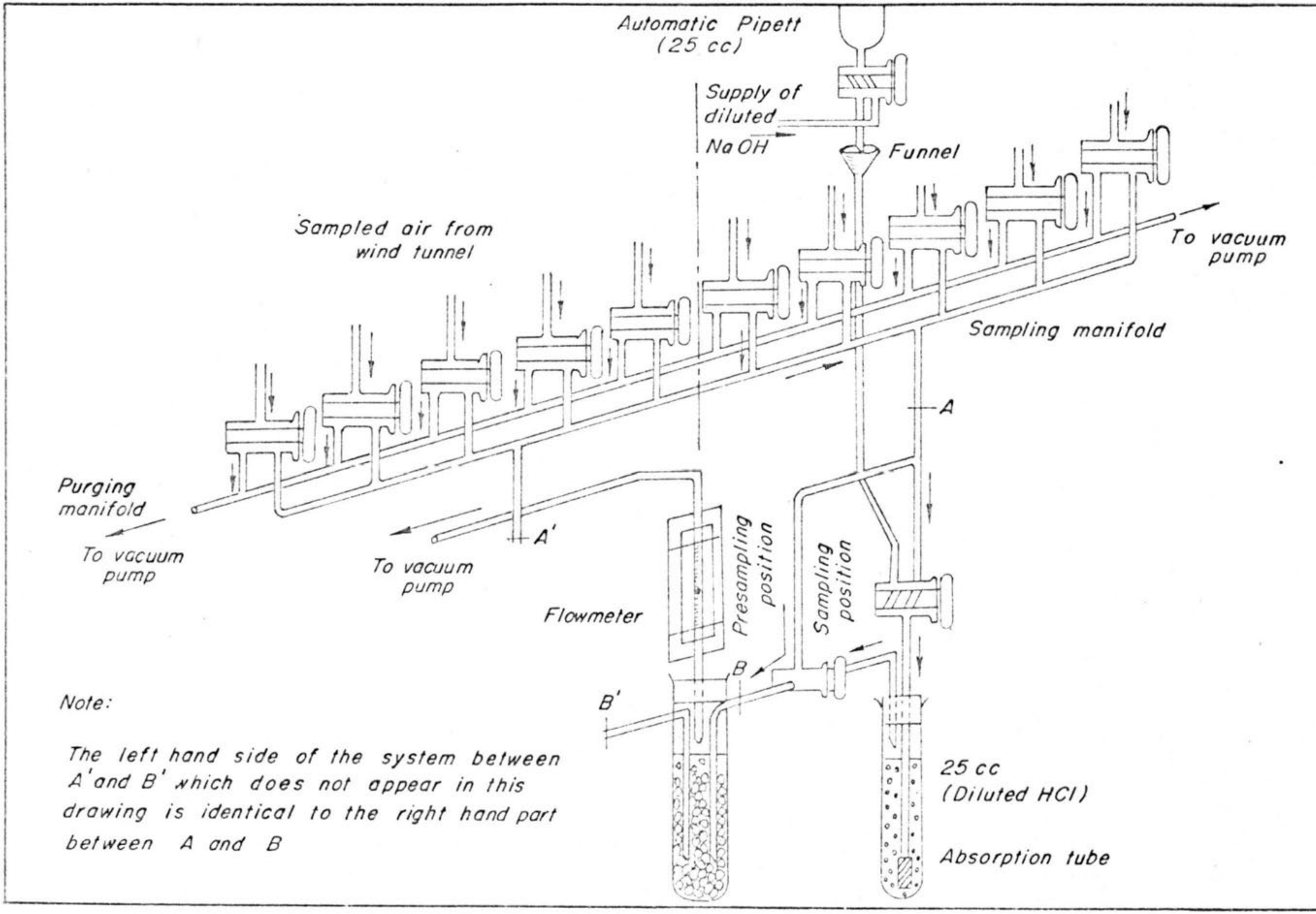

FIG. 2-5a SAMPLING SYSTEM

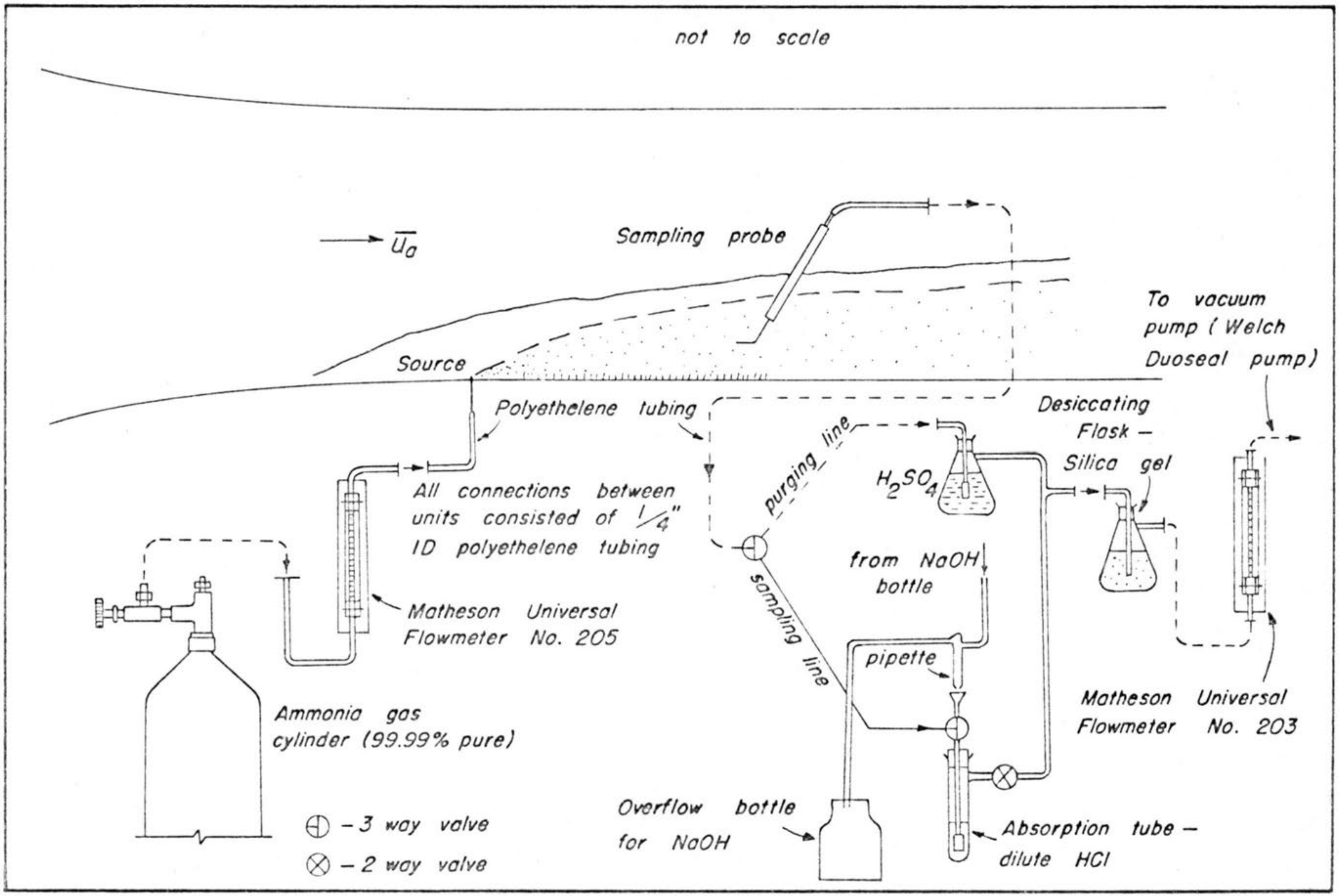

FIG. 2-5b FEED AND SAMPLING SYSTEM : SINGLE PROBE

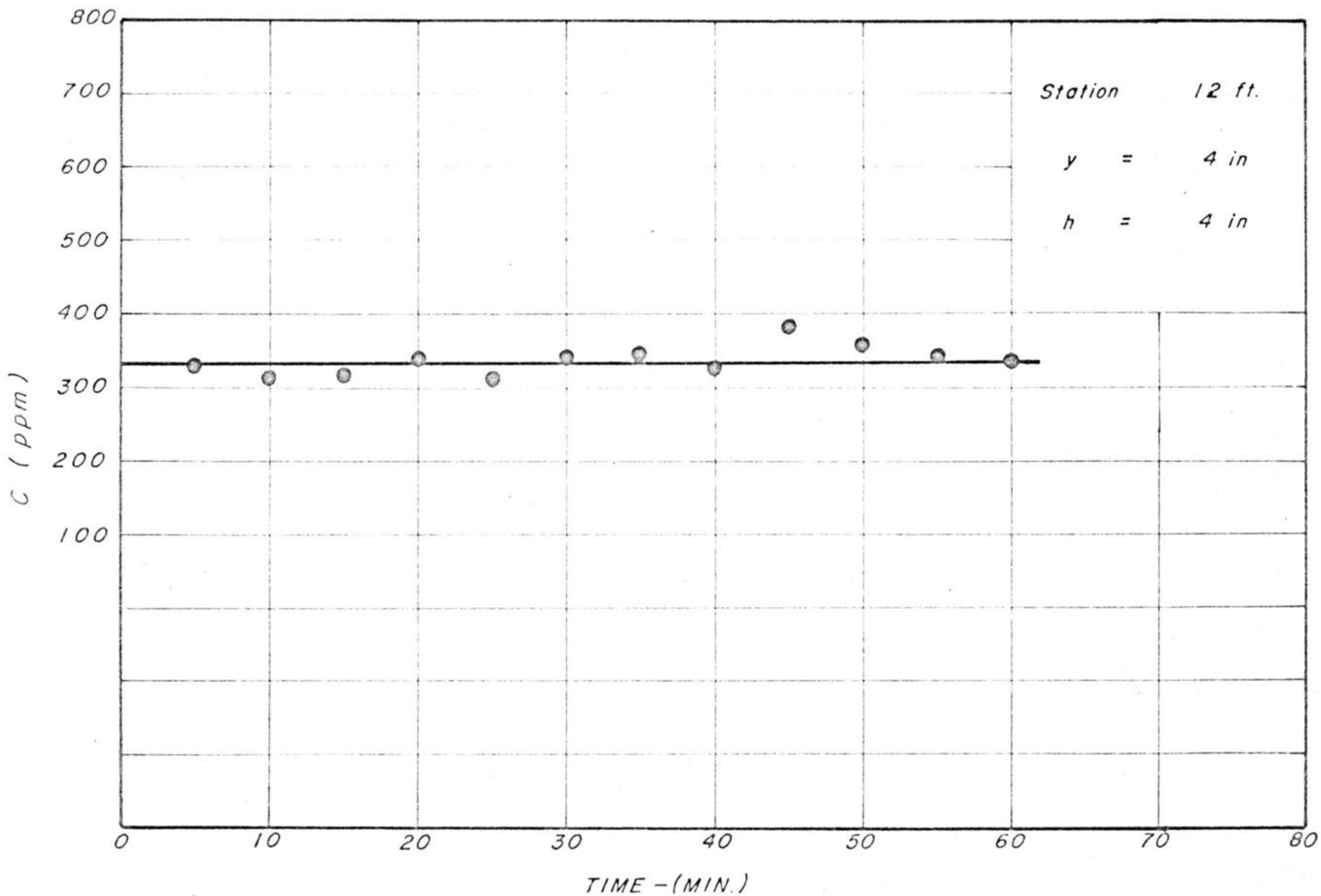

FIG. 2-6 STABILITY OF READING OF CONCENTRATION

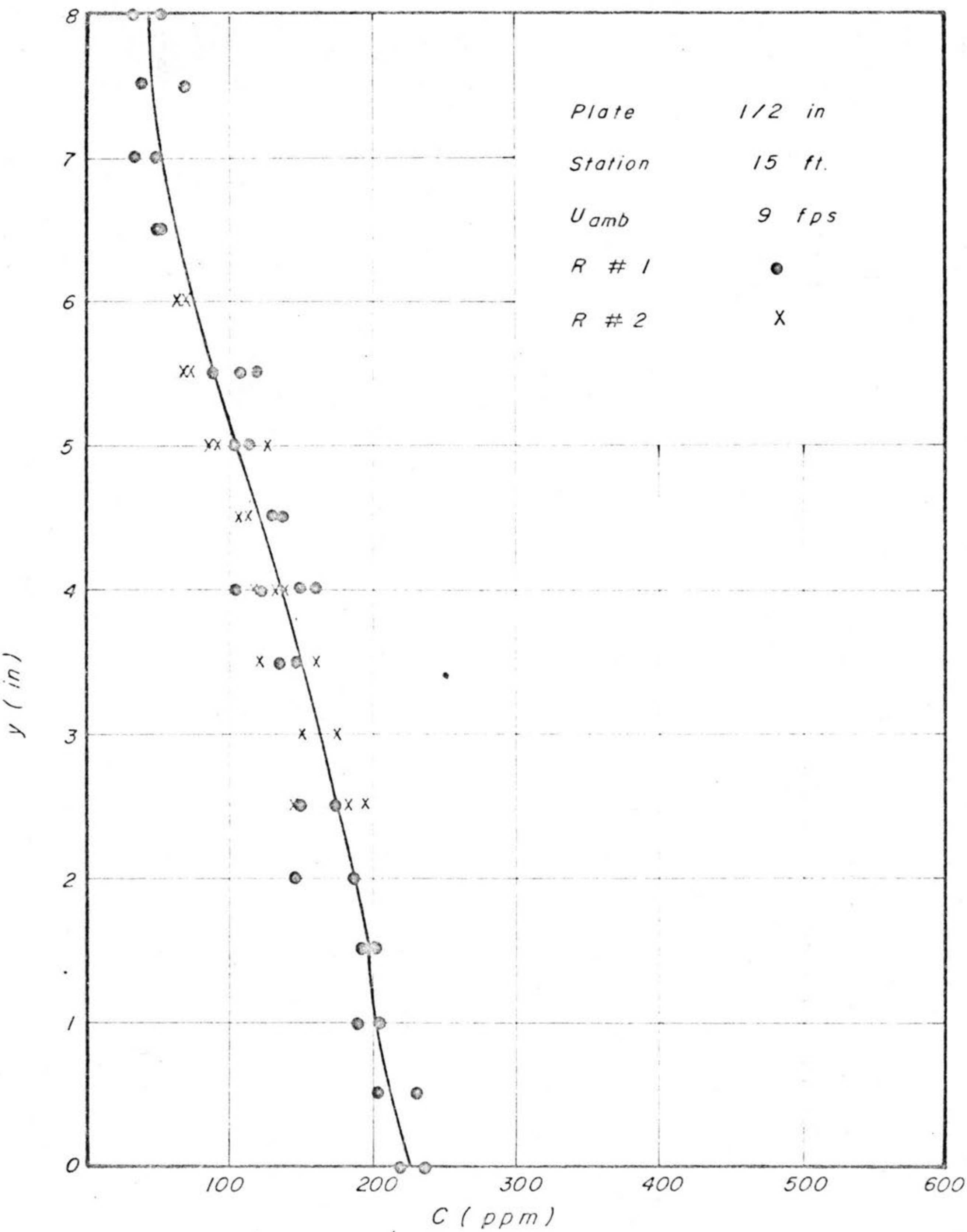

FIG. 2 - 7 TYPICAL CONCENTRATION PROFILE

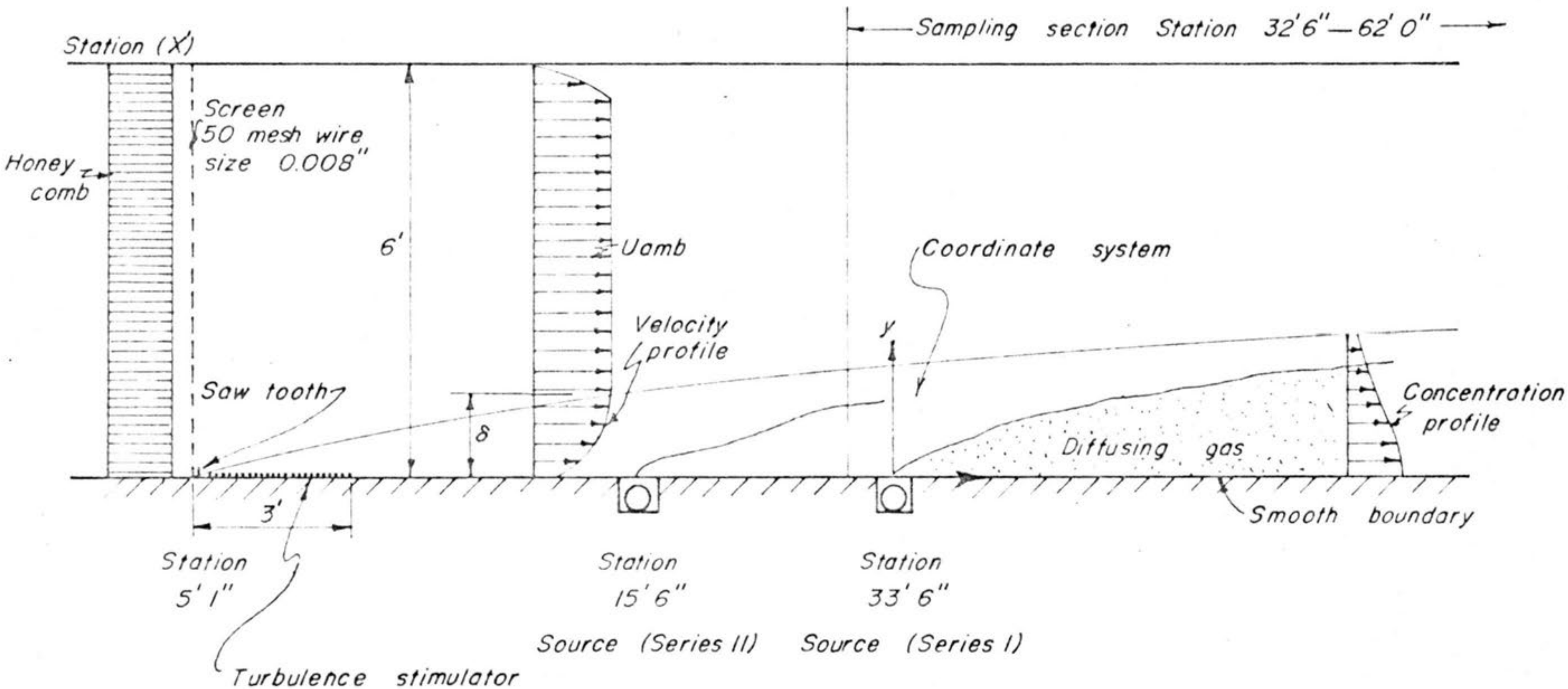

FIG. 3-1 TEST SECTION GEOMETRY

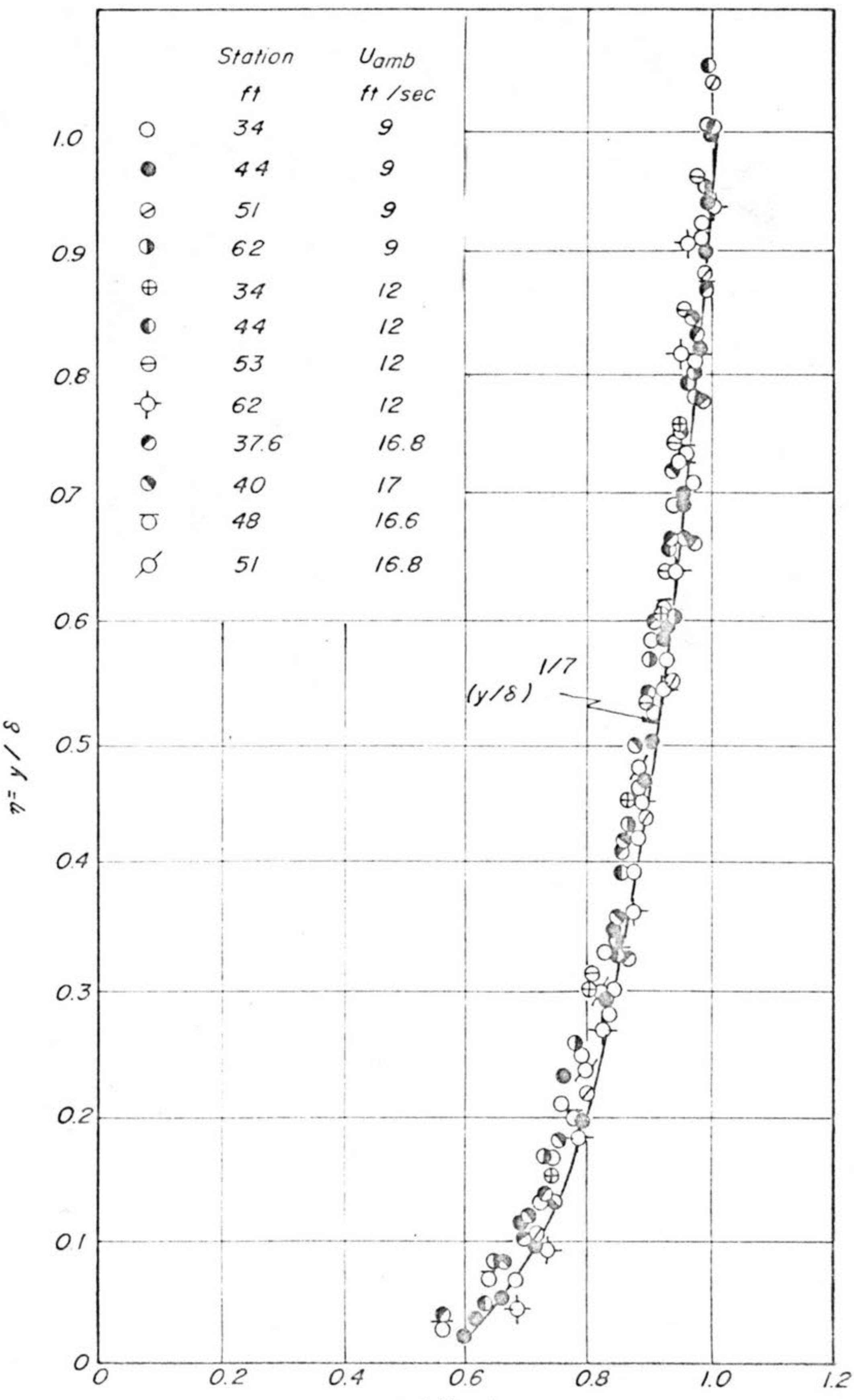

FIG. 3-2 UNIVERSAL VELOCITY PROFILE

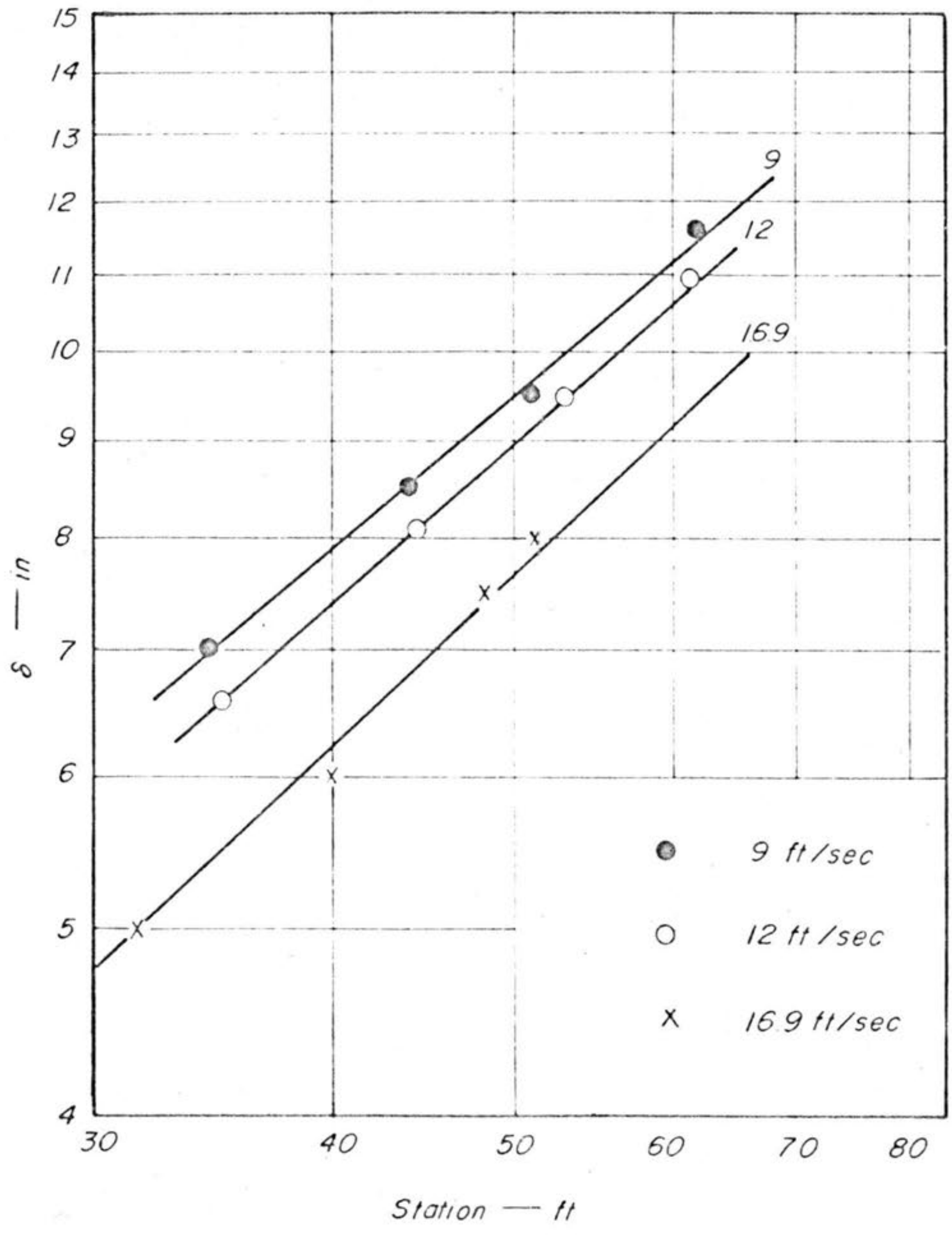

FIG. 3-3 VARIATION OF BOUNDARY LAYER THICKNESS

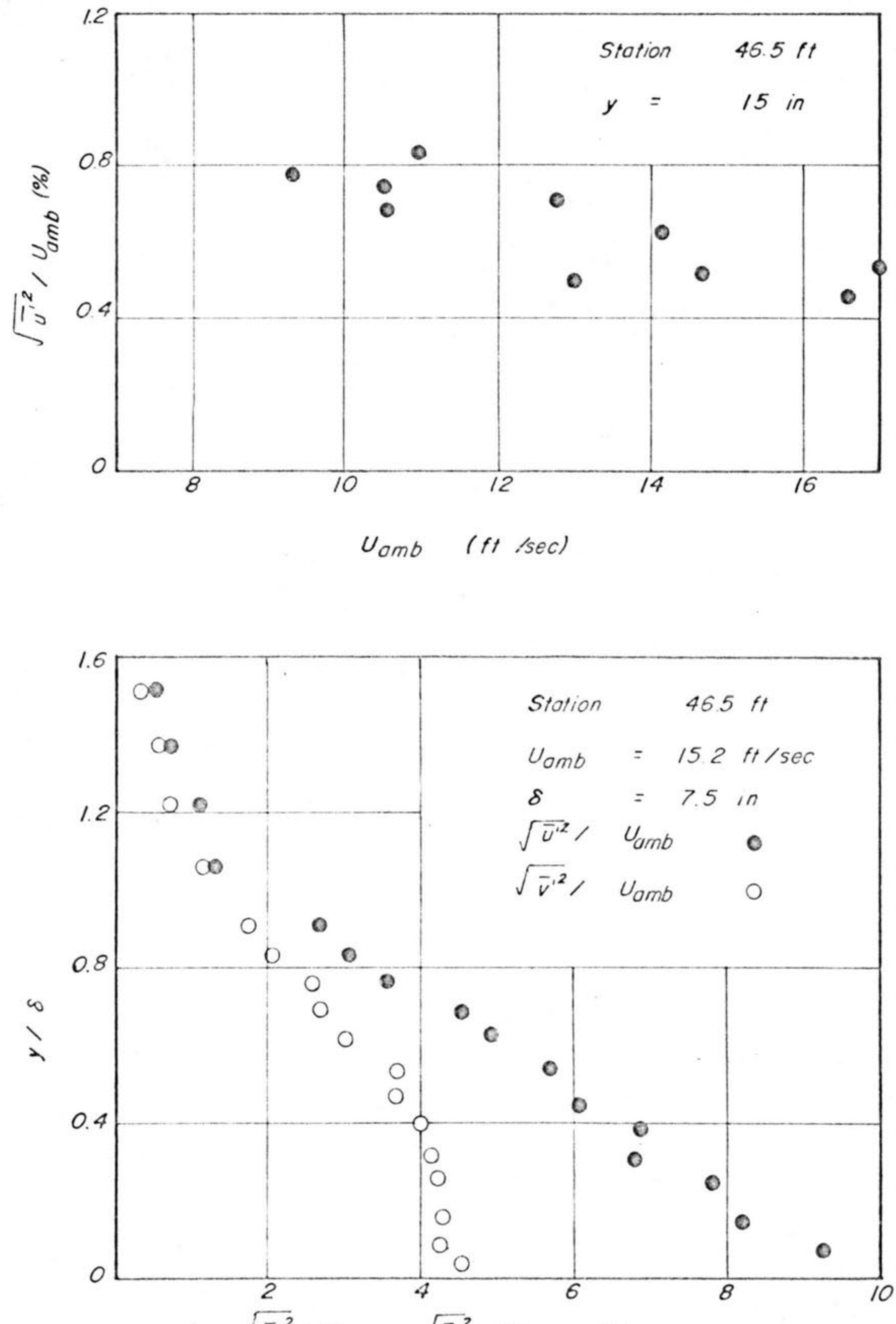

FIG. 3-4 TURBULENCE MEASUREMENT

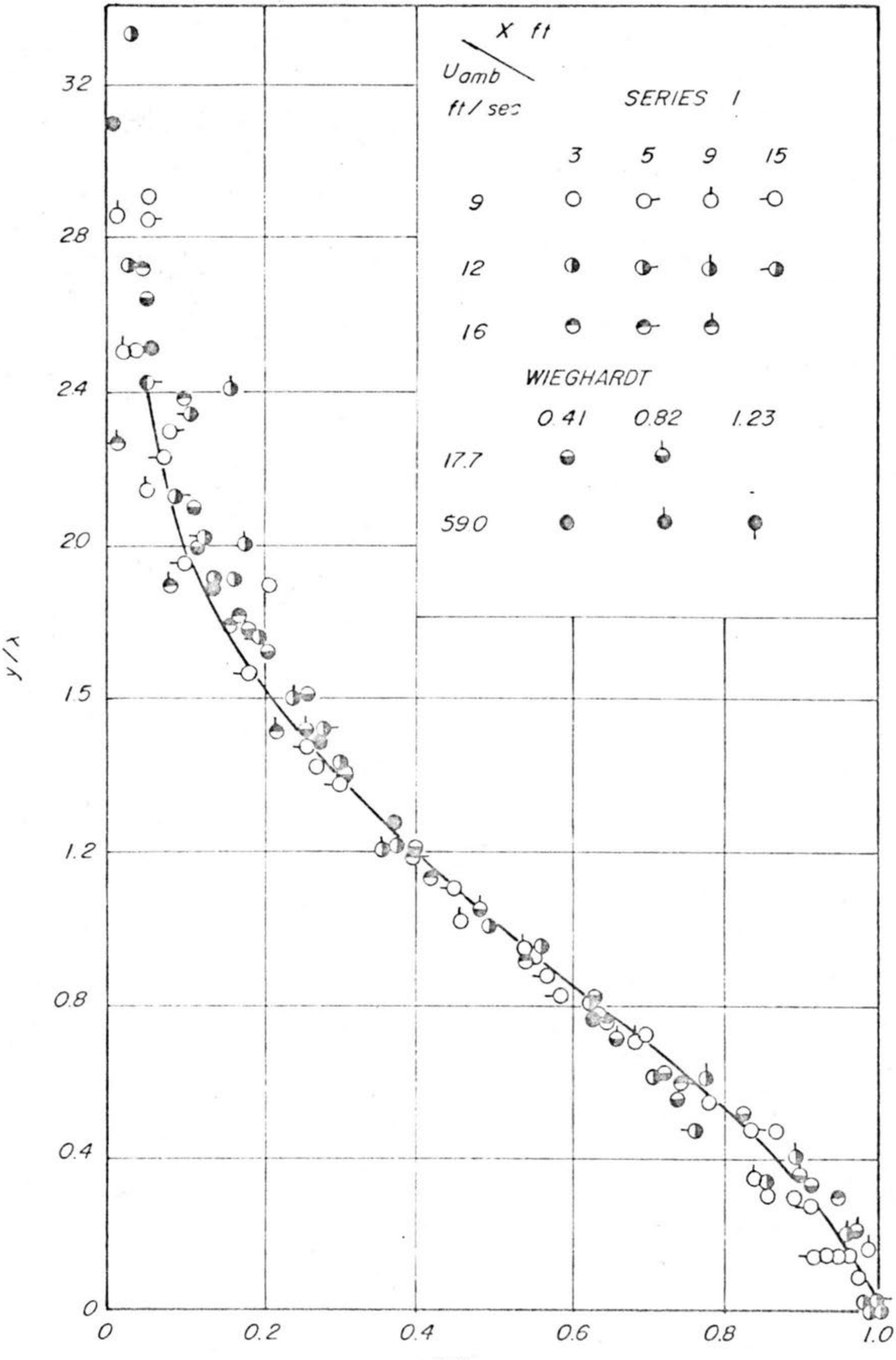

FIG. 3-5 c/C_{max} VS. y/λ IN THE INTERMEDIATE ZONE

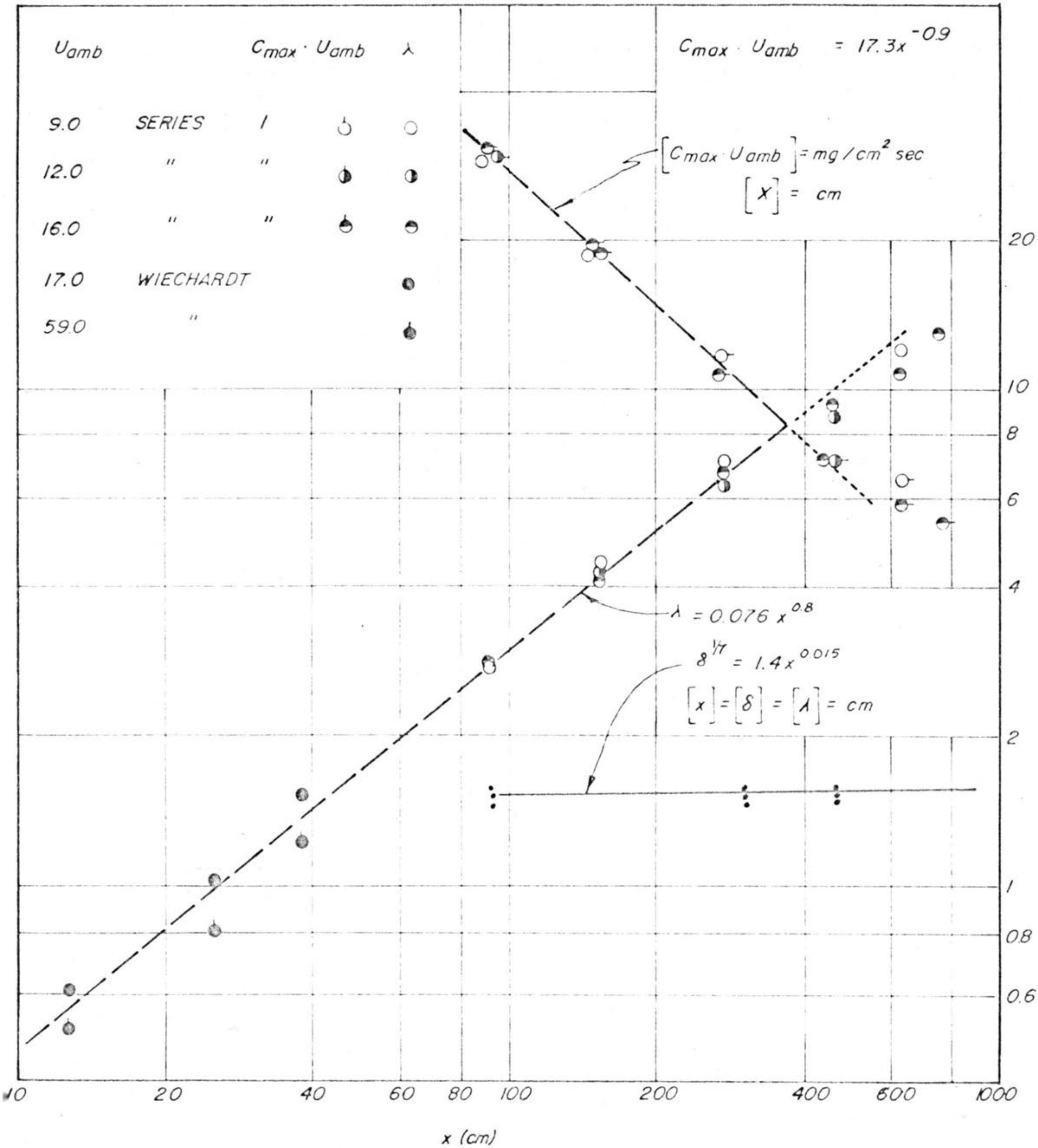

FIG. 3-6 VARIATION OF λ AND $U_{amb}C_{max}$ IN THE INTERMEDIATE ZONE

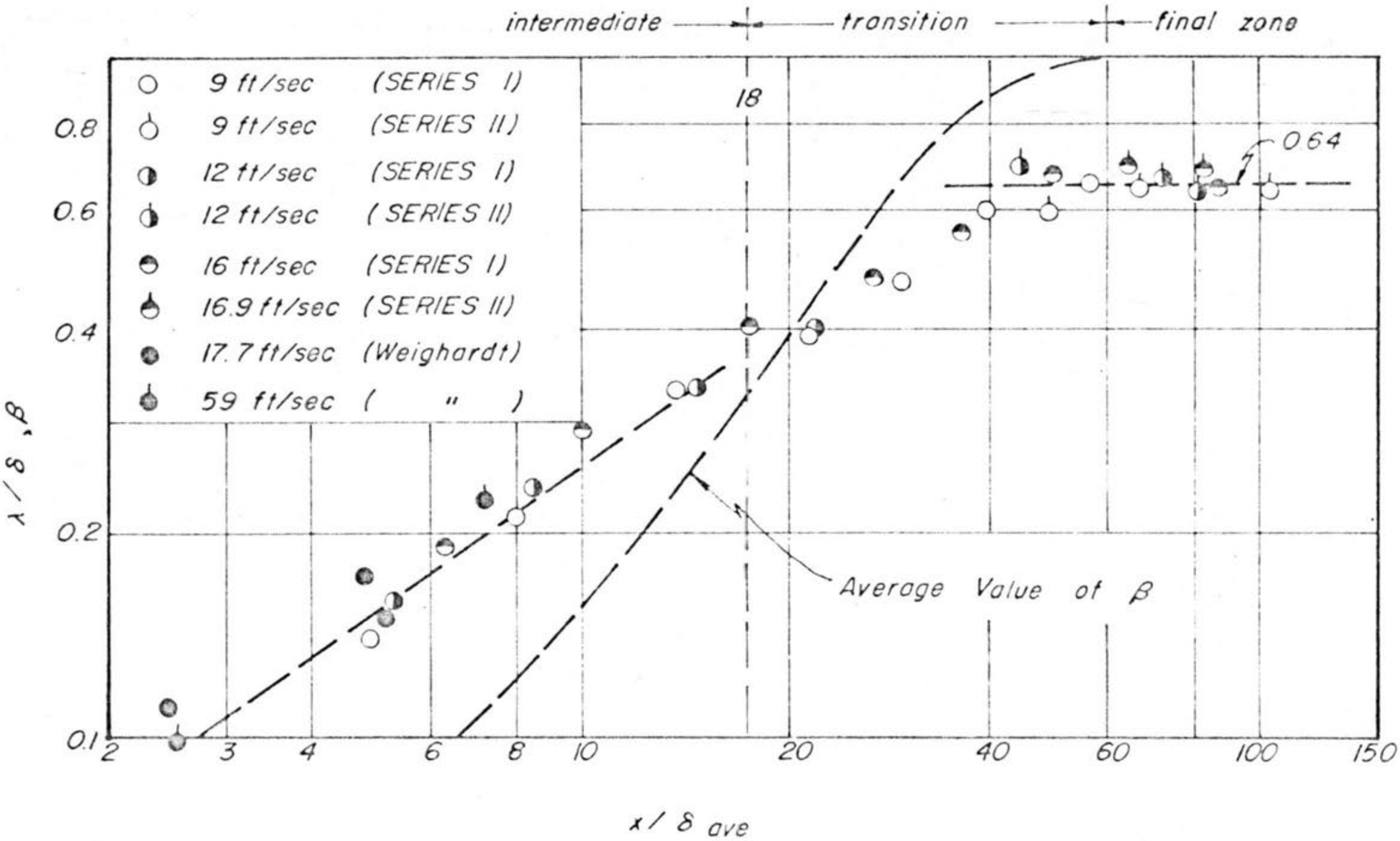

FIG. 3-7 THE VARIATION OF λ/δ AND β WITH X/δ_{ave}

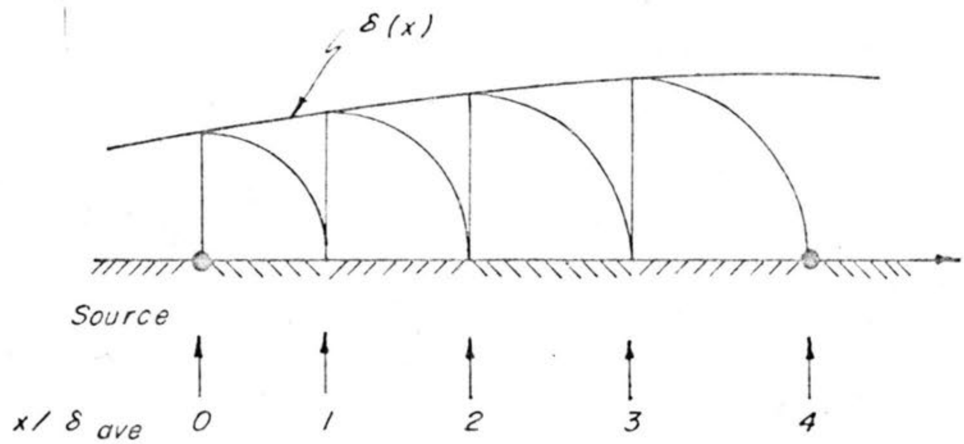

FIG. 3-8 DETERMINATION OF X/δ_{ave}

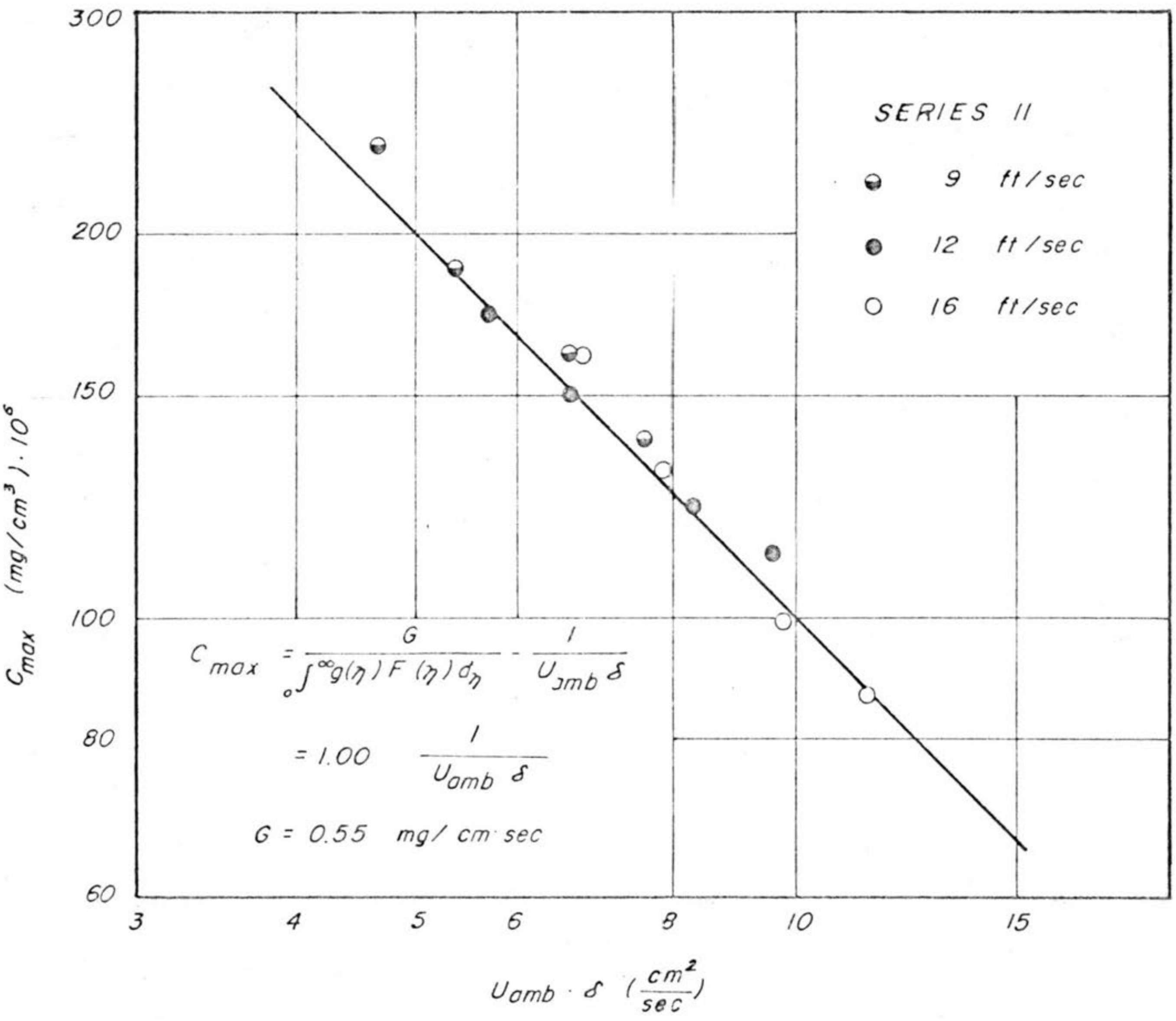

FIG. 3-9 THE VARIATION OF C_{max} VS. $U_{amb}\delta$ IN THE FINAL ZONE

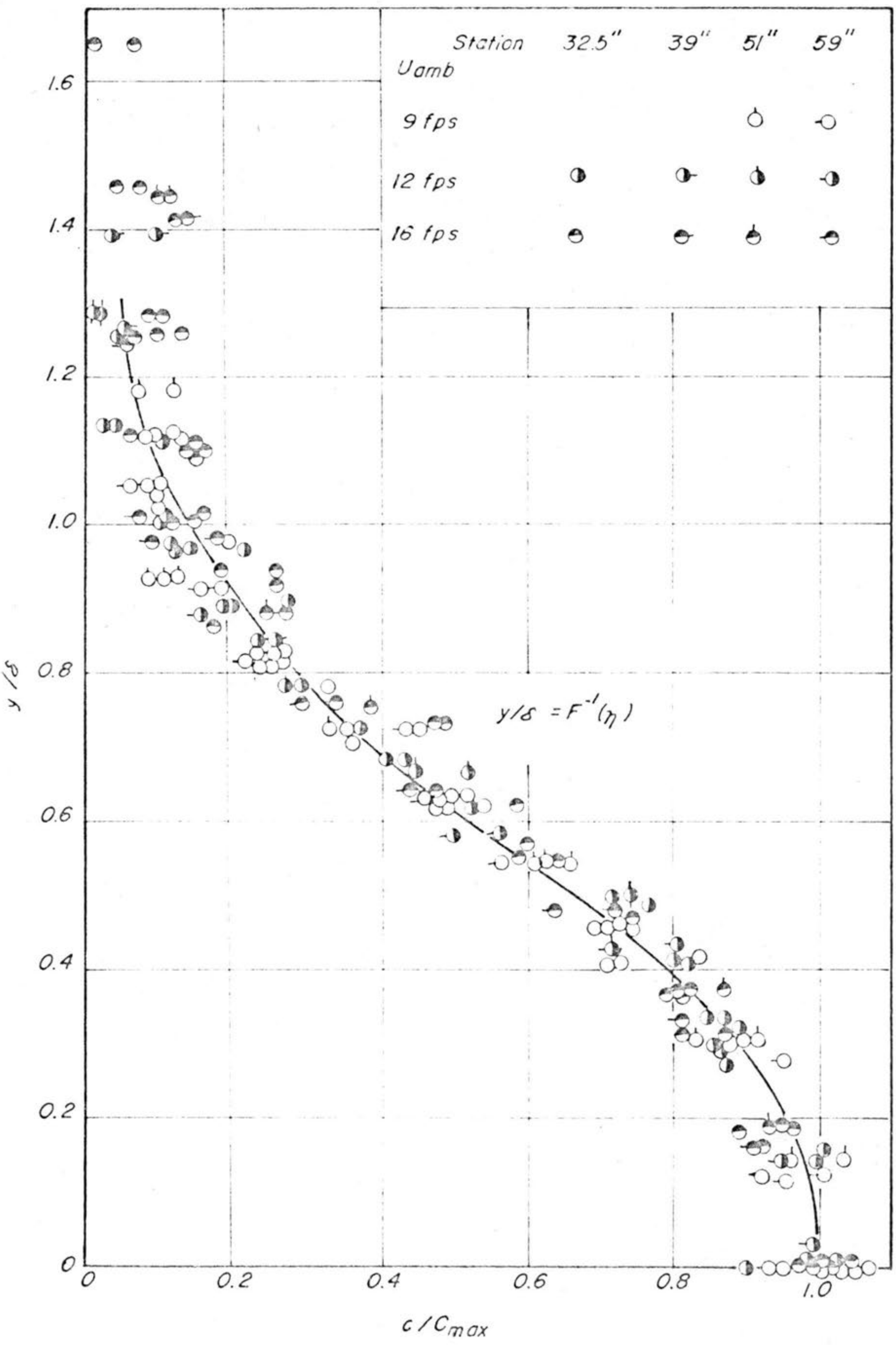

FIG. 3-10 c/C_{max} VS. y/δ IN FINAL ZONE

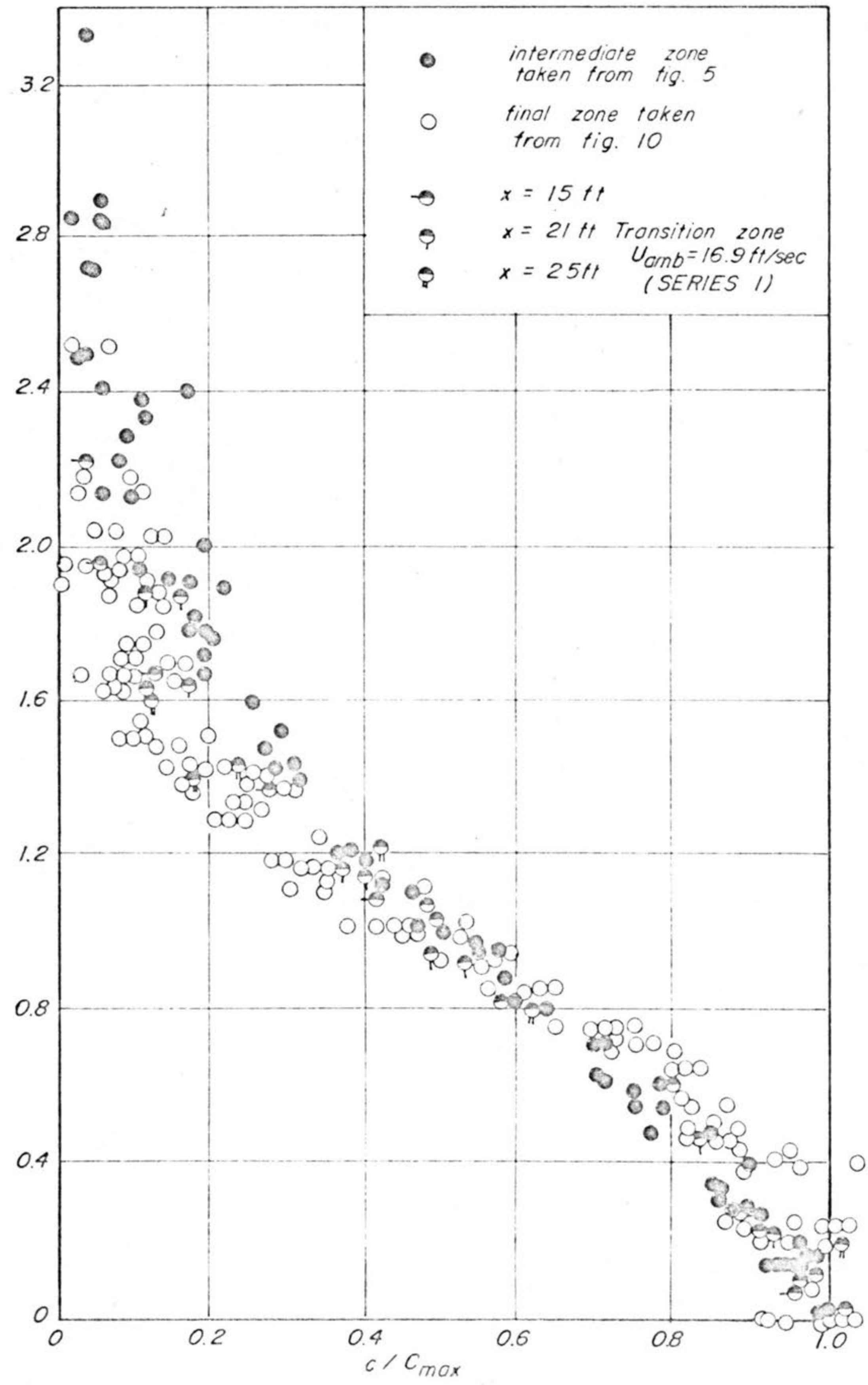

FIG. 3-11 c/C_{max} VS. y/λ IN VARIOUS ZONES

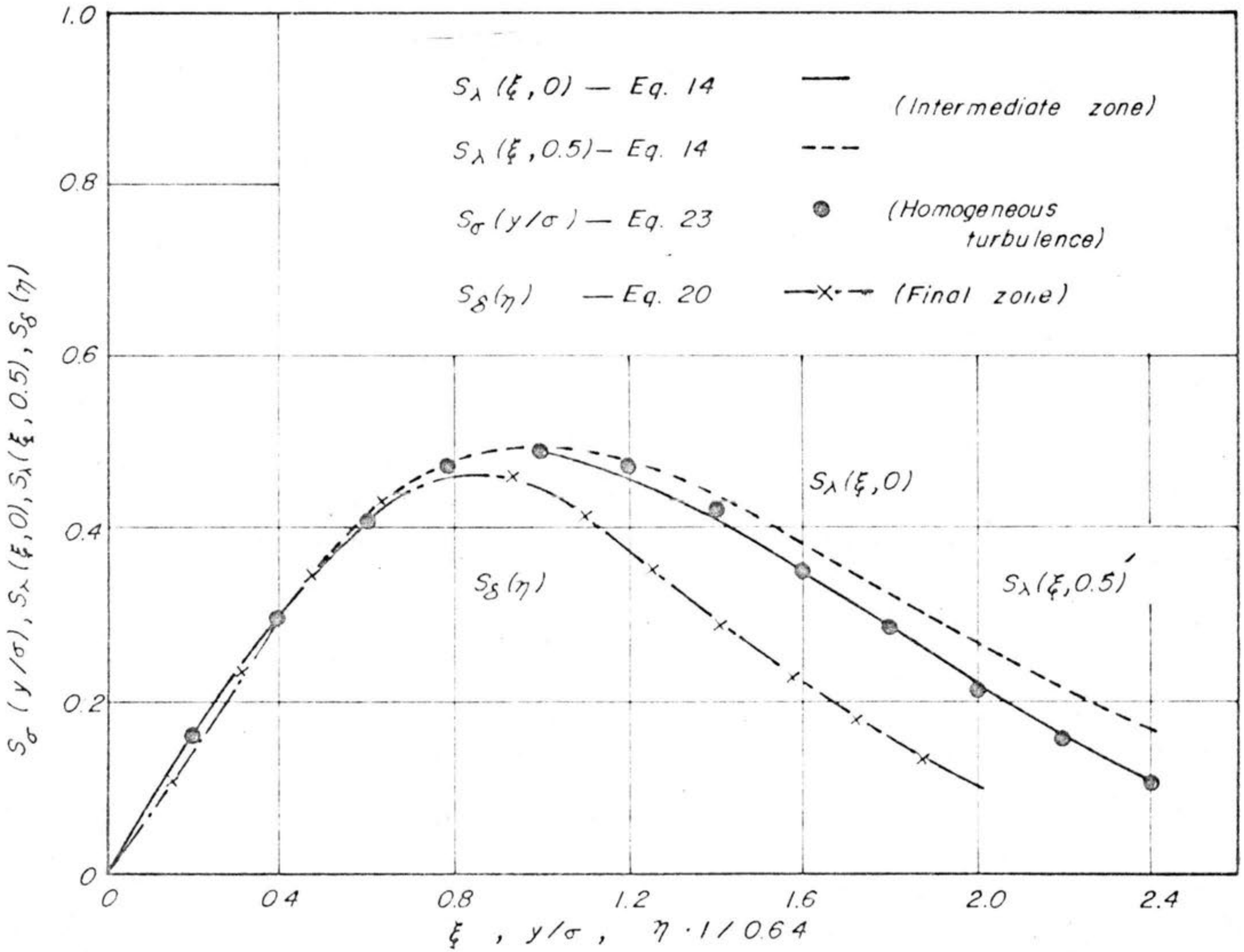

FIG. 3-12 DIMENSIONLESS FUNCTIONS RELATED TO $\overline{v'c'}$

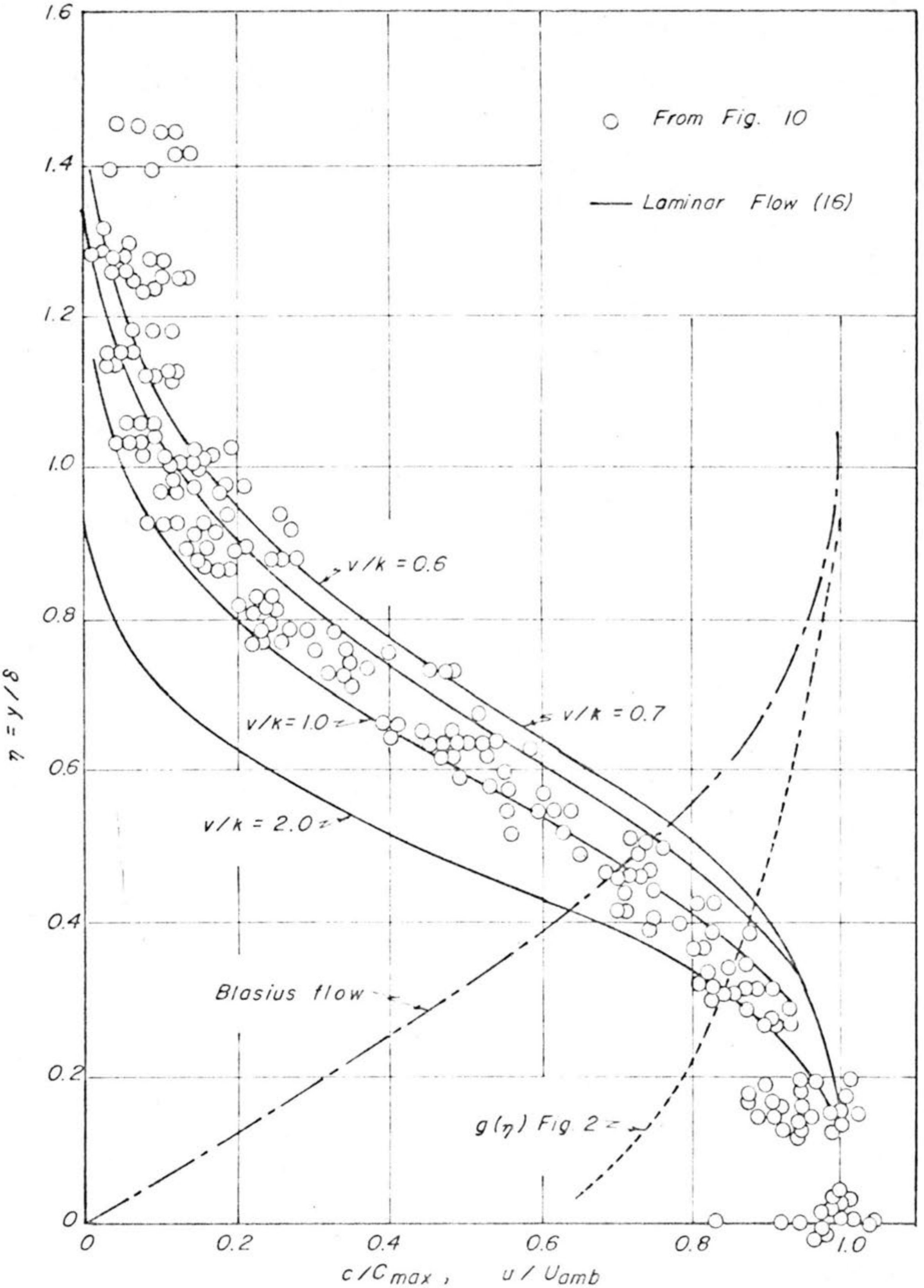

FIG. 3–13 COMPARISON OF LAMINAR AND TURBULENT DIFFUSION IN THE FINAL ZONE

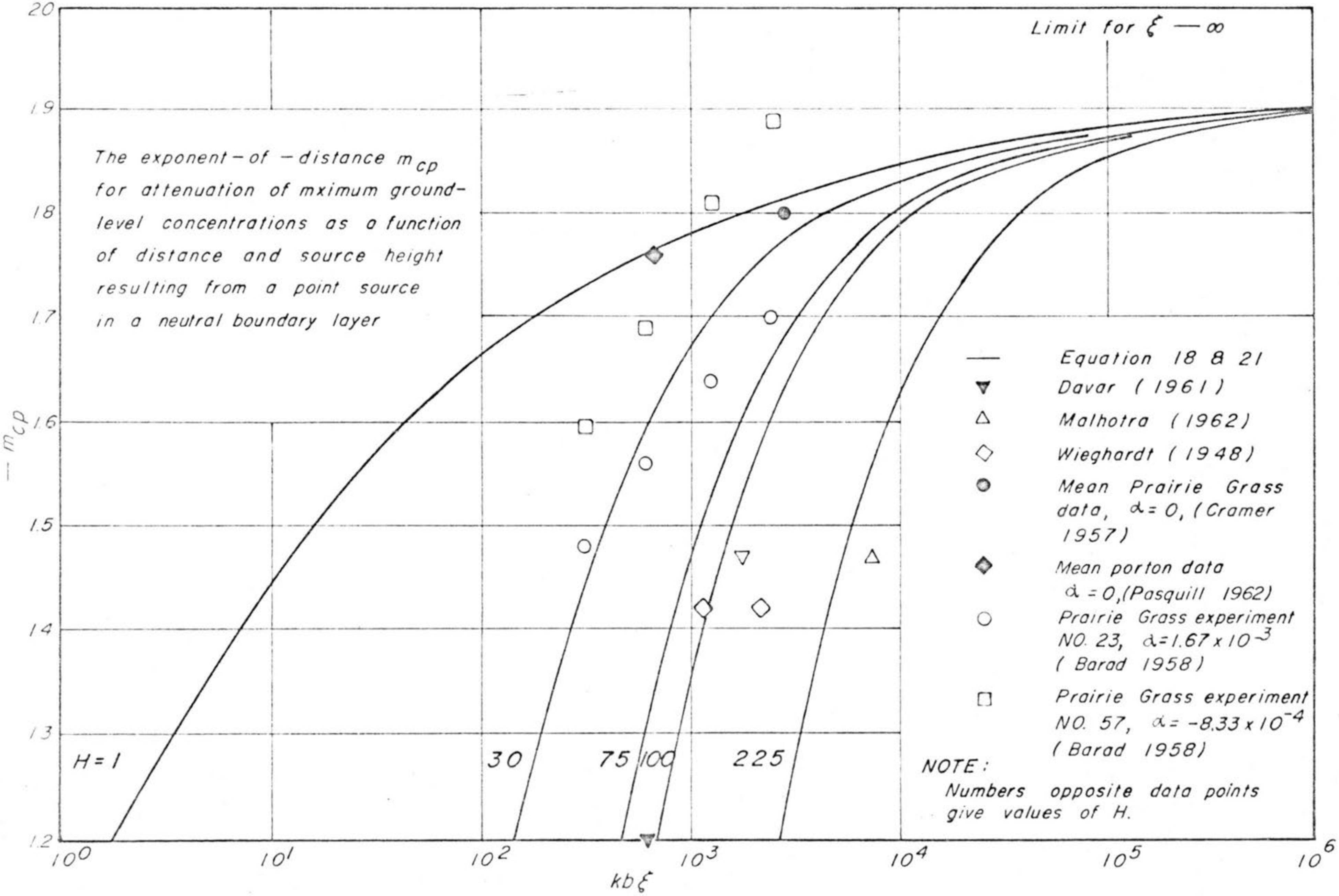

FIG. 4 - 1 COEFFICIENT OF GROUND LEVEL ATTENUATION OF POINT SOURCE (Cermak 4-6)

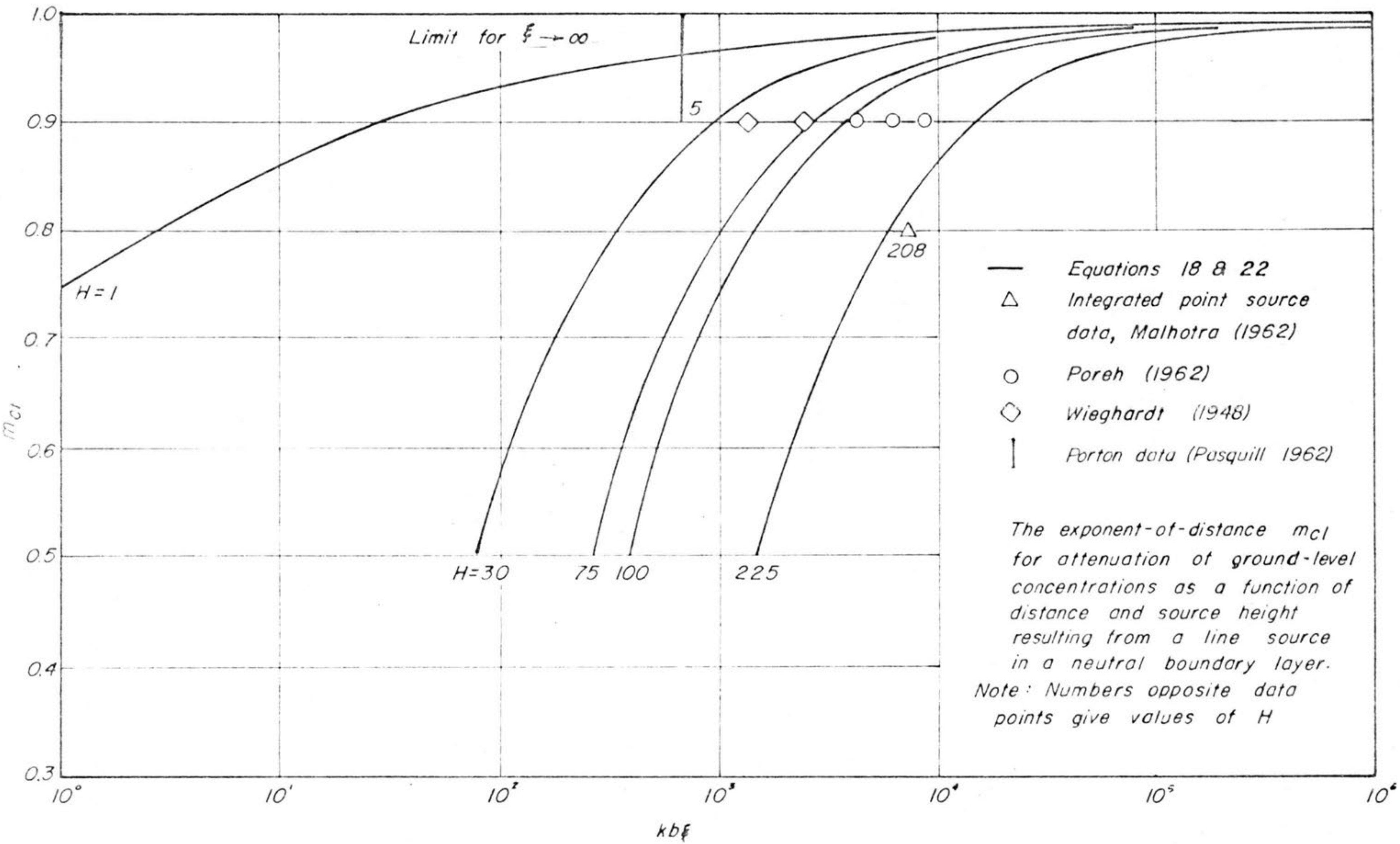

FIG. 4-2 COEFFICIENT OF GROUND LEVEL ATTENUATION OF LINE SOURCE (Cermak 4 – 6)

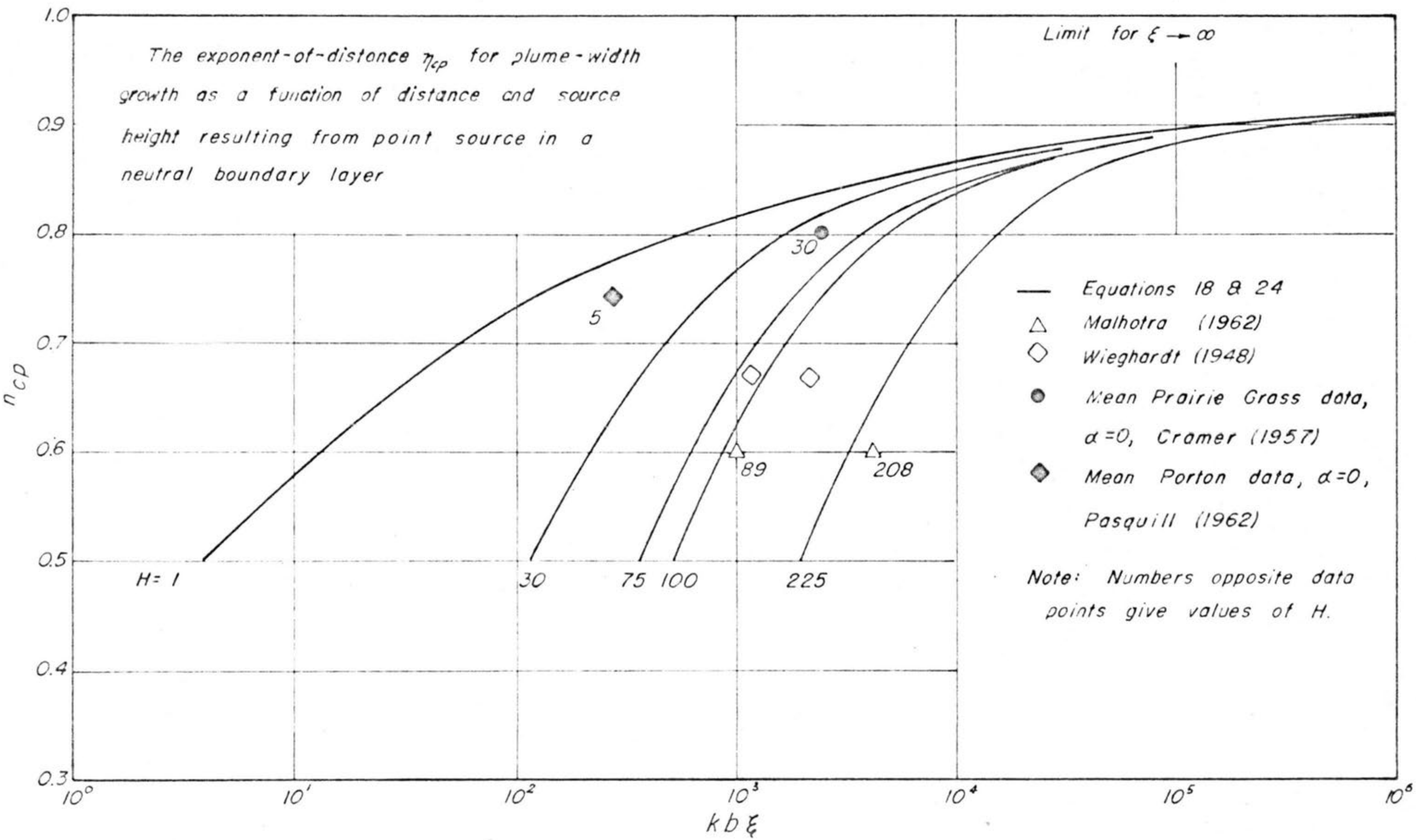

FIG. 4-3 COEFFICIENT OF PLUME-WIDTH GROWTH FOR A POINT SOURCE (Cermak 4-6)

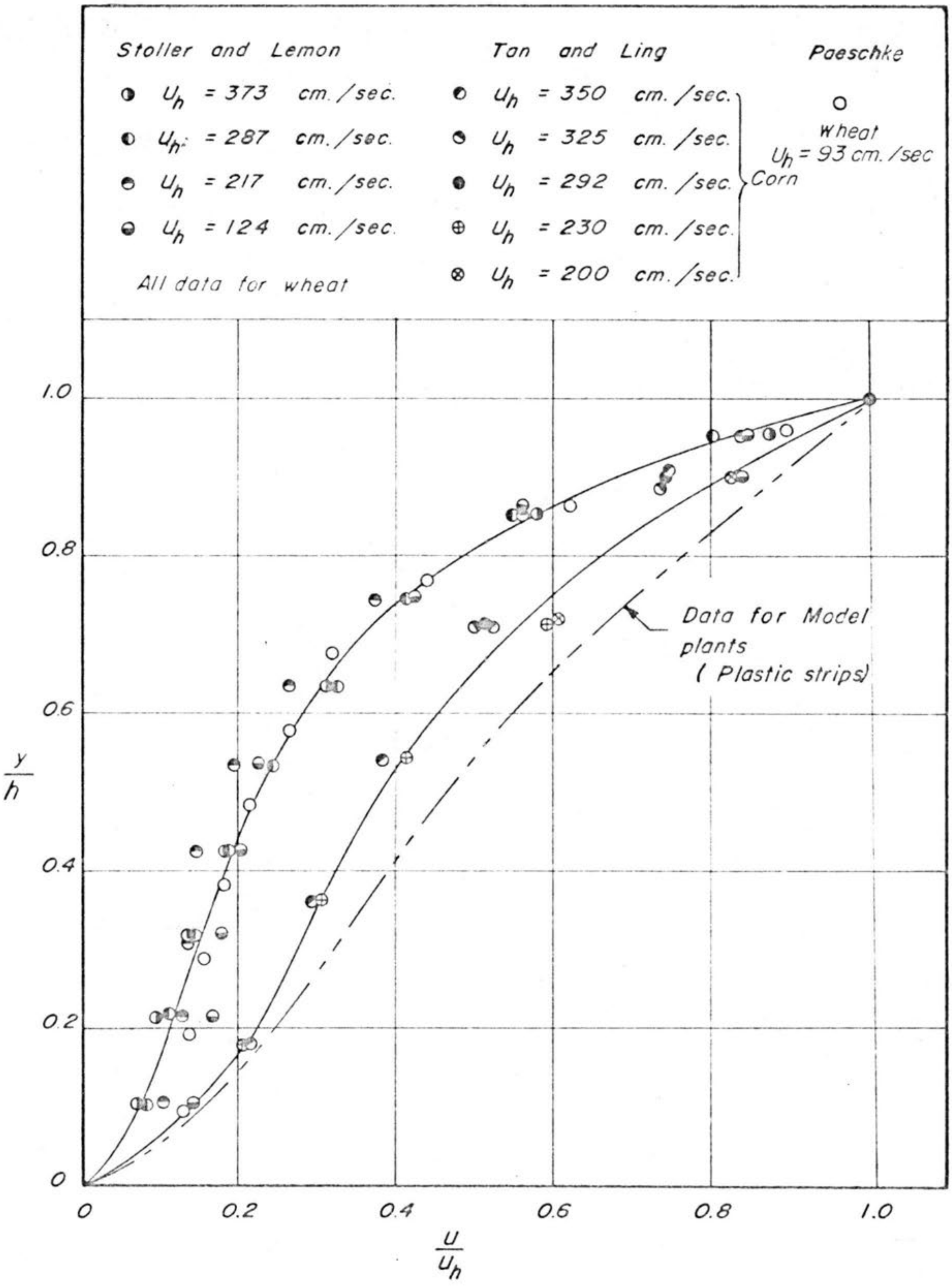

FIG. 5 – 1 VELOCITY DISTRIBUTION IN CANOPY : FIELD DATA

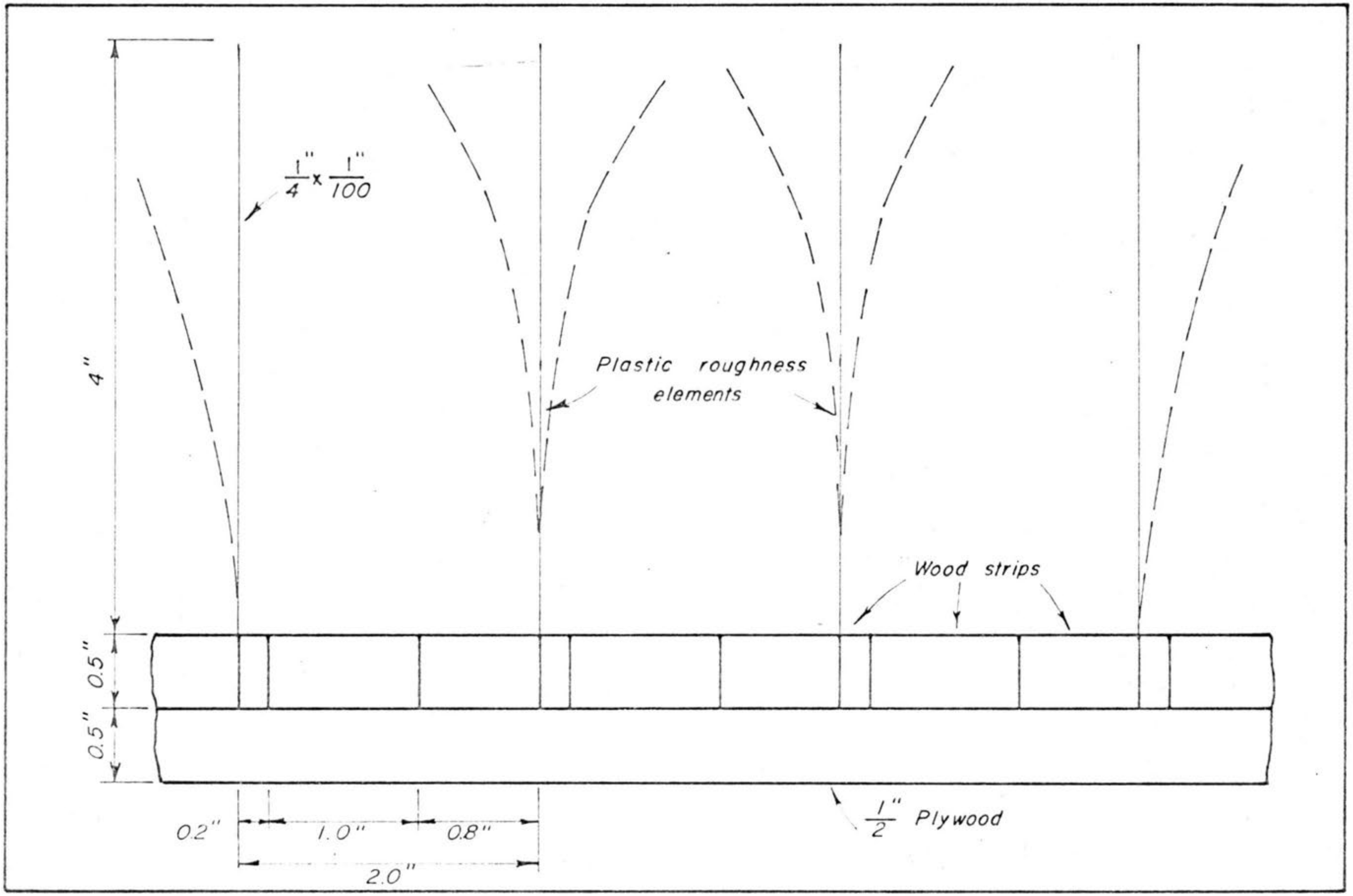

FIG. 5-2 FLEXIBLE ROUGHNESS ELEMENTS

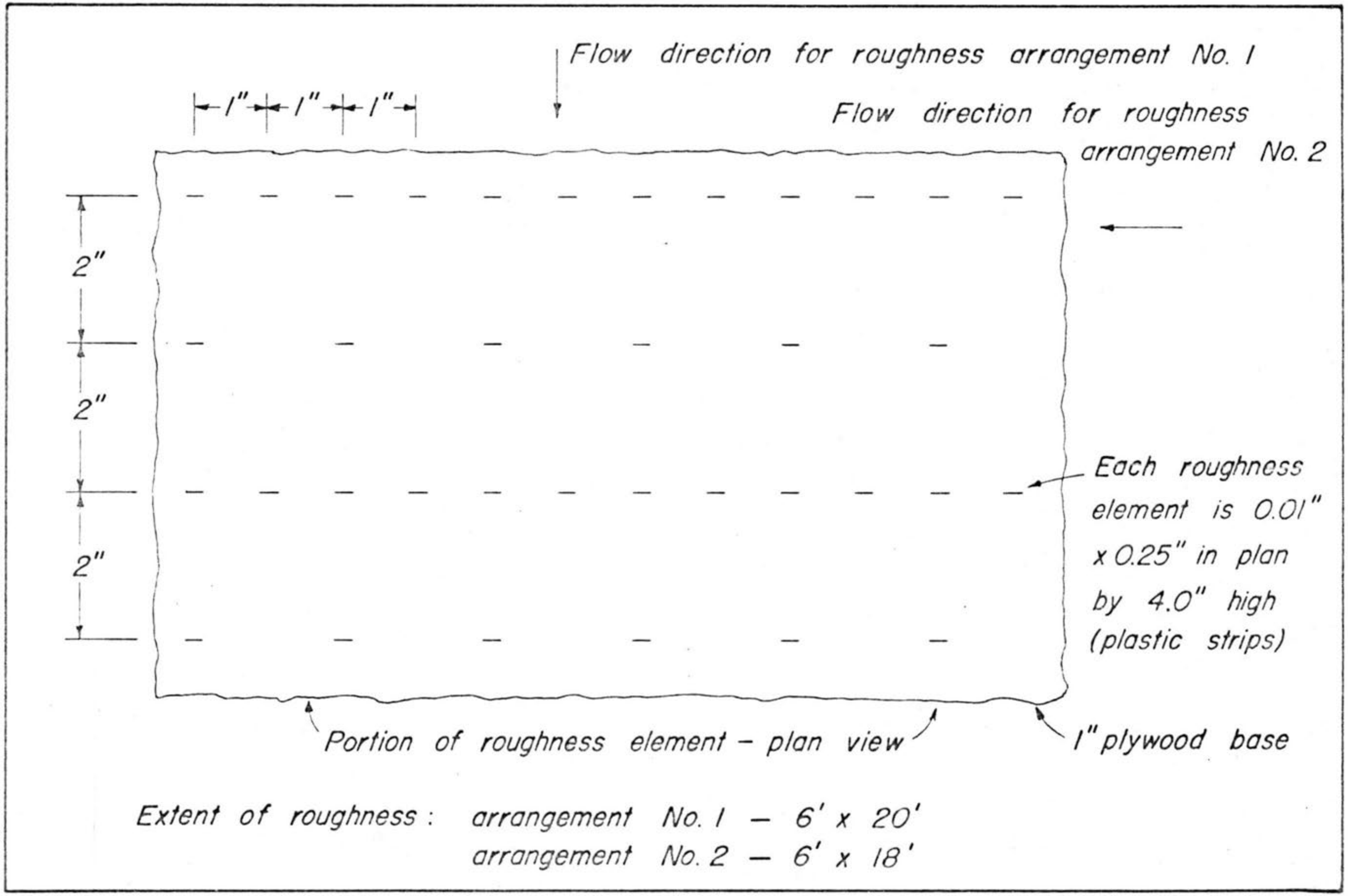

FIG. 5-3 ARRANGEMENT 1 AND 2 OF ROUGHNESS ELEMENTS

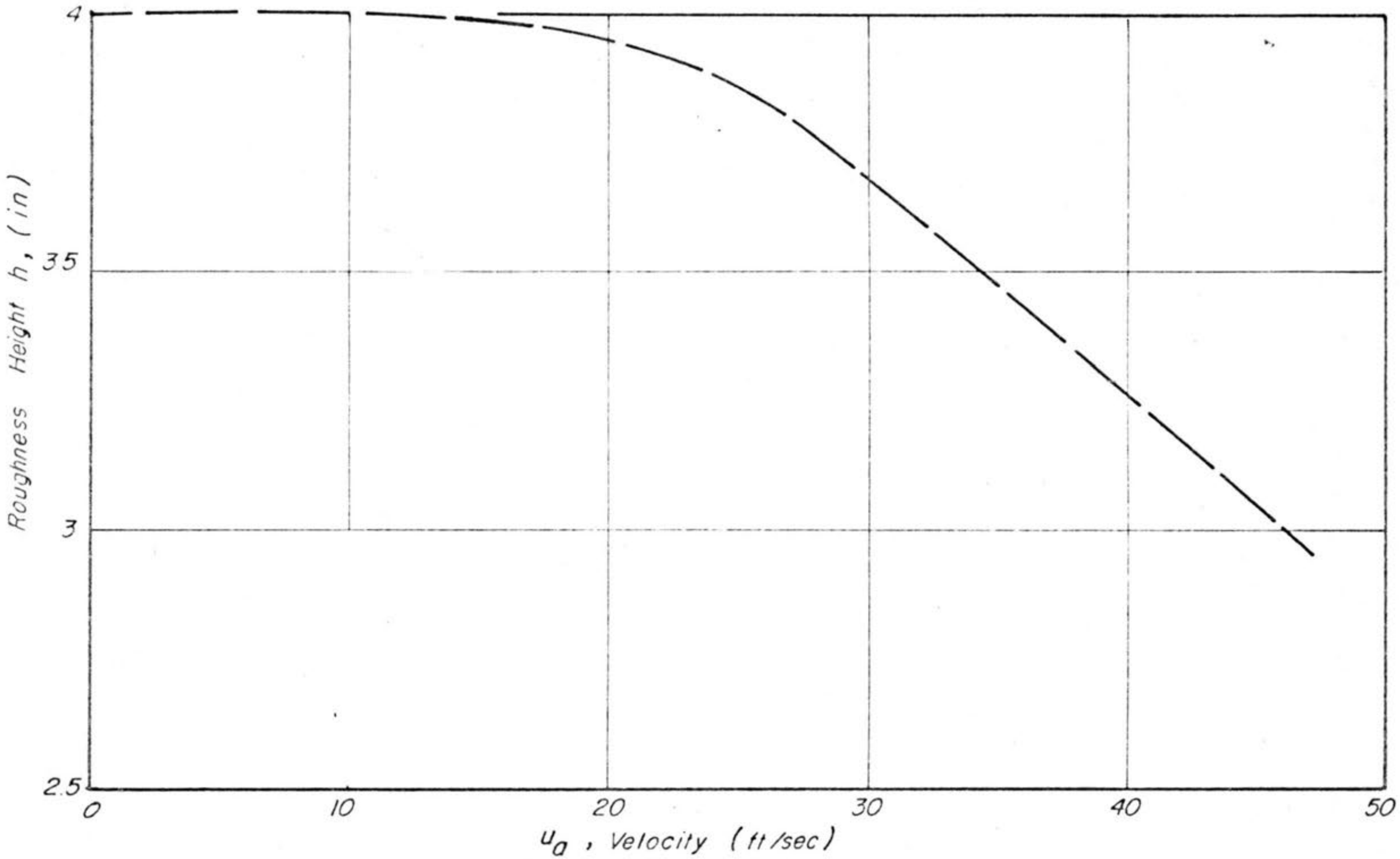

FIG. 5-4 CHANGE OF FLEXIBLE ROUGHNESS HEIGHT WITH WIND VELOCITY

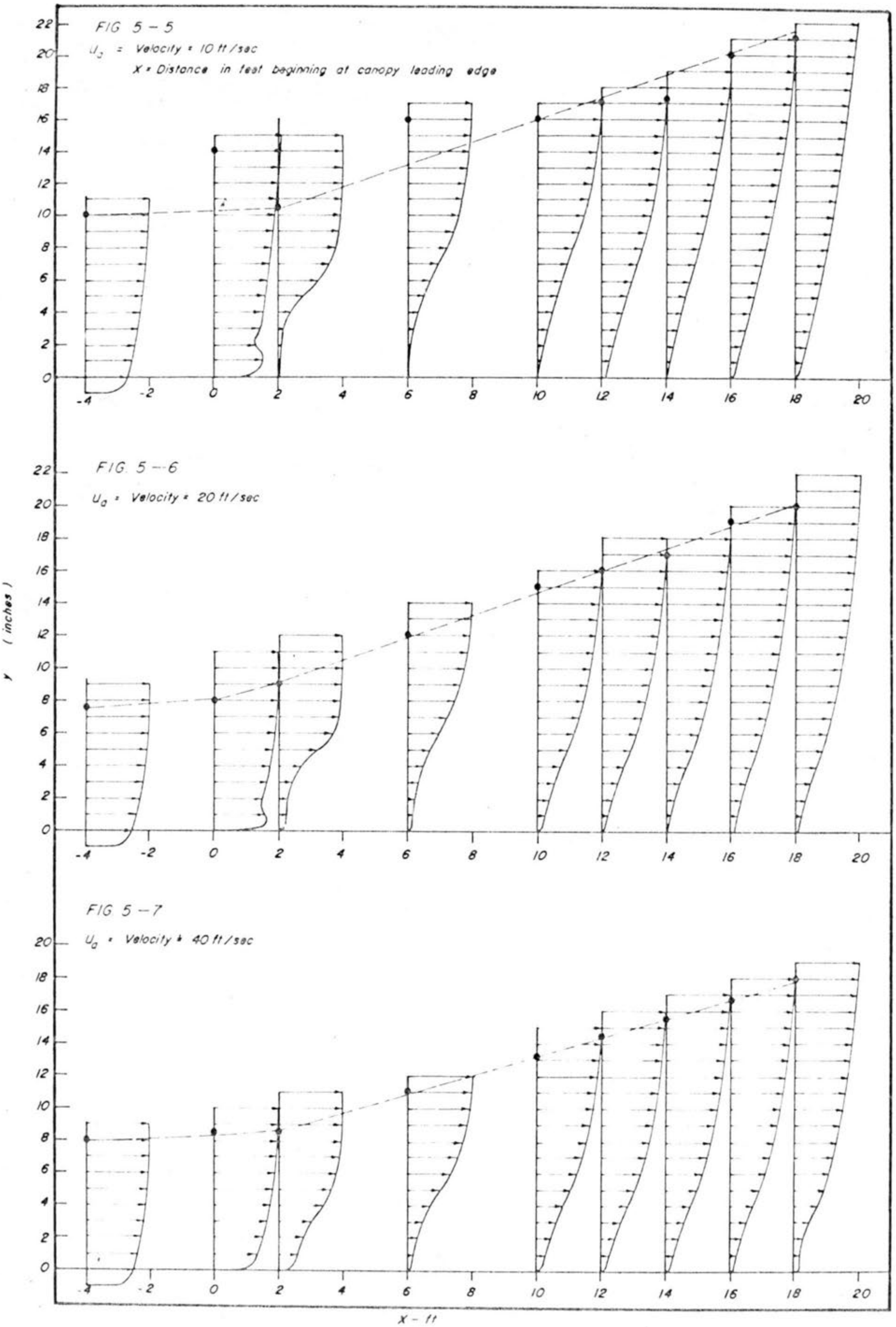

FIGS 5-5, 6 & 7 VELOCITY PROFILES

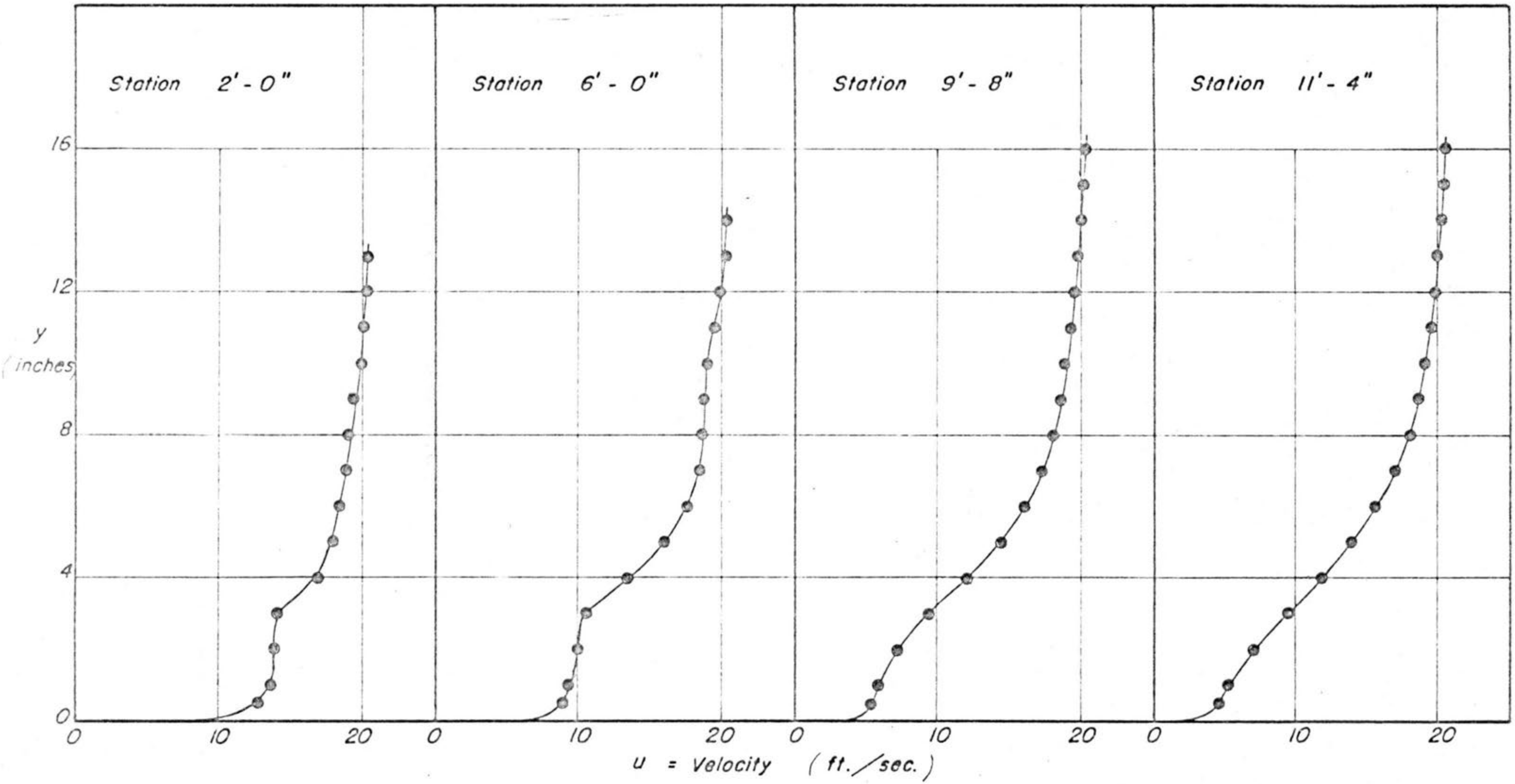

FIG. 5-8a VELOCITY PROFILES FOR ARRANGEMENT 2

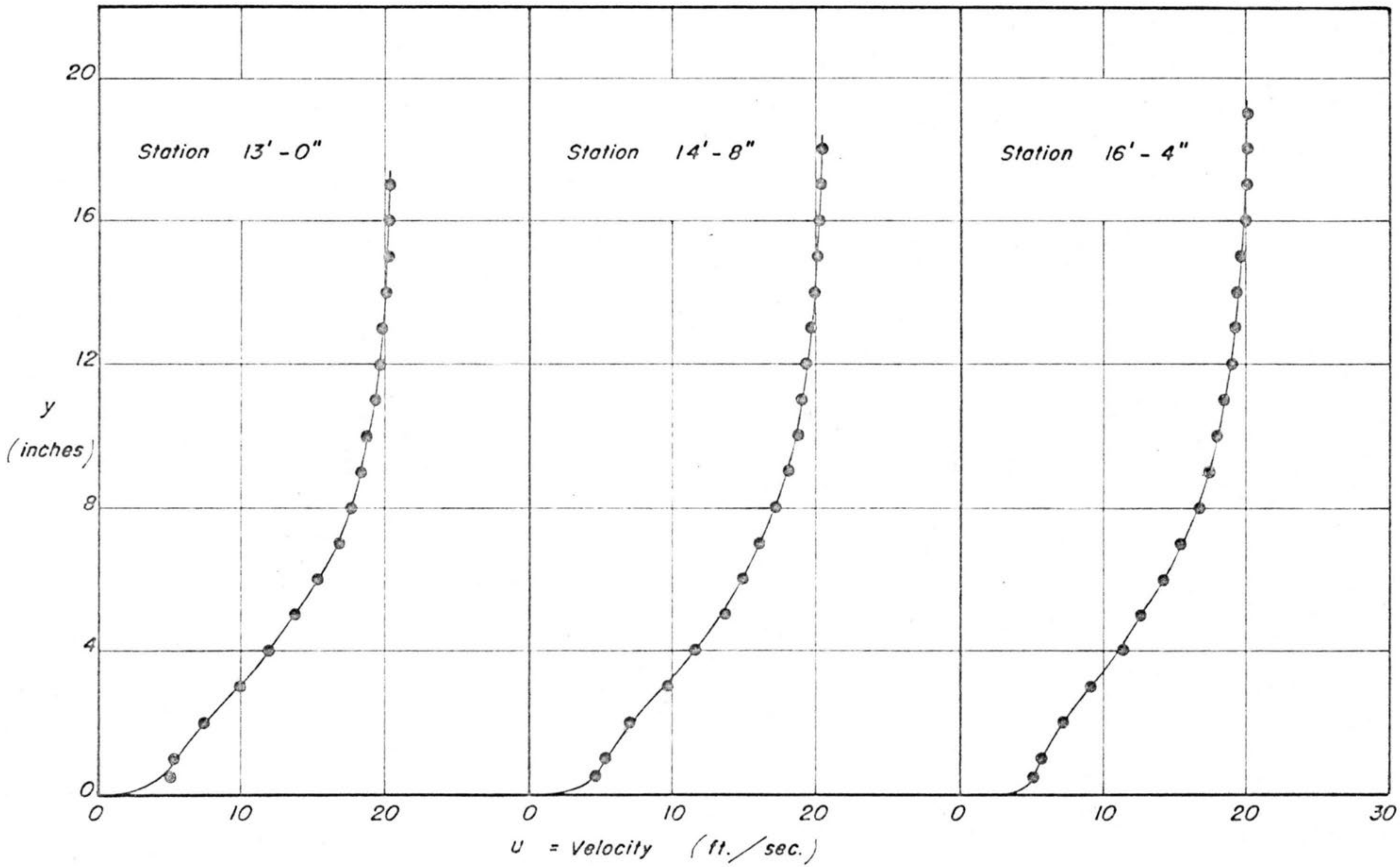

FIG. 5-8 b VELOCITY PROFILES FOR ARRANGEMENT 2

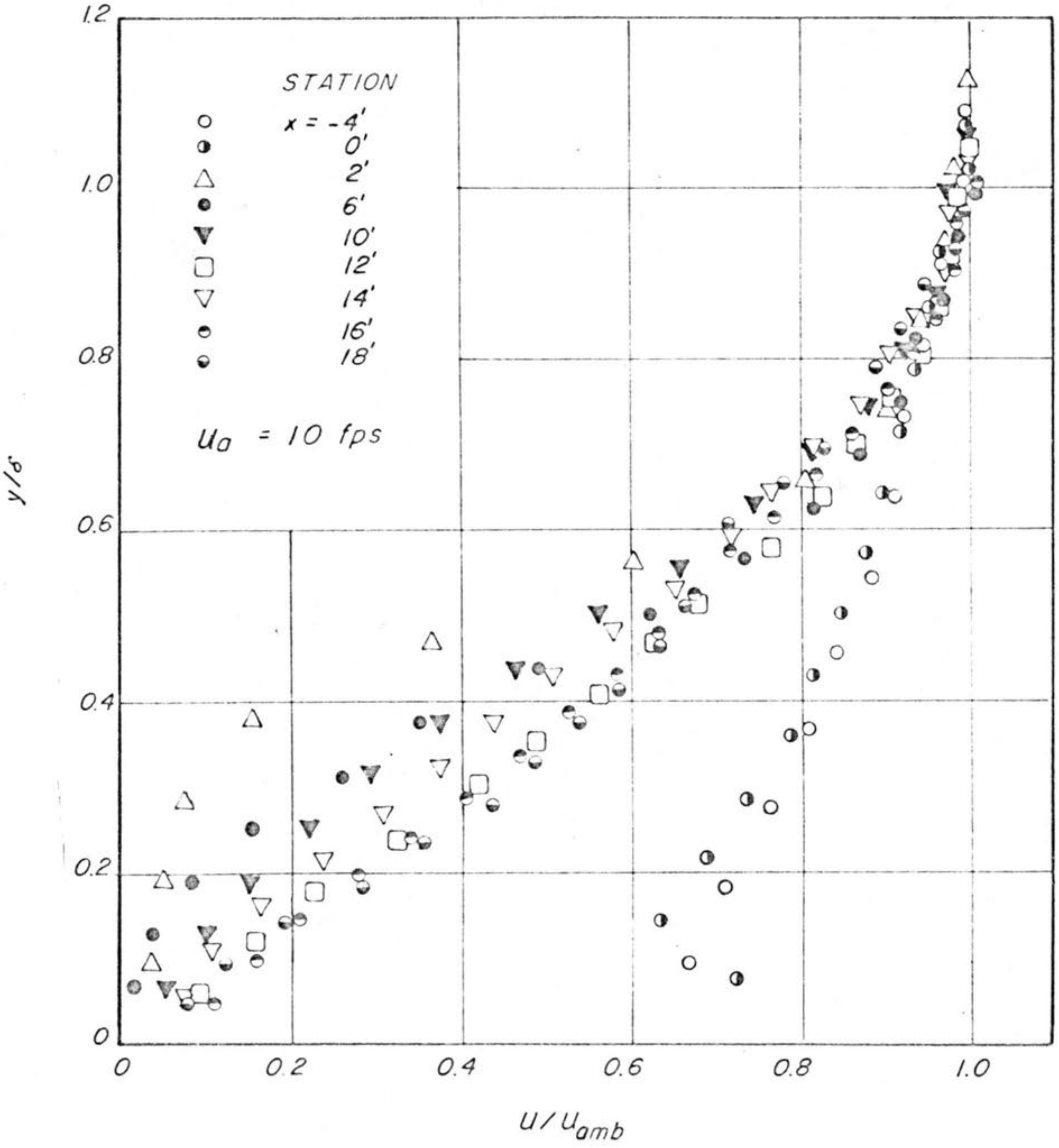

FIG. 5-9 DIMENSIONLESS VELOCITY PROFILES
ARRANGEMENT I

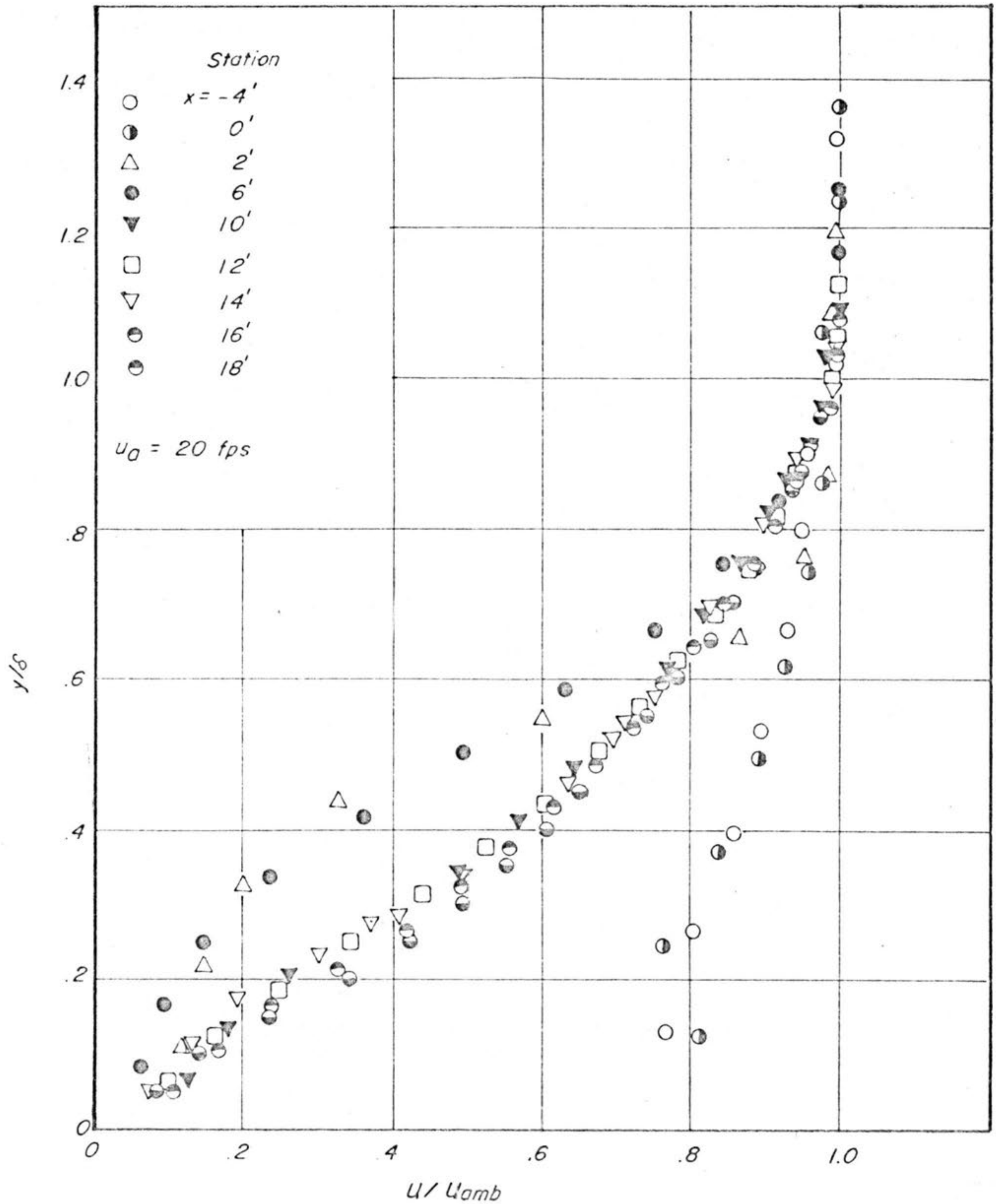

FIG. 5-10 DIMENSIONLESS VELOCITY PROFILES
ARRANGEMENT I

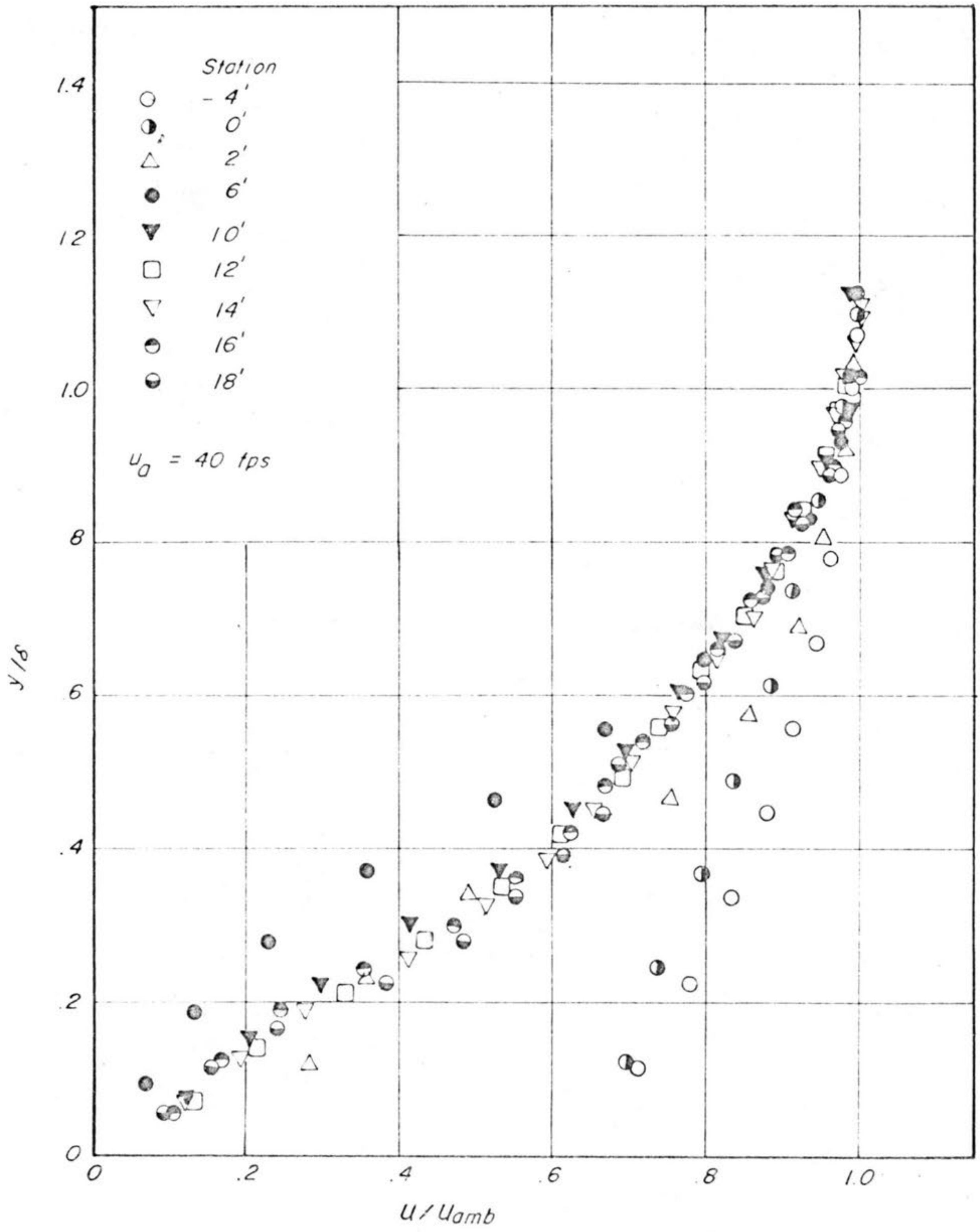

FIG. 5-11 DIMENSIONLESS VELOCITY PROFILES ARRANGEMENT I

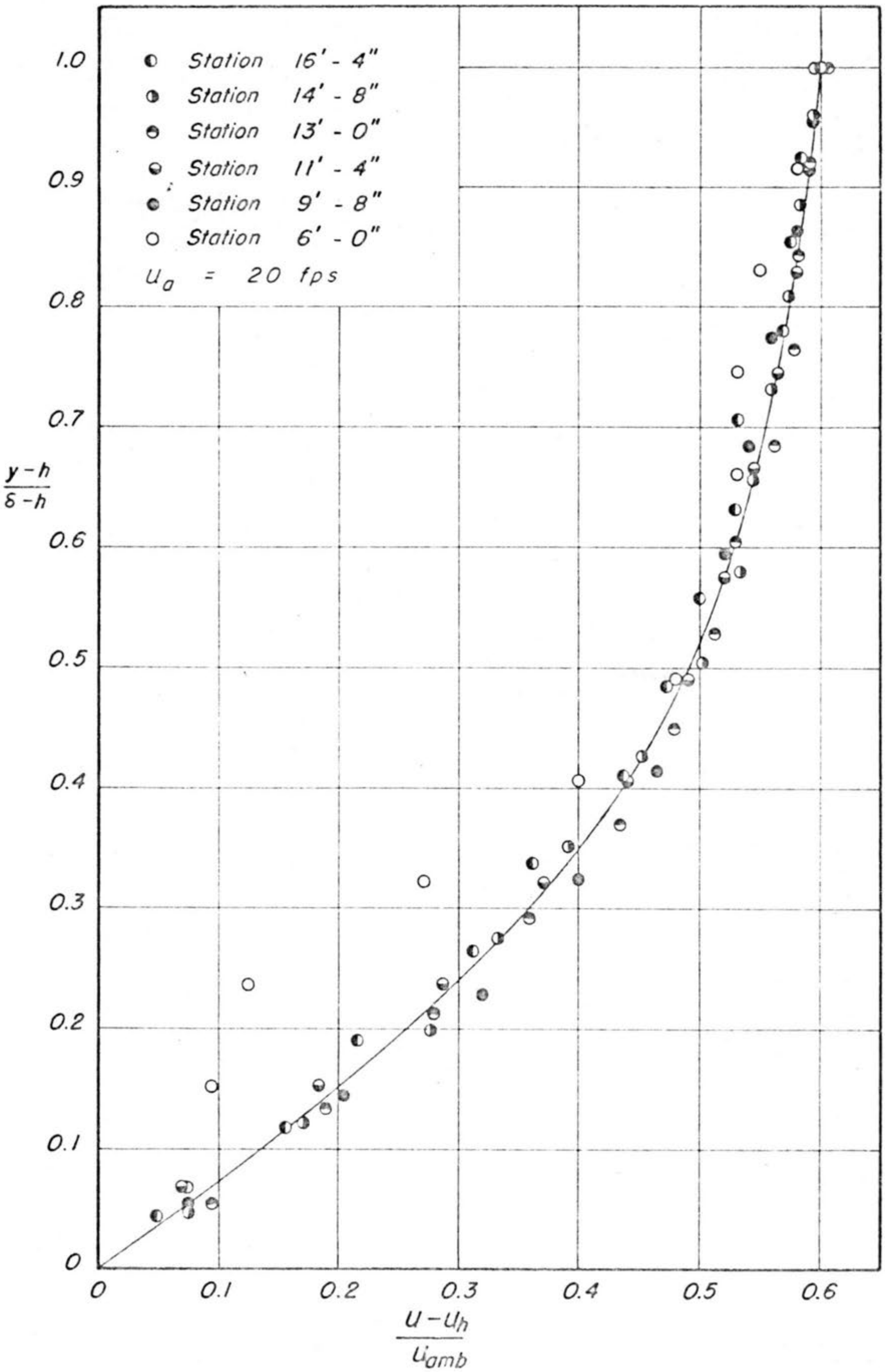

FIG. 5-12 DIMENSIONLESS VELOCITY PROFILES: ARRANGEMENT 2

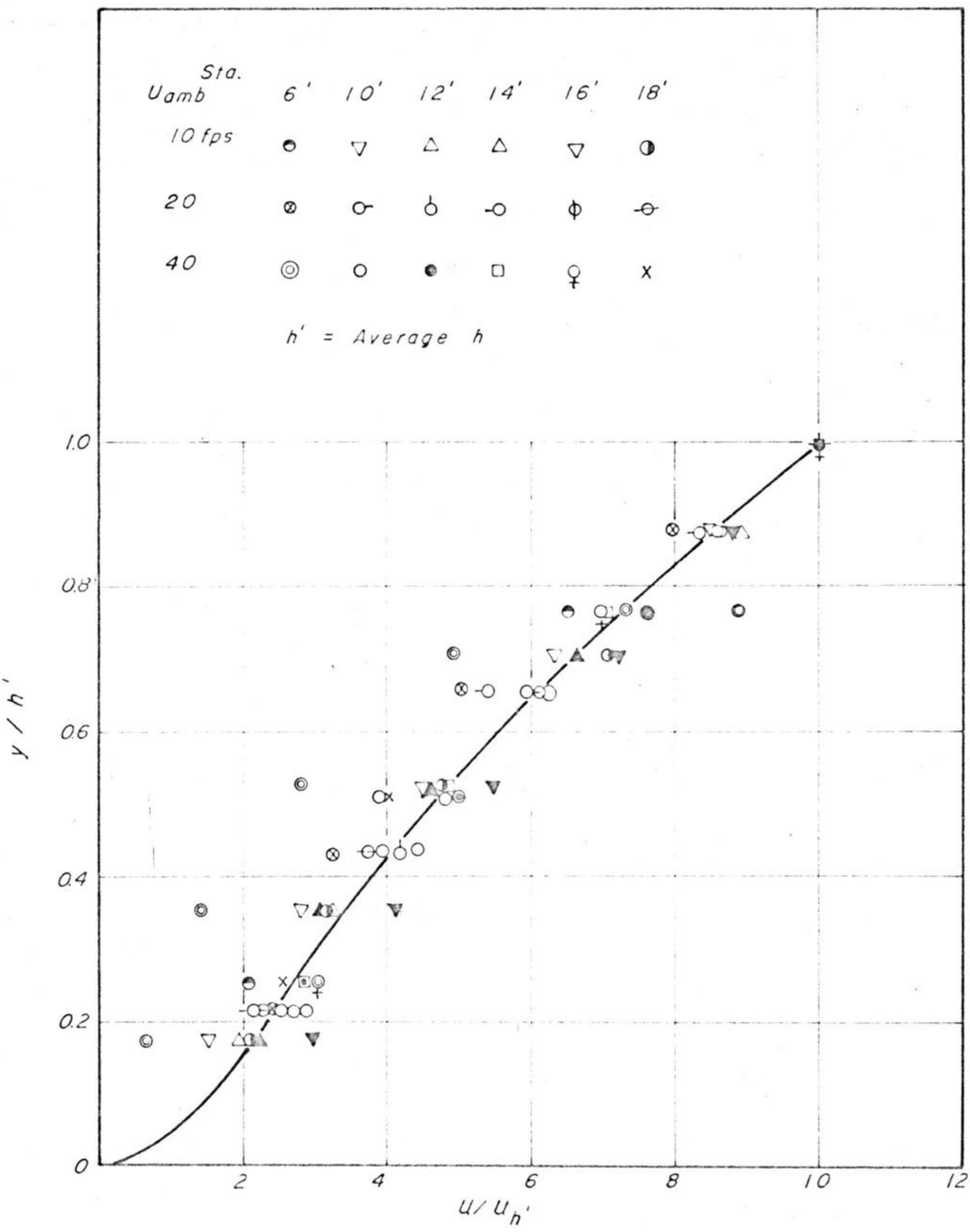

FIG. 5-13 DIMENSIONLESS PROFILES IN CANOPY ARRANGEMENT I

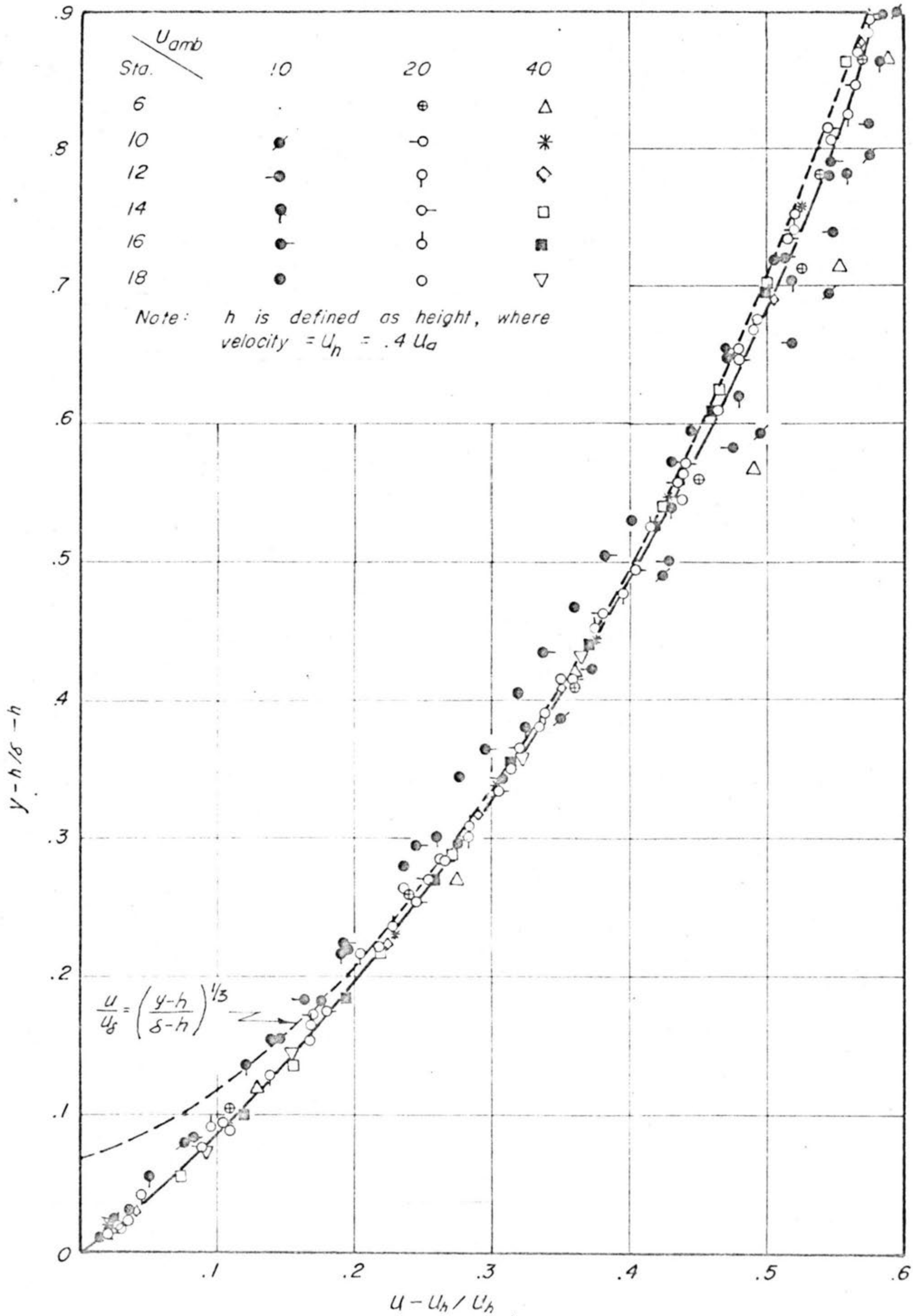

FIG. 5-14 DIMENSIONLESS VELOCITY PROFILES ABOVE CANOPY ARRANGEMENT I

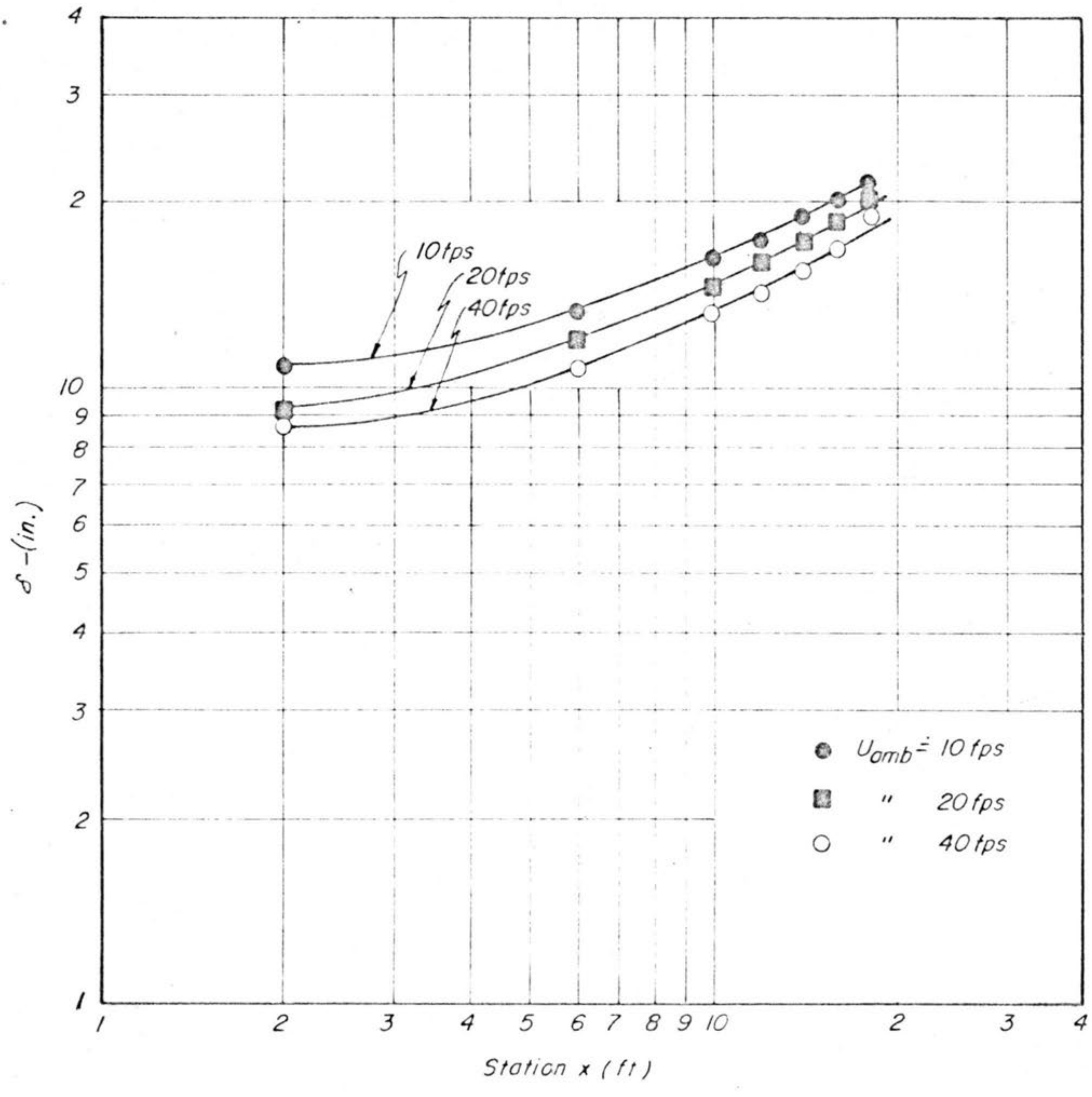

FIG. 5-15 BOUNDARY-LAYER THICKNESS DEVELOPMENT
ARRANGEMENT I

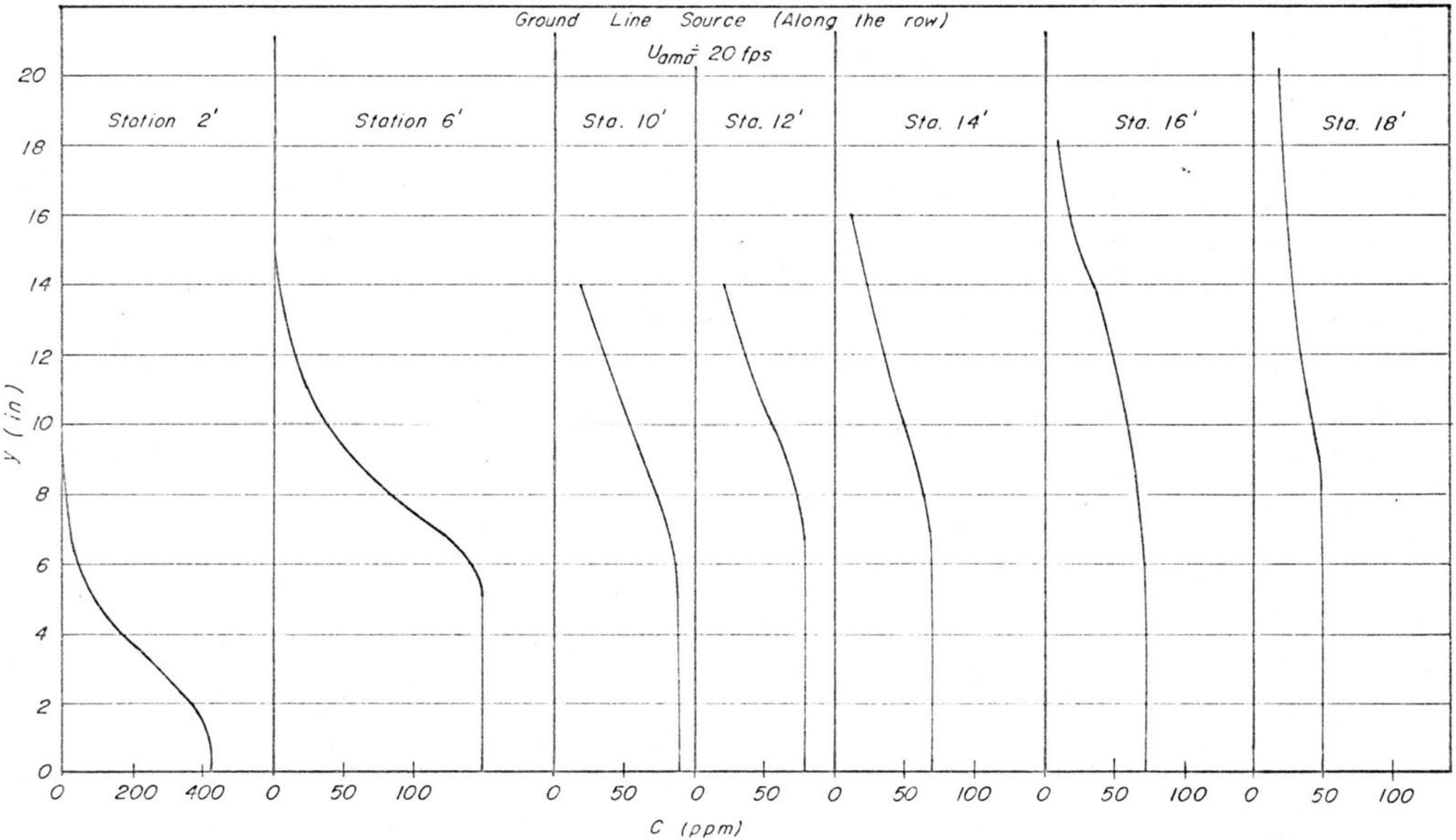

FIG. 5-16 CONCENTRATION PROFILES
ARRANGEMENT I

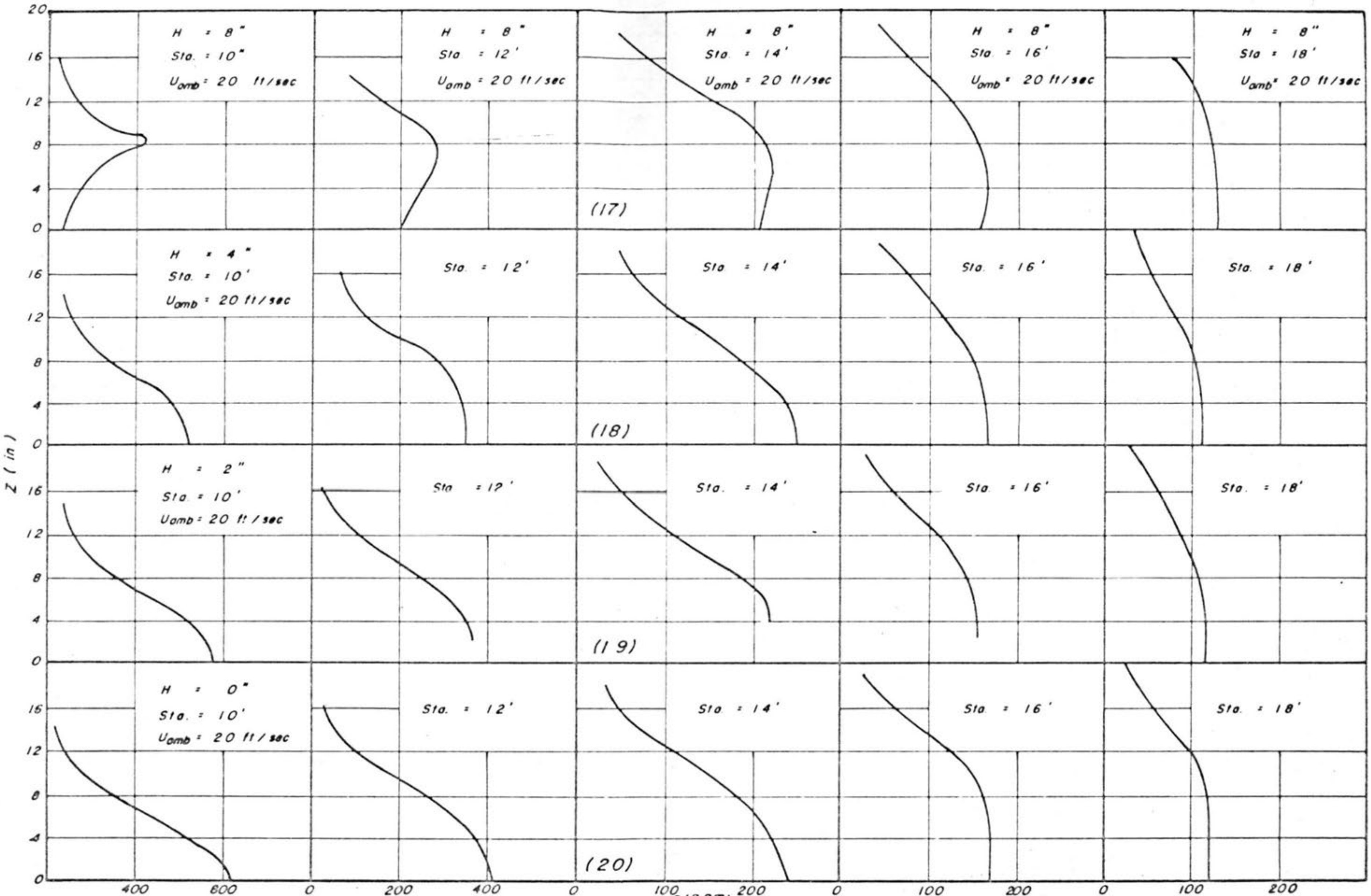

FIG. 5 - 17, 18, 19, & 20 CONCENTRATION PROFILES

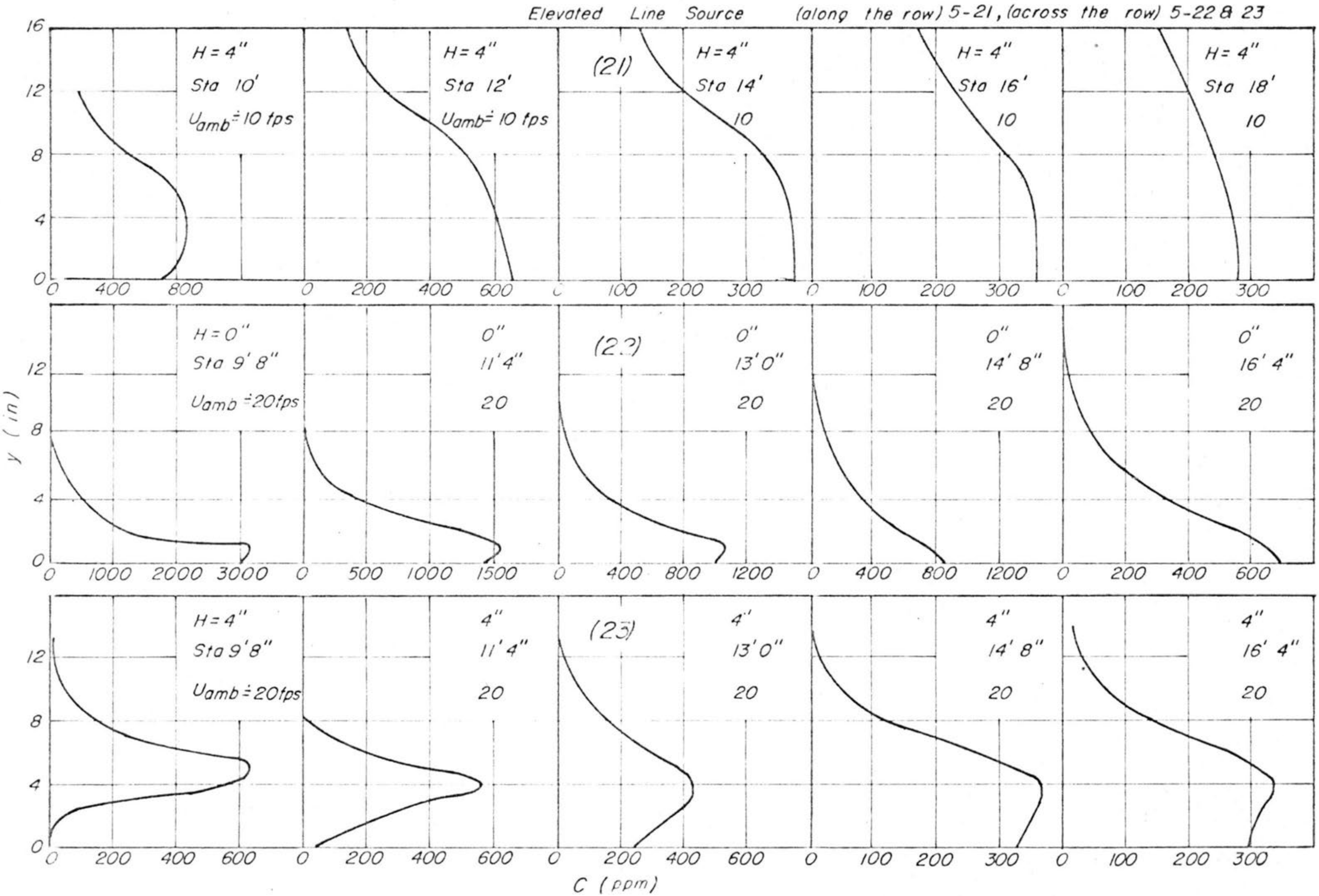

FIGS. 5-21, 22 & 23 CONCENTRATION PROFILES: ALONG THE ROW ARRANGEMENT 1
ACROSS THE ROW ARRANGEMENT 2

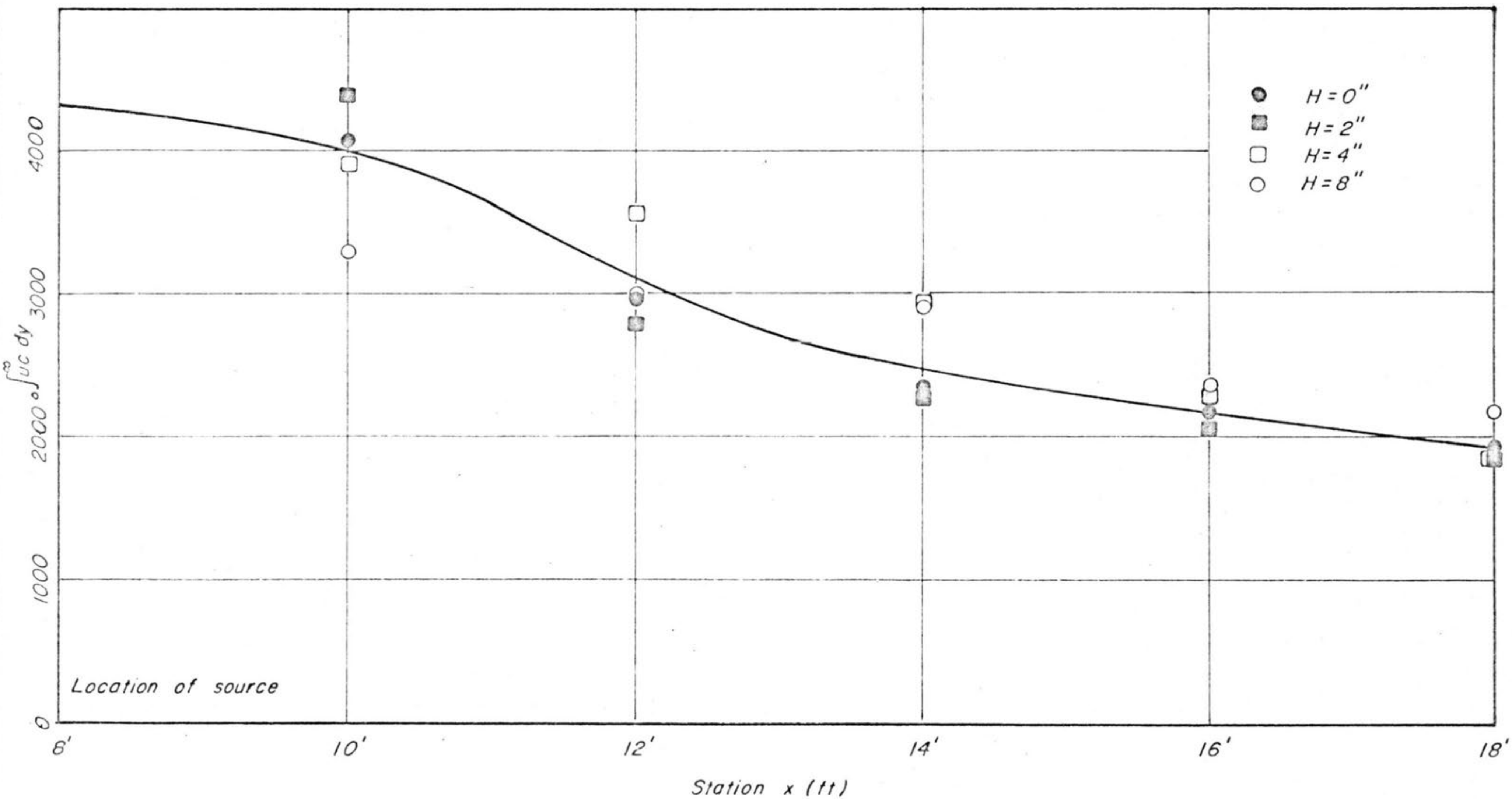

FIG. 5-24 INTEGRATED DISCHARGE OF AMMONIUM

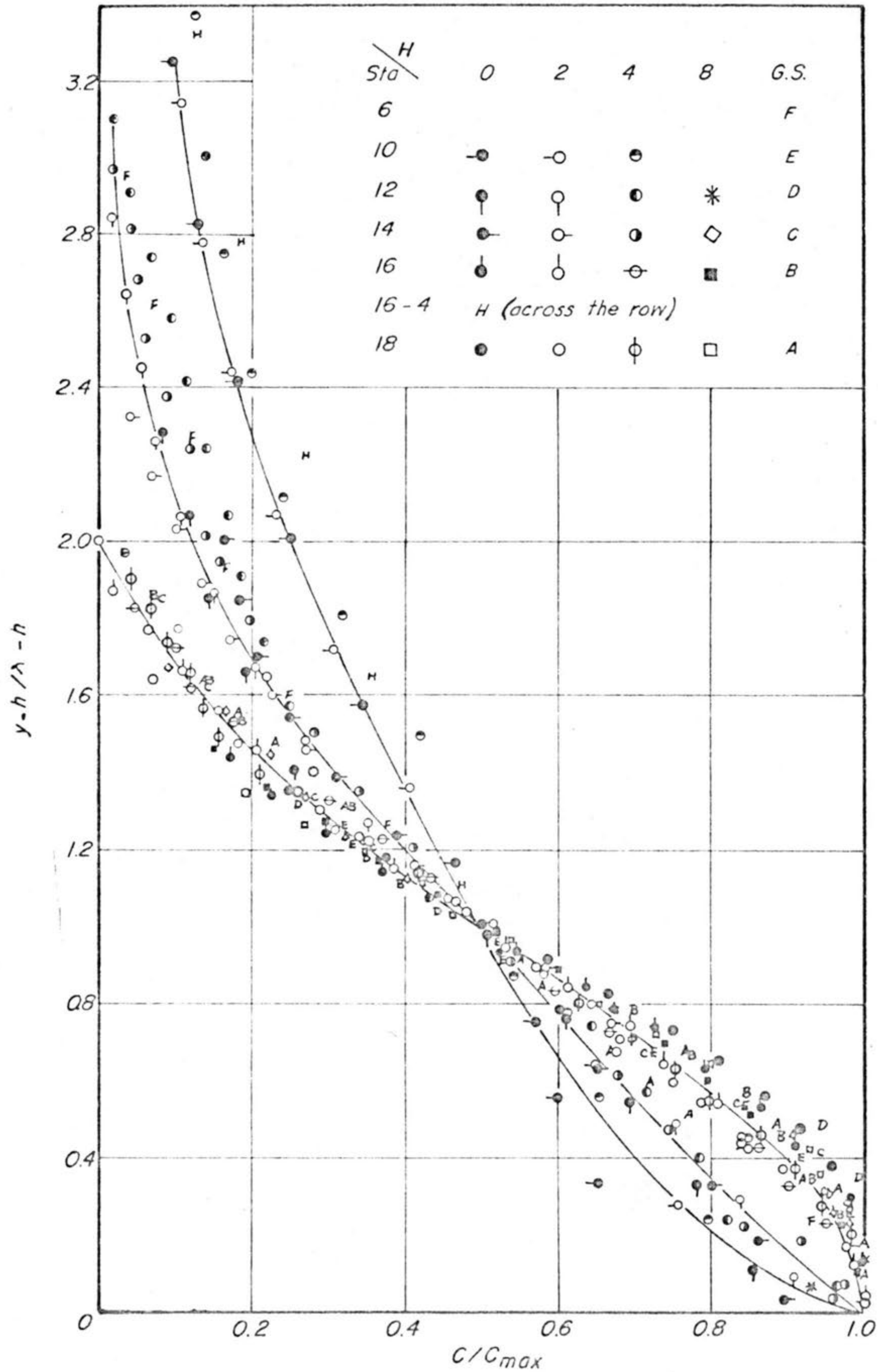

FIG. 5-25 DIMENSIONLESS CONCENTRATIONS ABOVE COVER

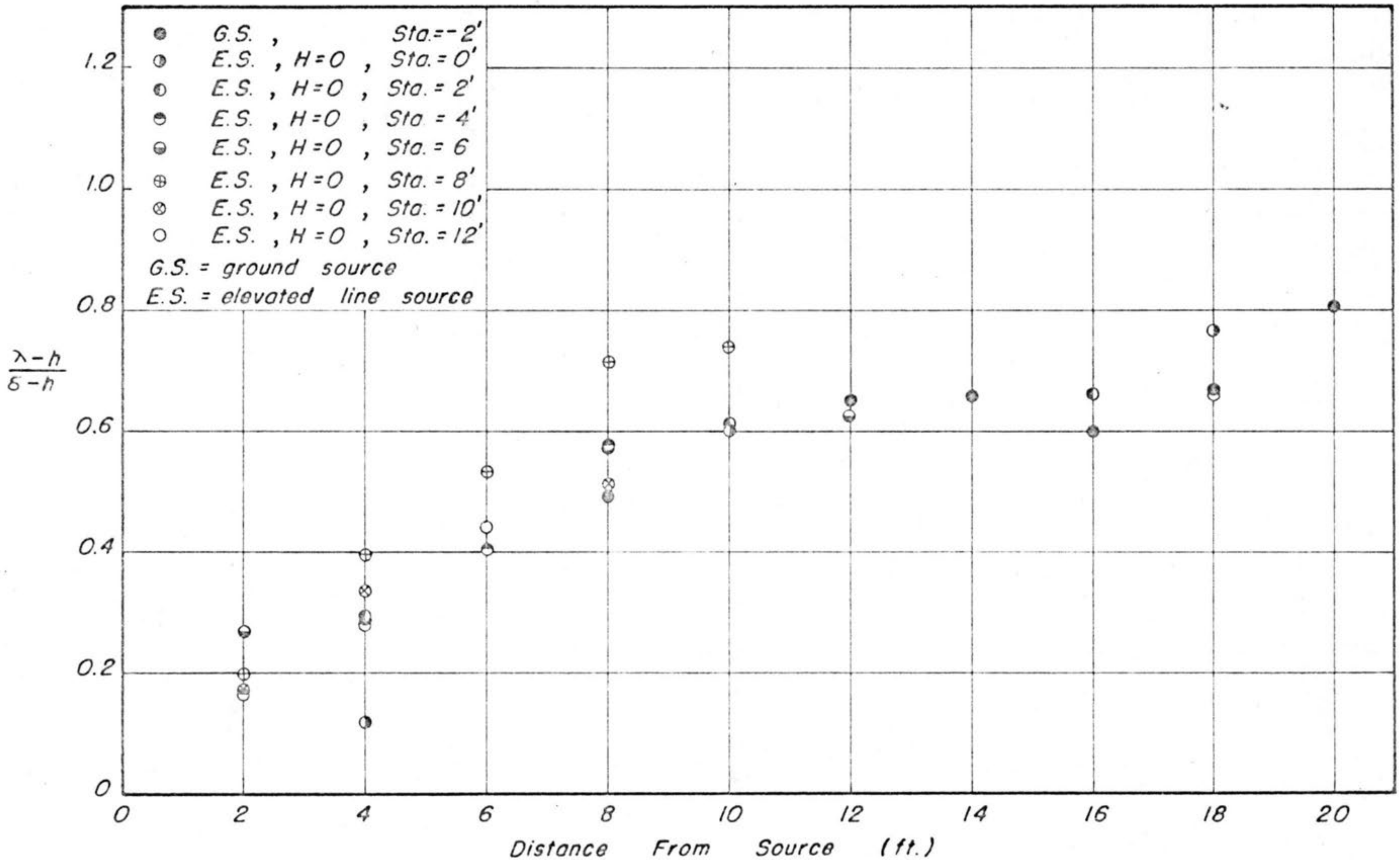

FIG. 5-26 $\lambda - h / \delta - h$ FOR THE THREE ZONES

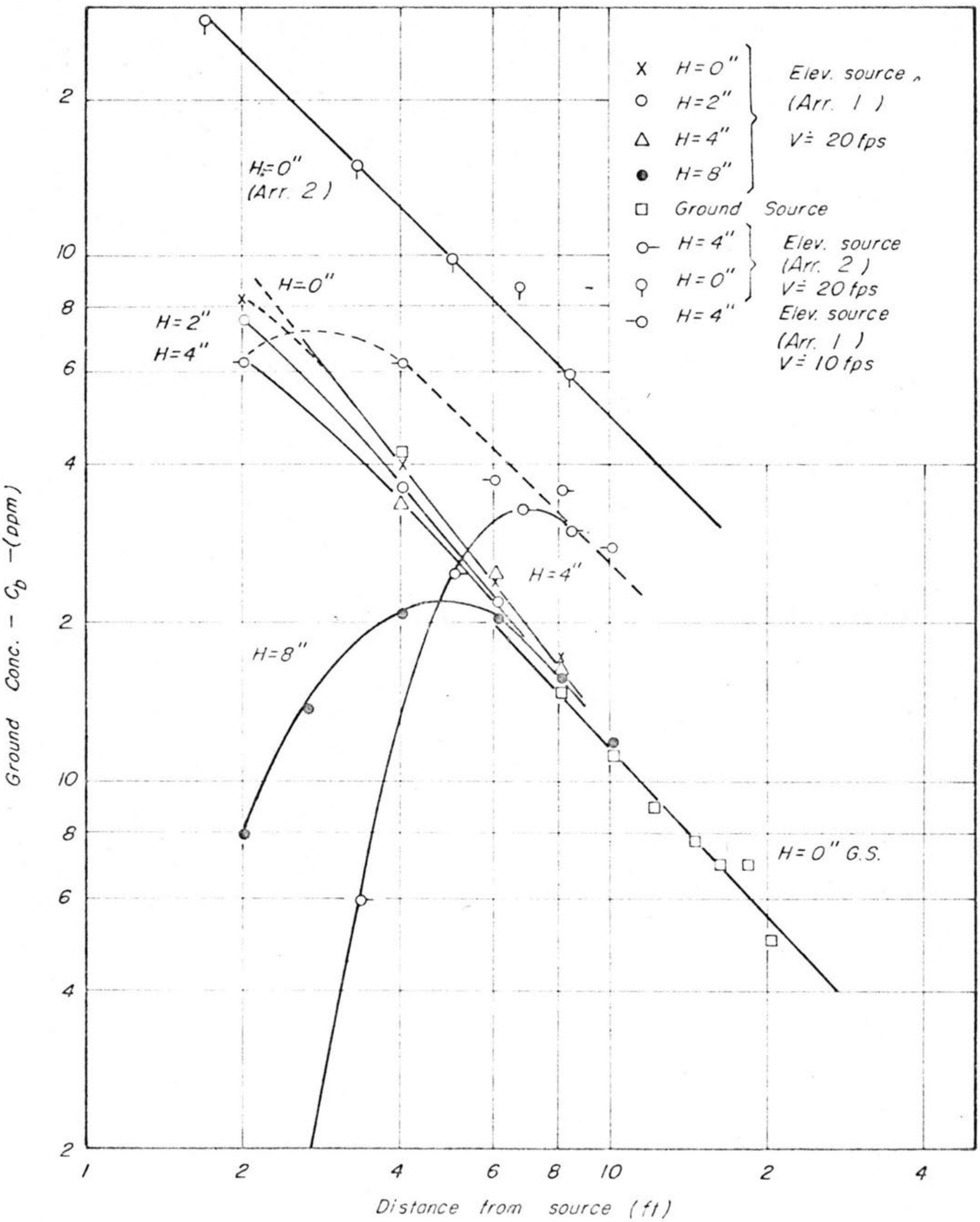

FIG. 5-27 C_{max} AS FUNCTION OF X

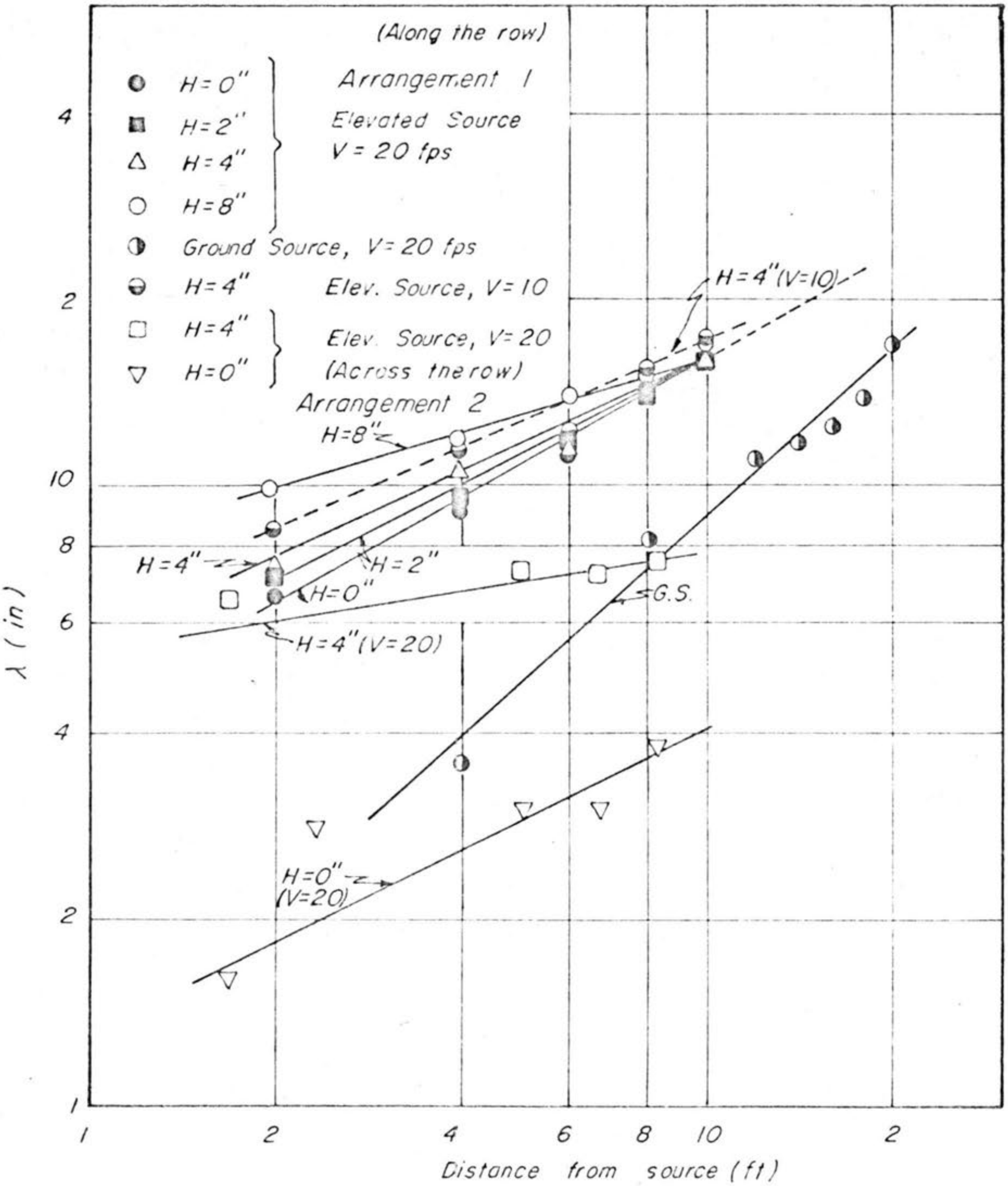

FIG 5-28 λ AS FUNCTION OF X

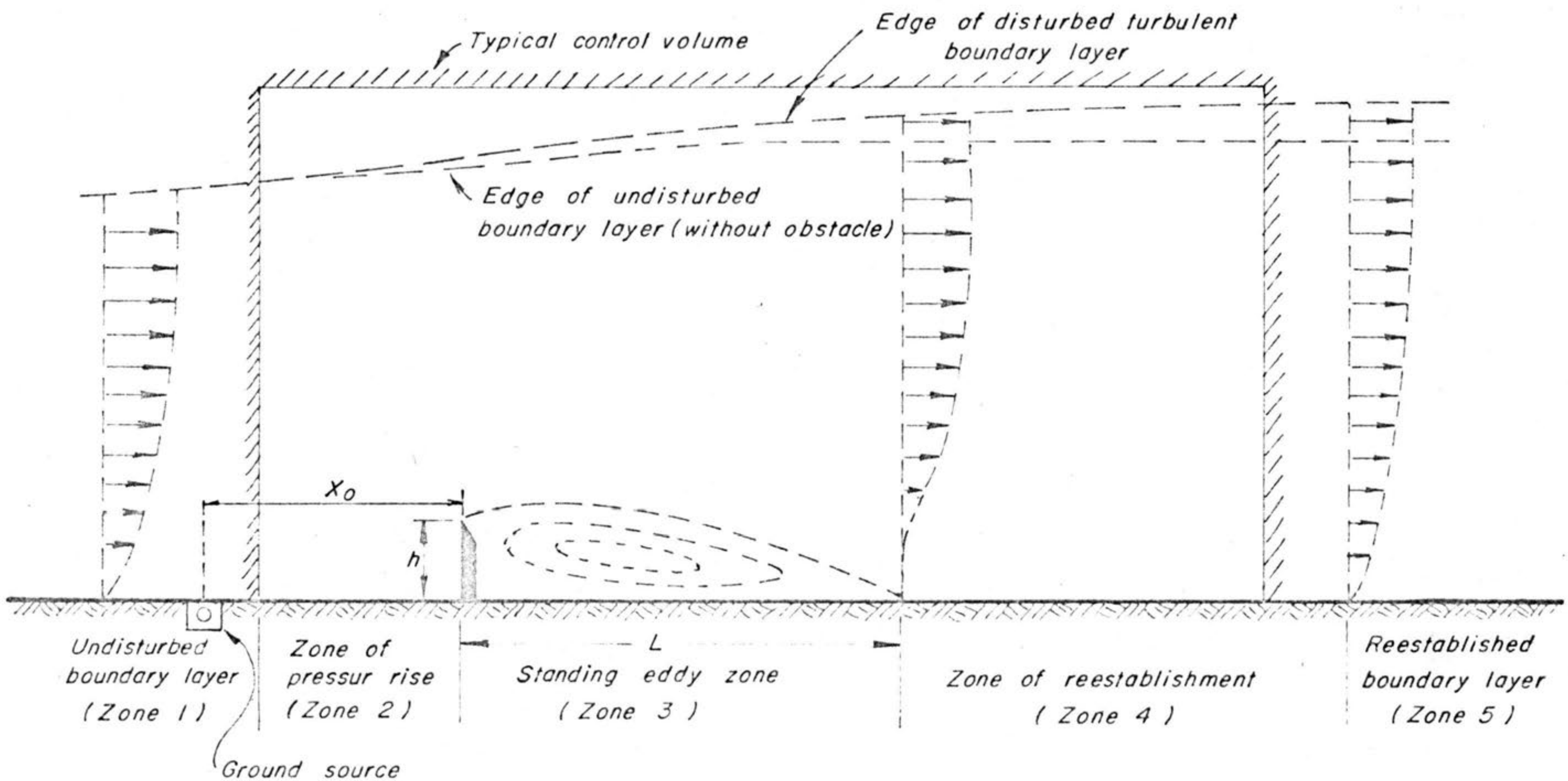

FIG. 6-1 THE ZONES OF THE FLOW DISTURBED BY A PLATE

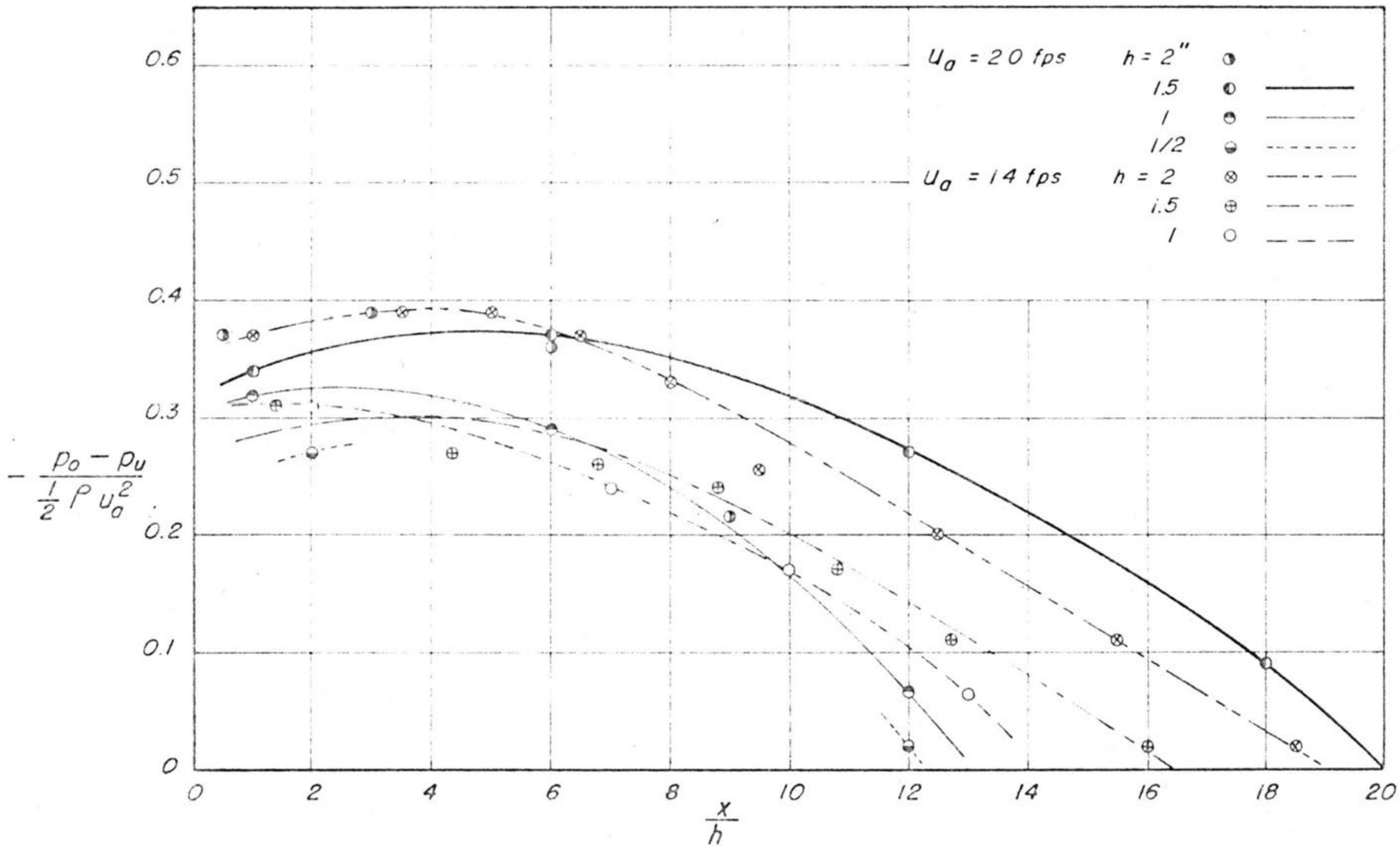

FIG. 6 – 2 PRESSURE DISTRIBUTION DOWNSTREAM FROM WALL

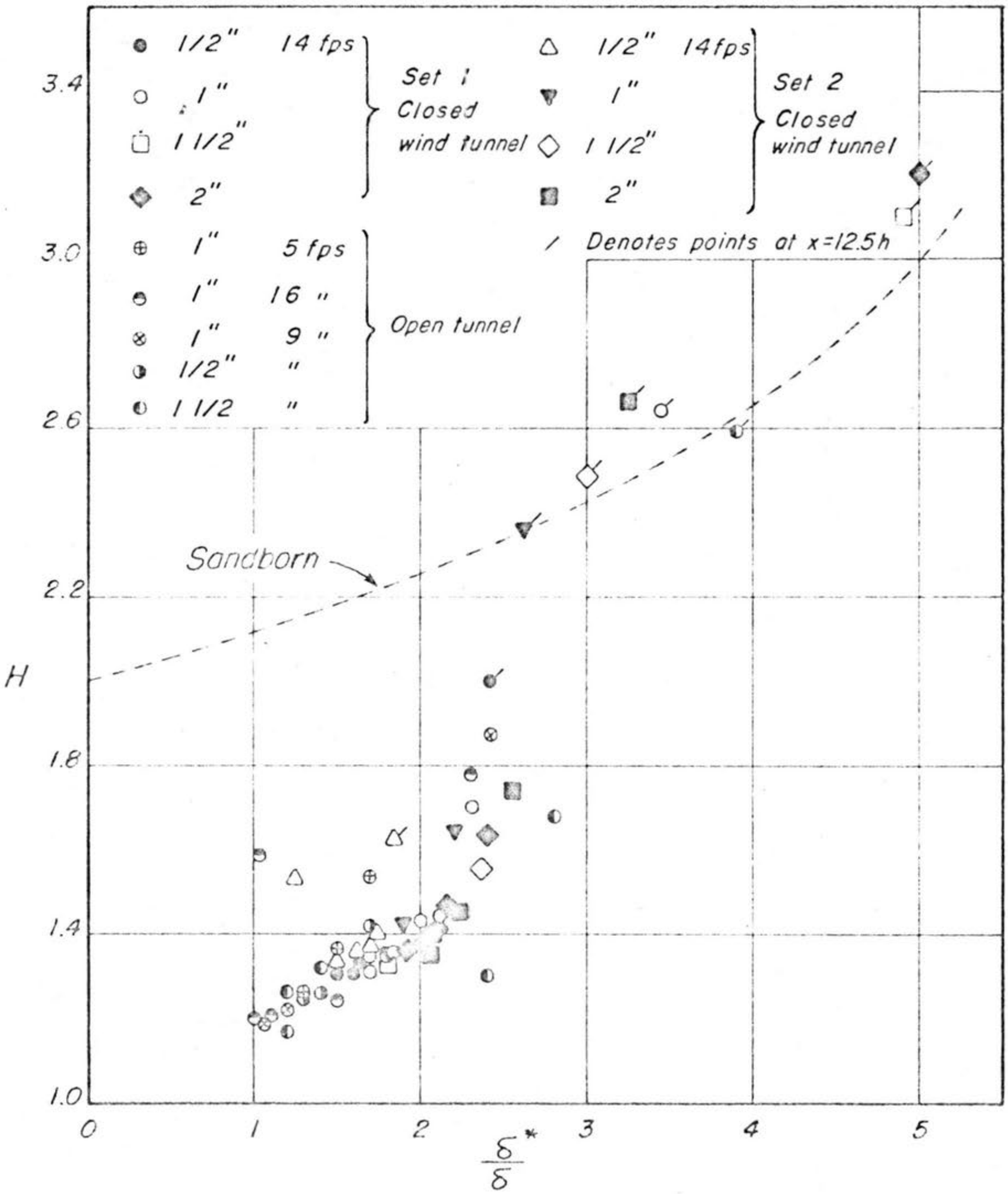

FIG. 6-3 APPLICATION OF SANDBORN'S SEPARATION CRITERIUM TO REATTACHMENT

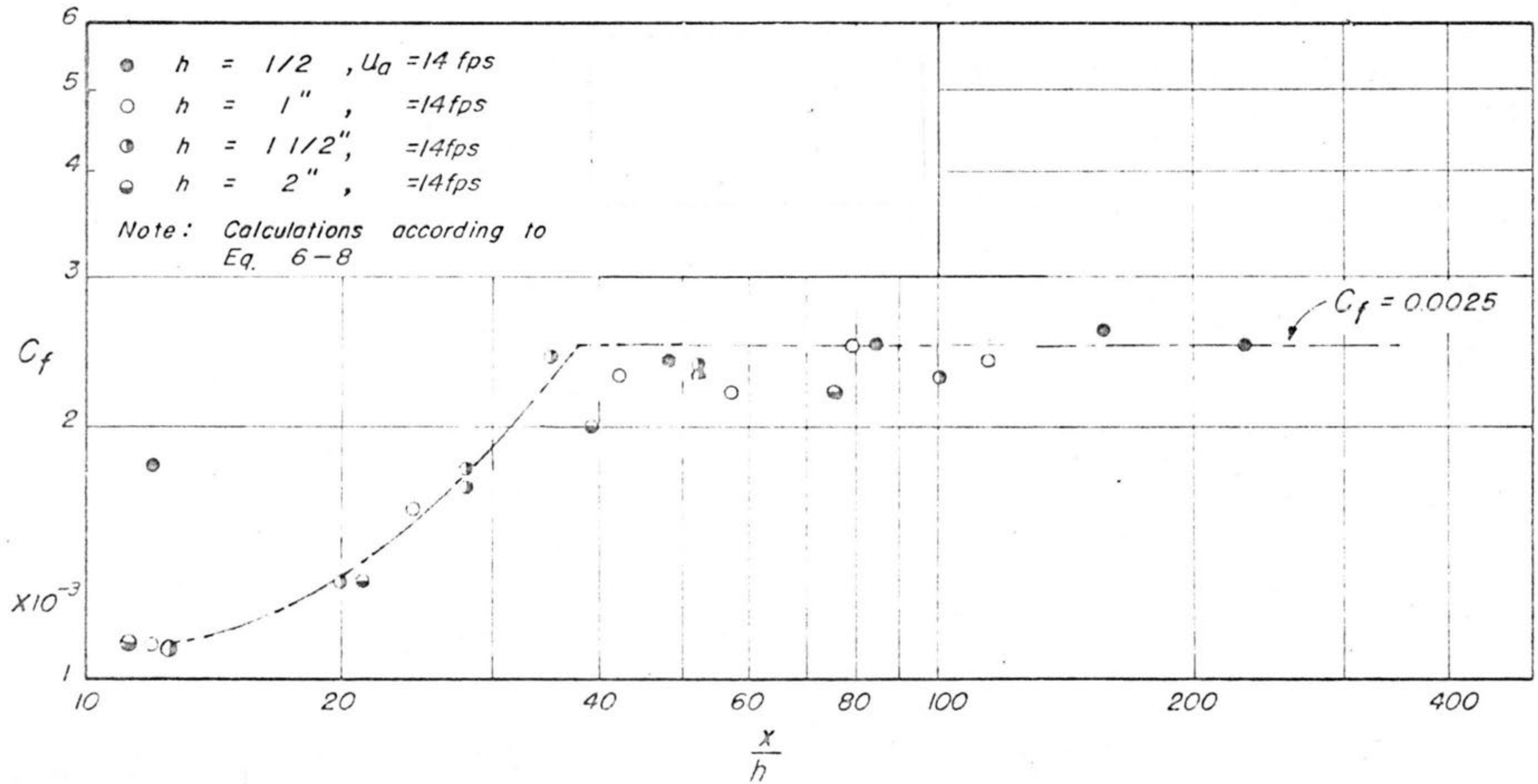

FIG. 6-4 FRICTION FACTOR C_f VS x/h

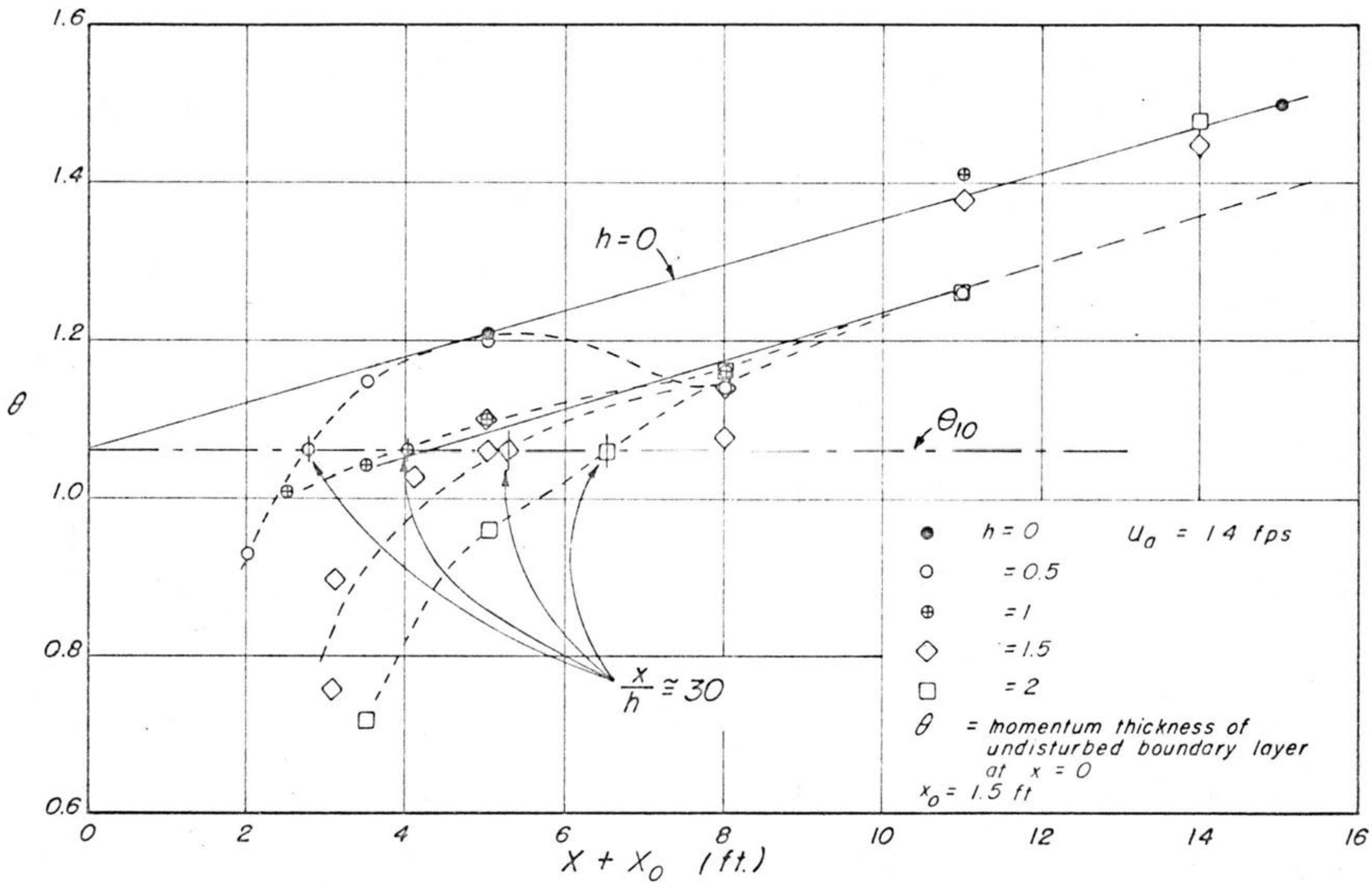

FIG. 6-5 MOMENTUM THICKNESS VS. DISTANCE FROM WALL

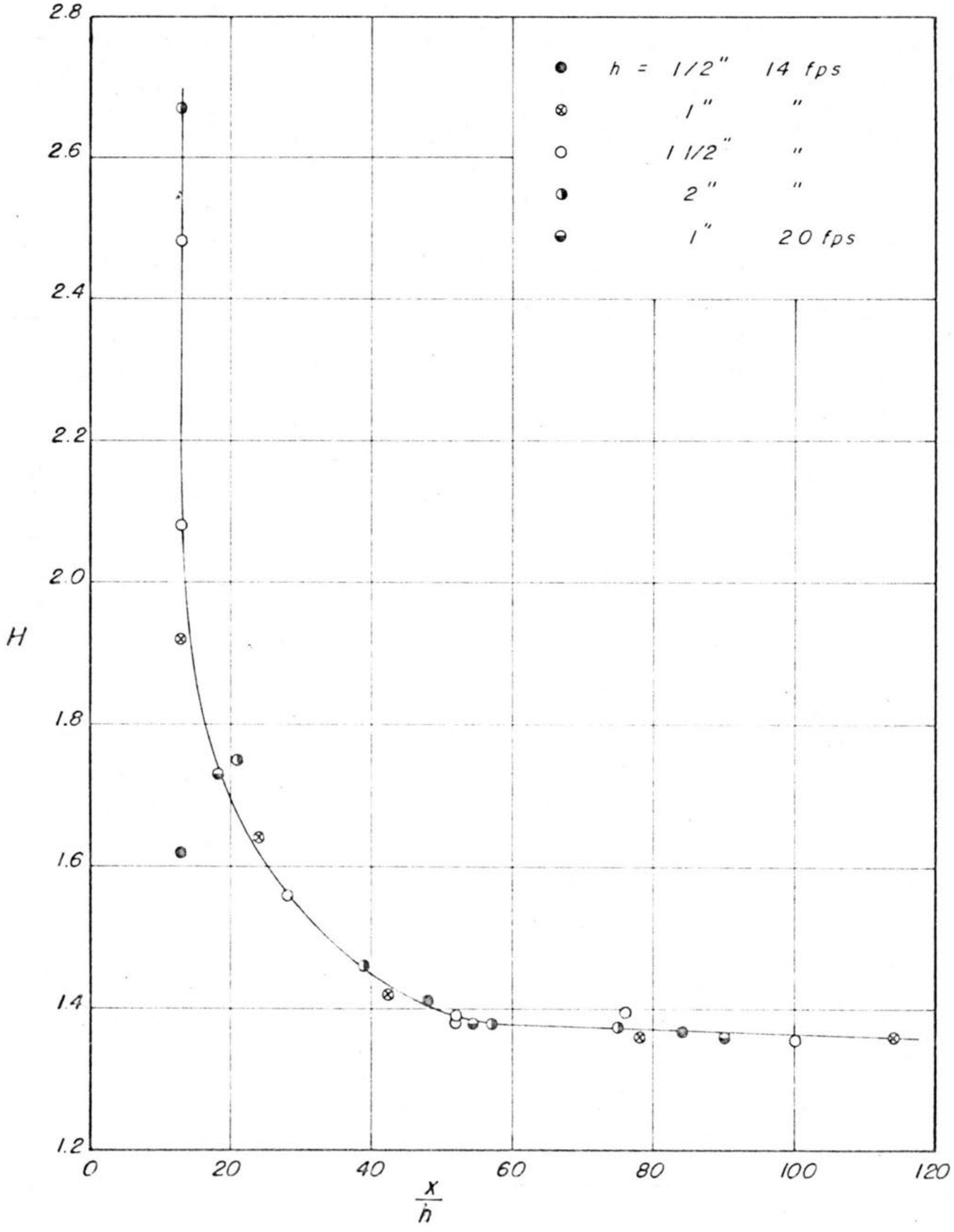

FIG. 6—6 SHAPE FACTOR AS FUNCTION OF DISTANCE FROM WALL

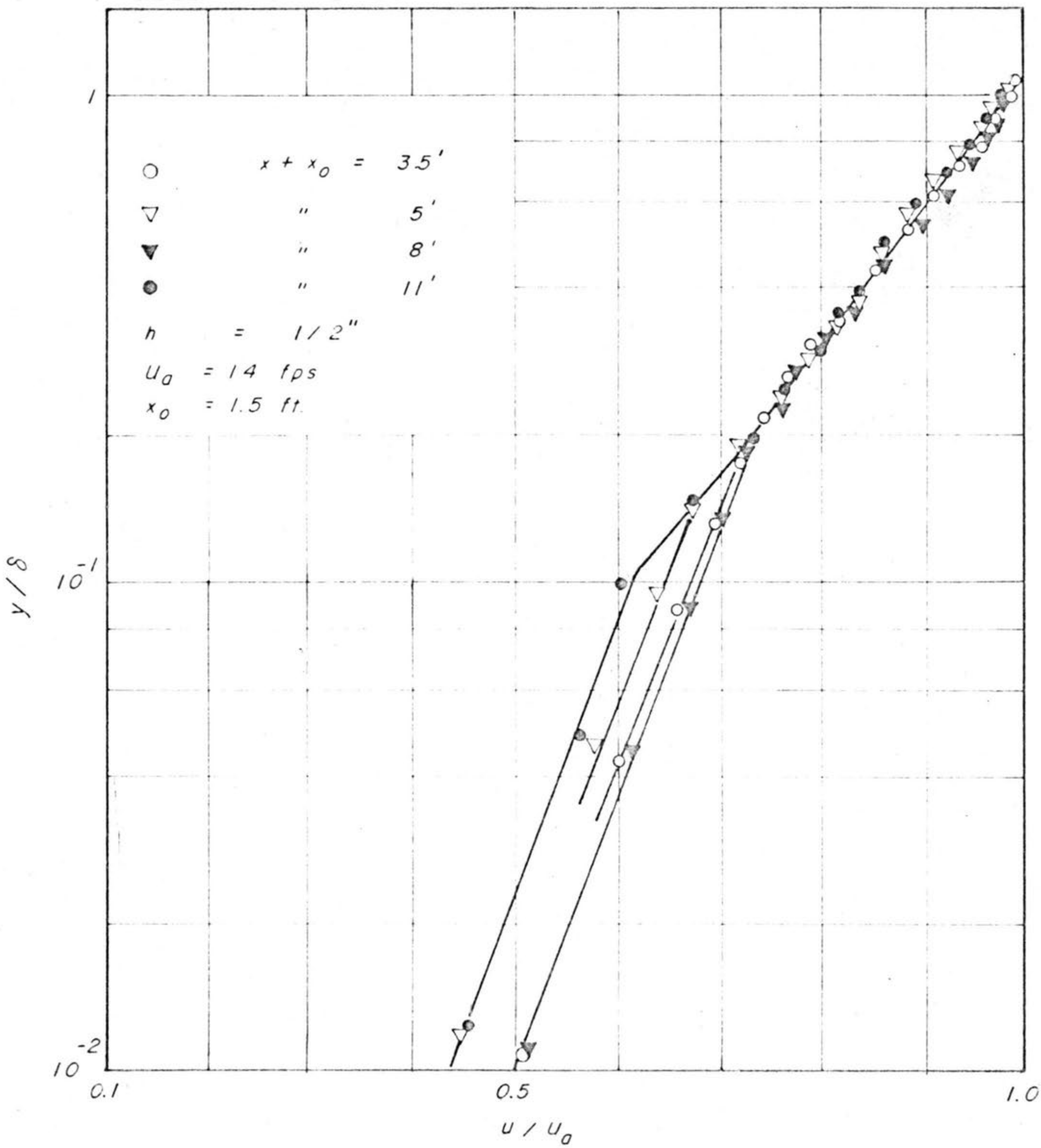

FIG. 6 - 7 DIMENSIONLESS VELOCITY PROFILES

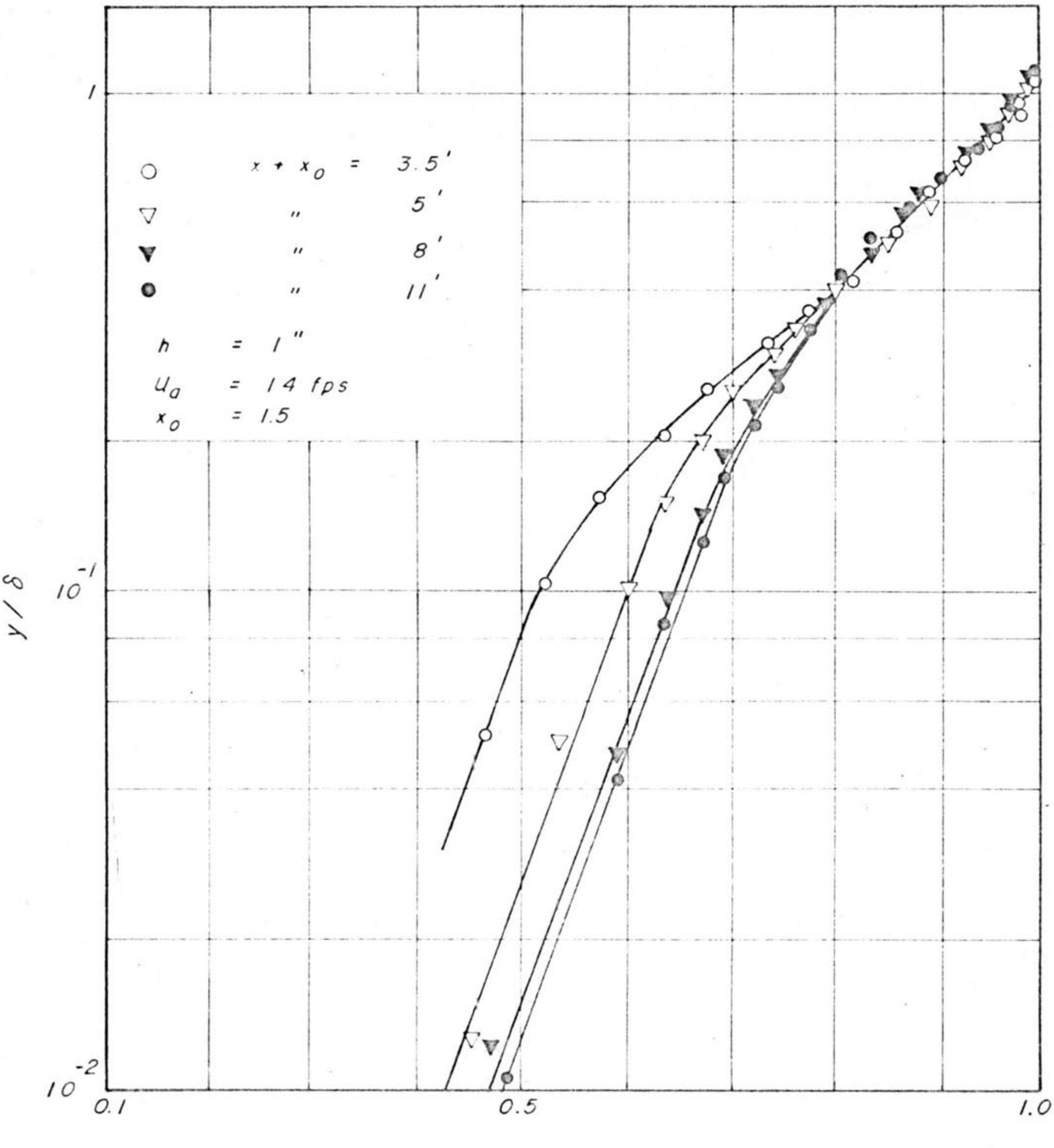

FIG. 6 — 8 DIMENSIONLESS VELOCITY PROFILES

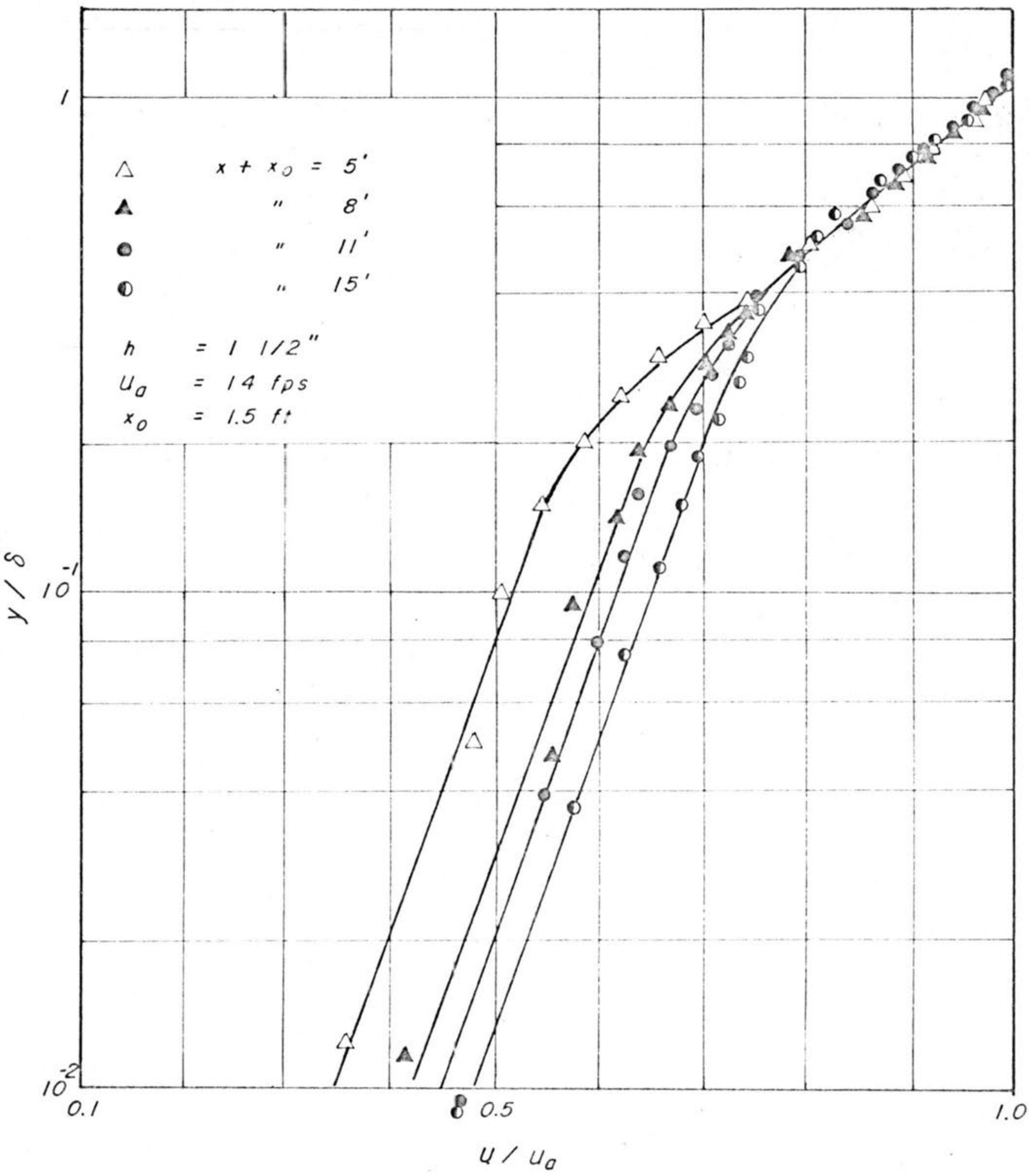

FIG. 6 – 9 DIMENSIONLESS VELOCITY PROFILES

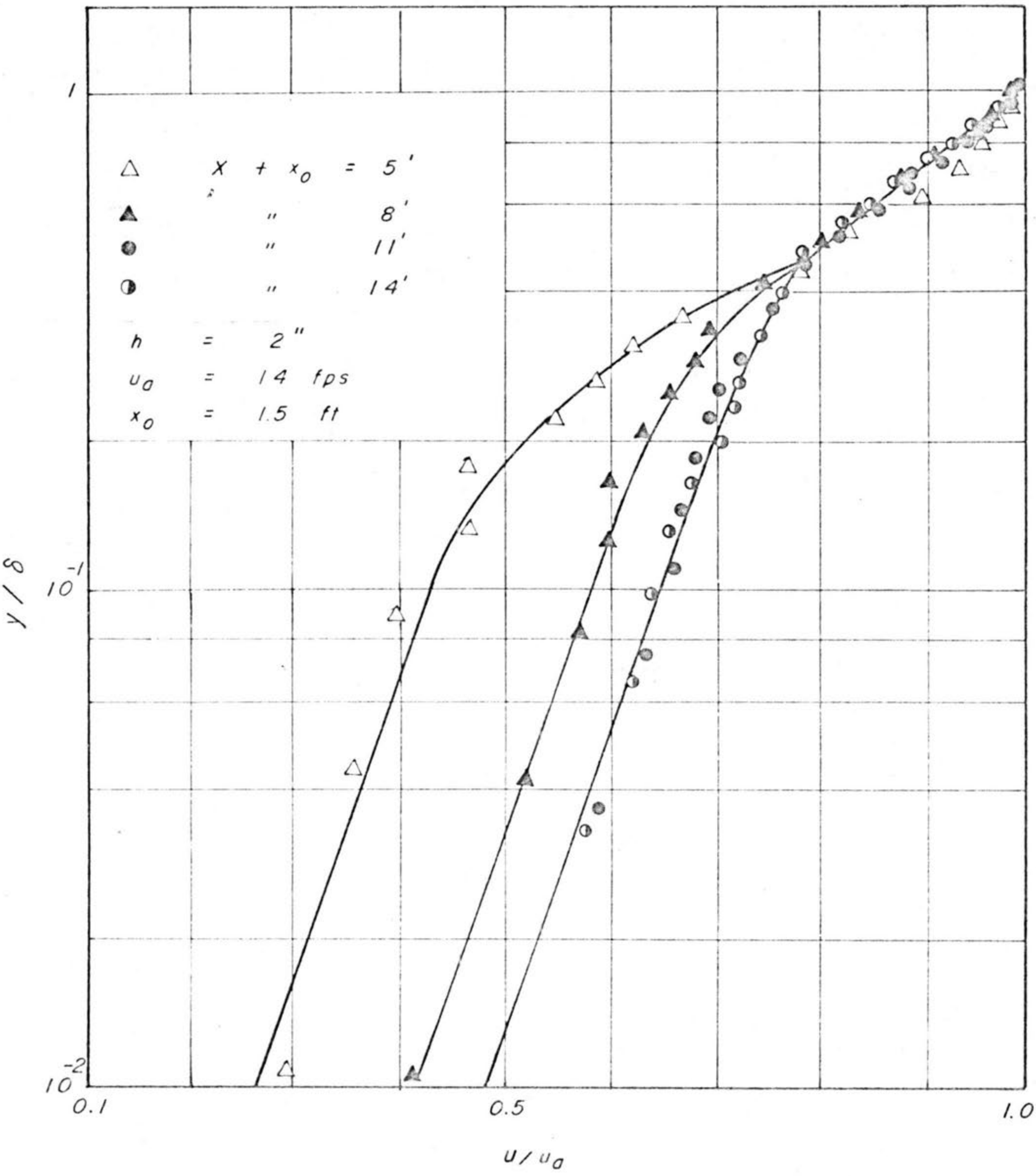

FIG. 6-10 DIMENSIONLESS VELOCITY PROFILES

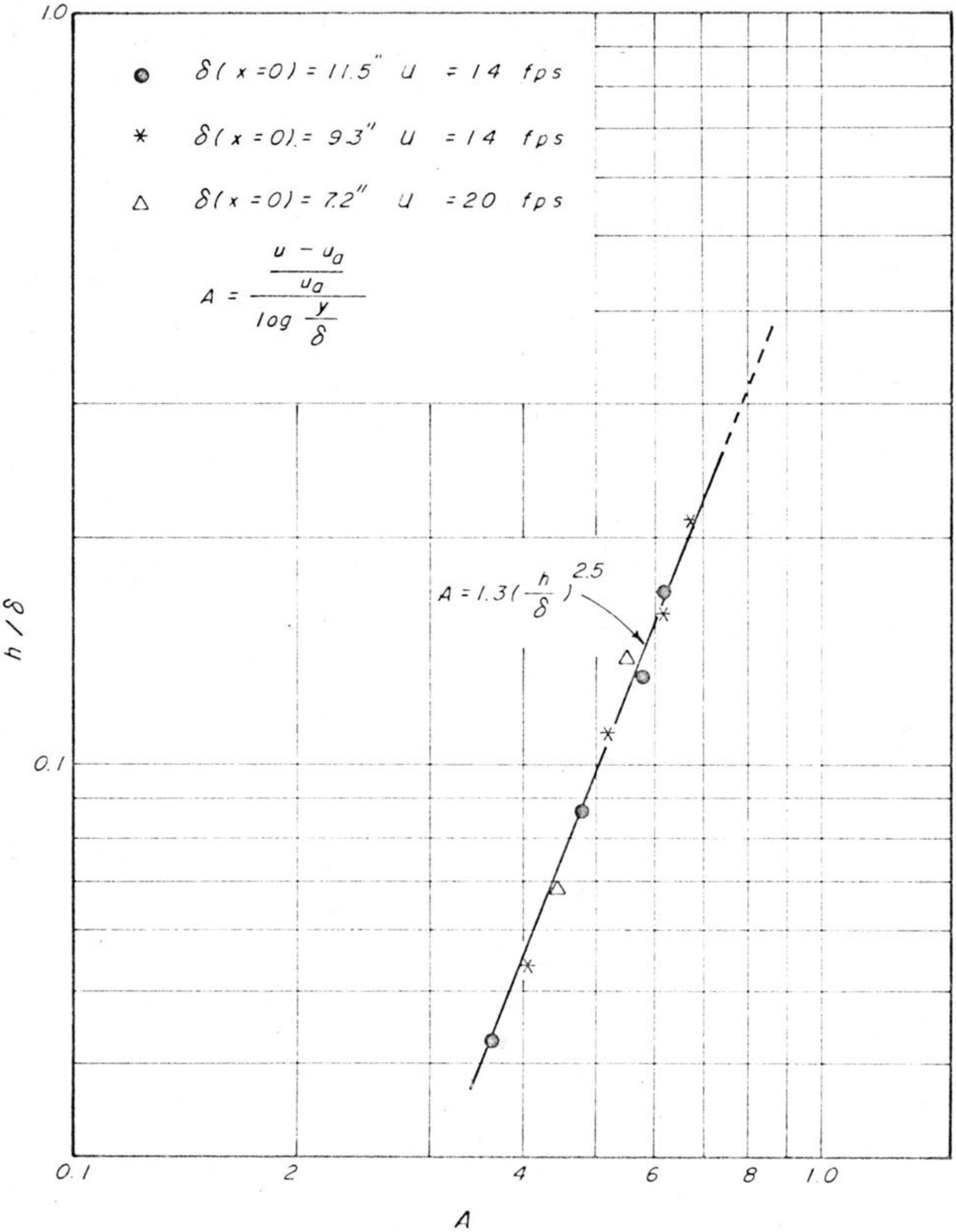

FIG. 6-11 OUTER PROFILE, A vs h/δ

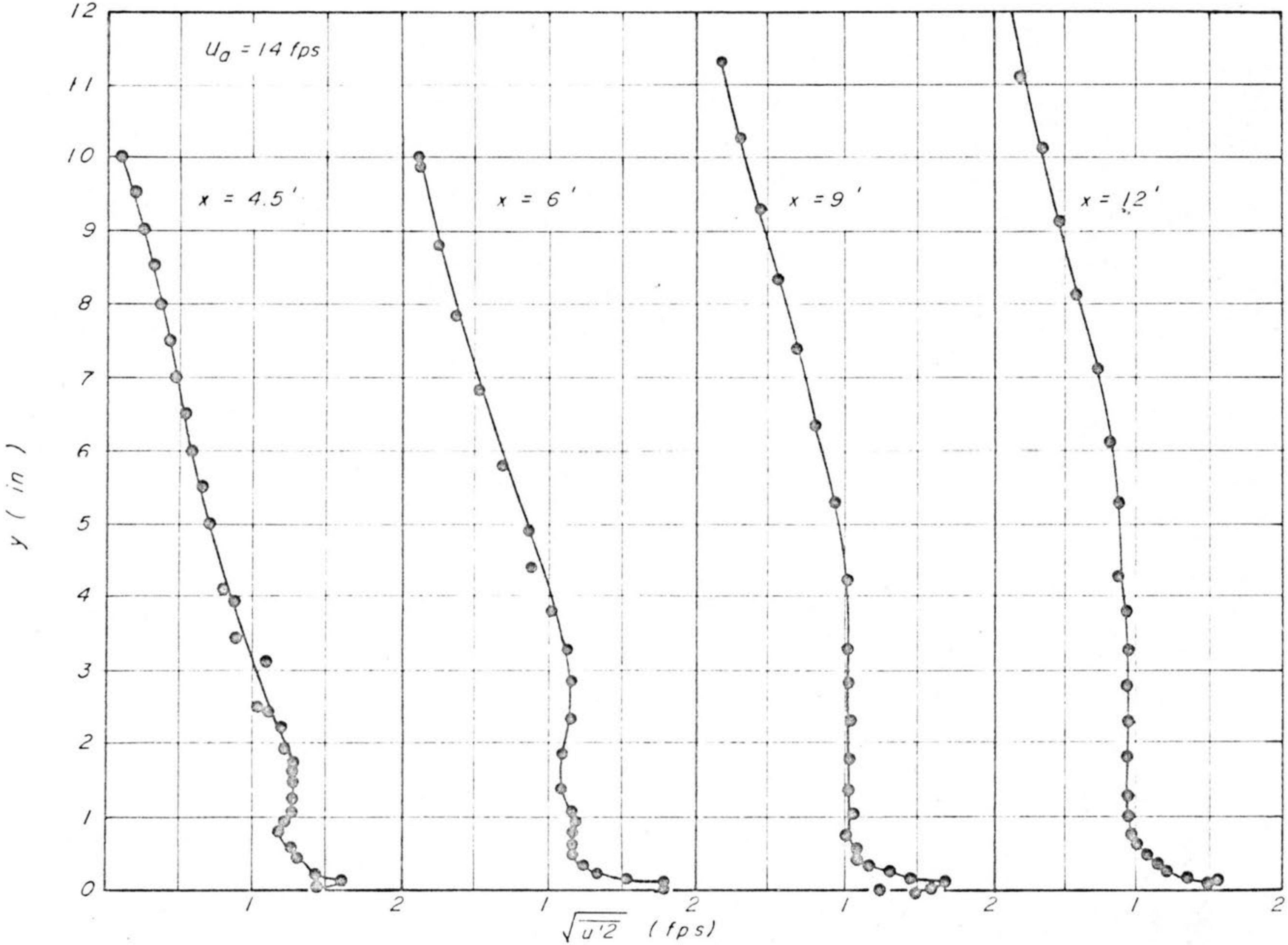

FIG. 6-12 TURBULENT INTENSITY DISTRIBUTIONS, h = 1/2"

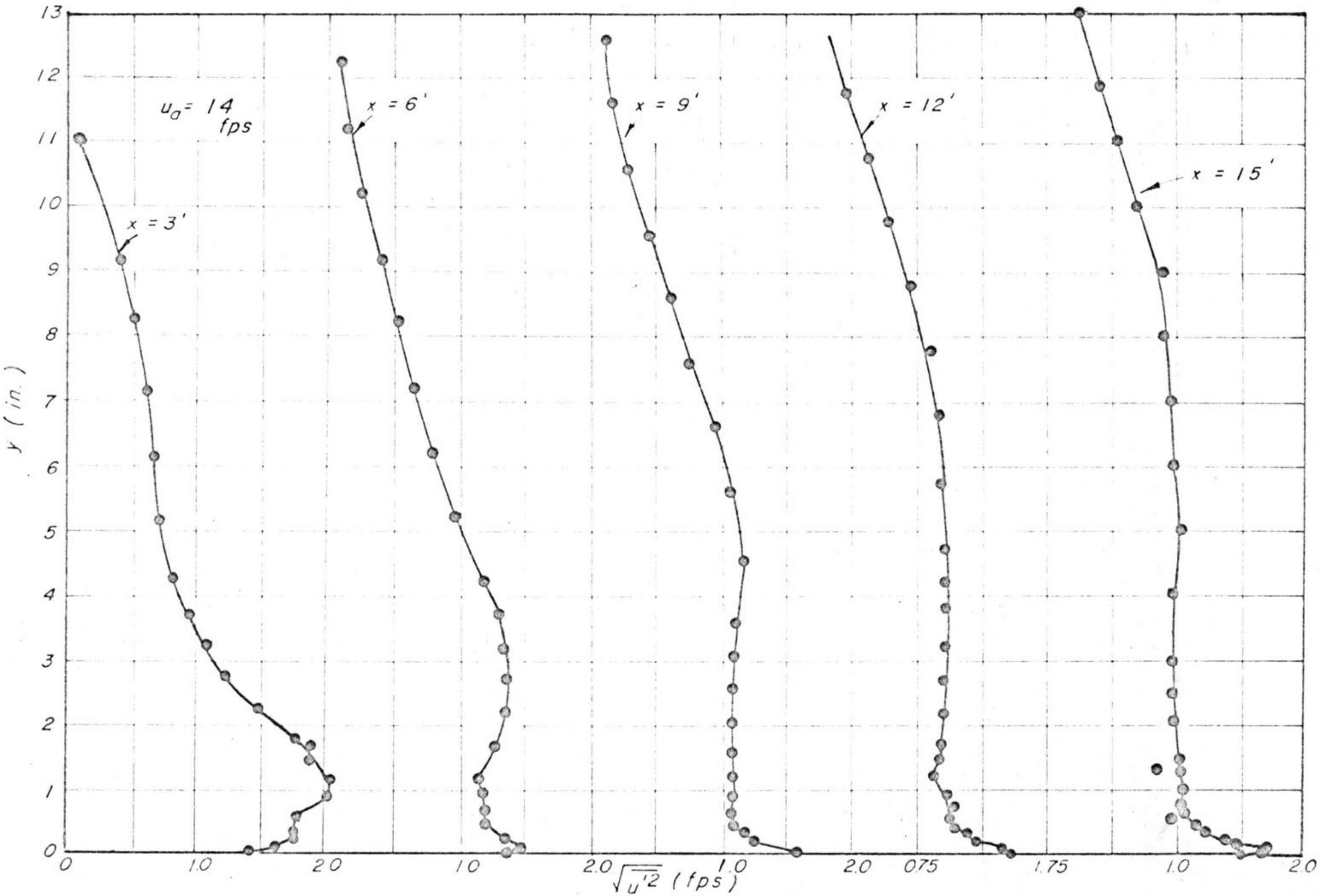

FIG. 6 - 13 TURBULENT INTENSITY DISTRIBUTIONS, h = 1"

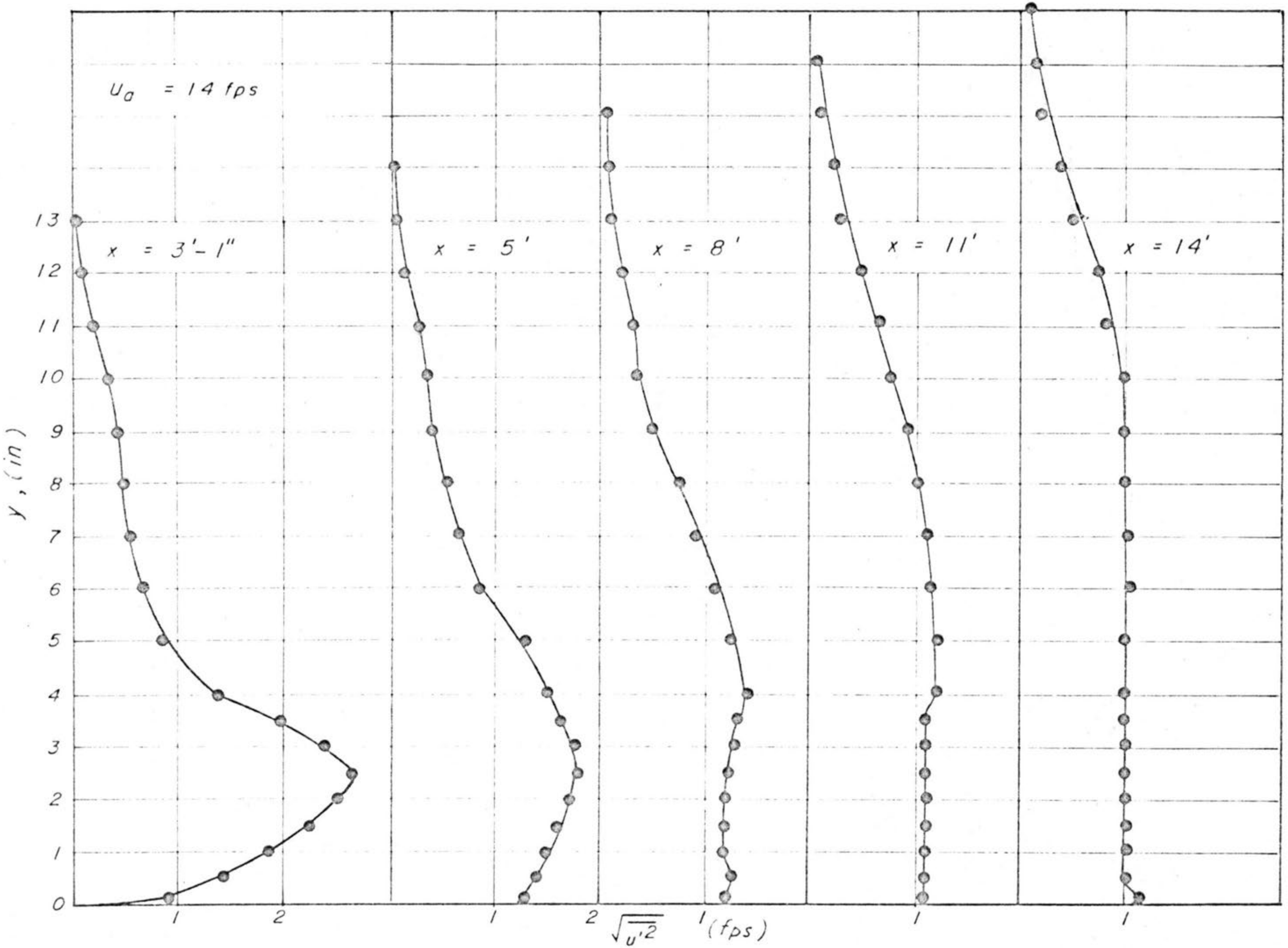

FIG. 6-14 TURBULENT INTENSITY DISTRIBUTIONS, h = 1.5"

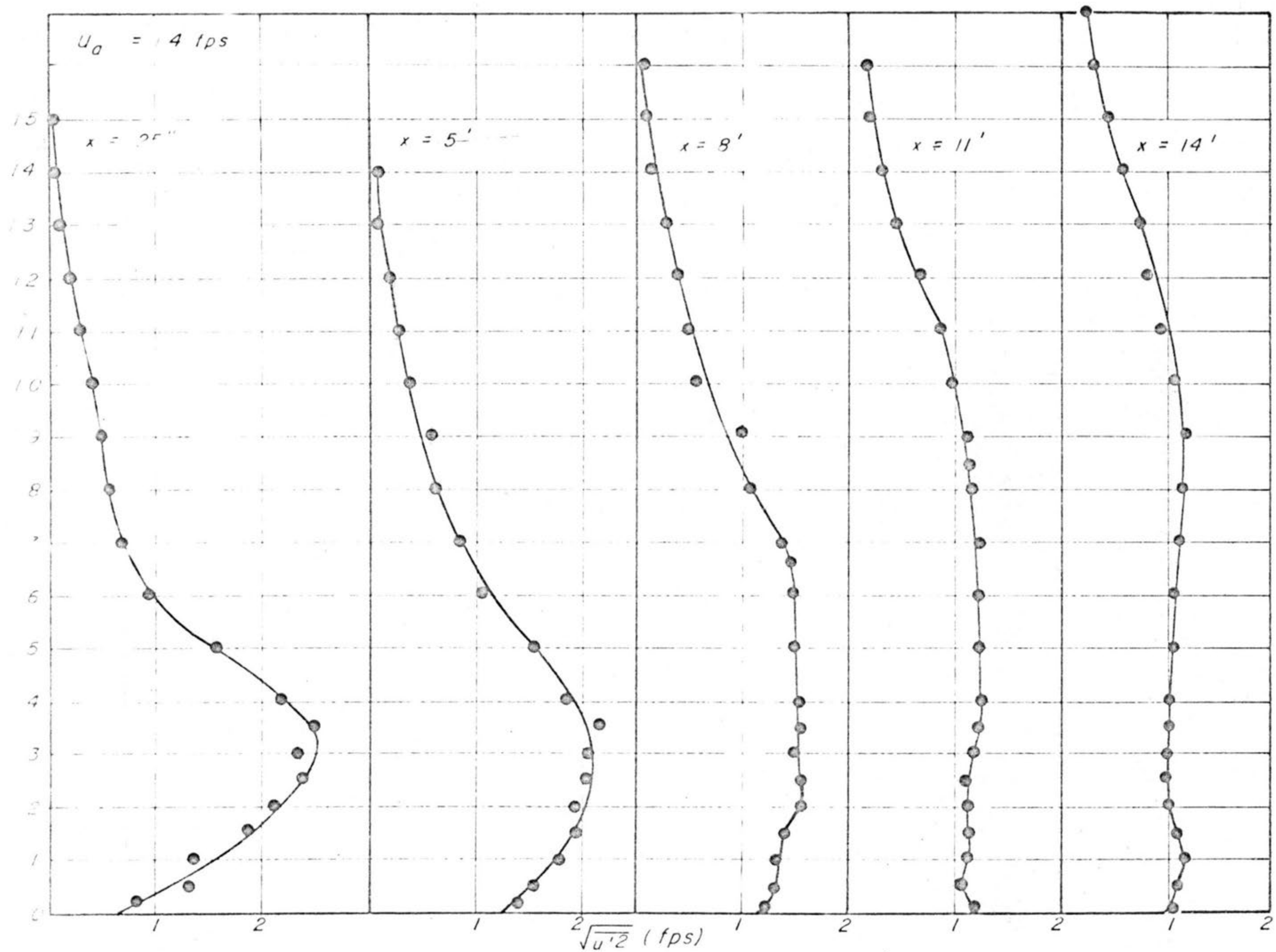

FIG. 6-15 TURBULENT INTENSITY DISTRIBUTIONS, h = 2"

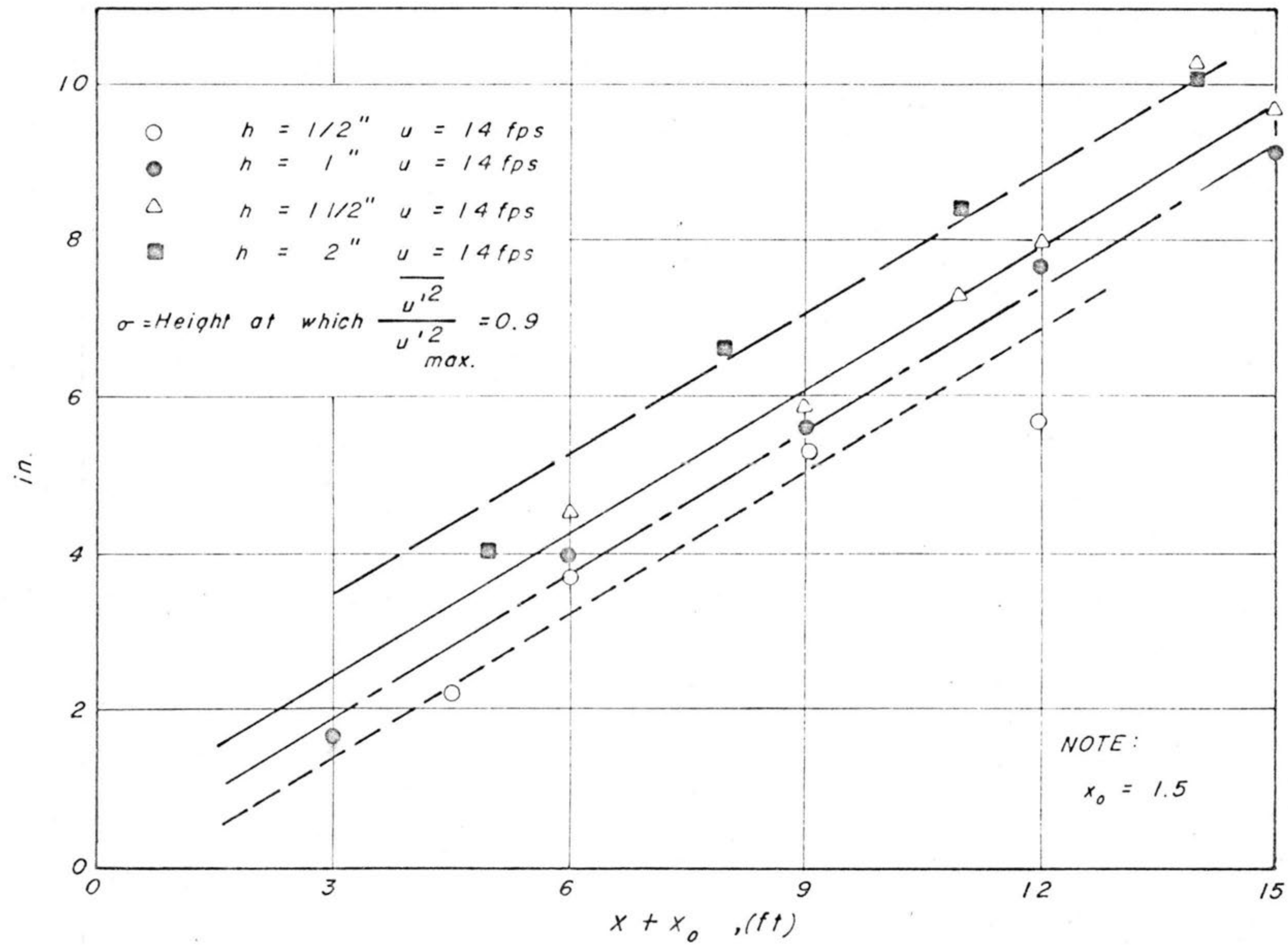

FIG. 6-16 SPREADING OF WALL GENERATED TURBULENCE

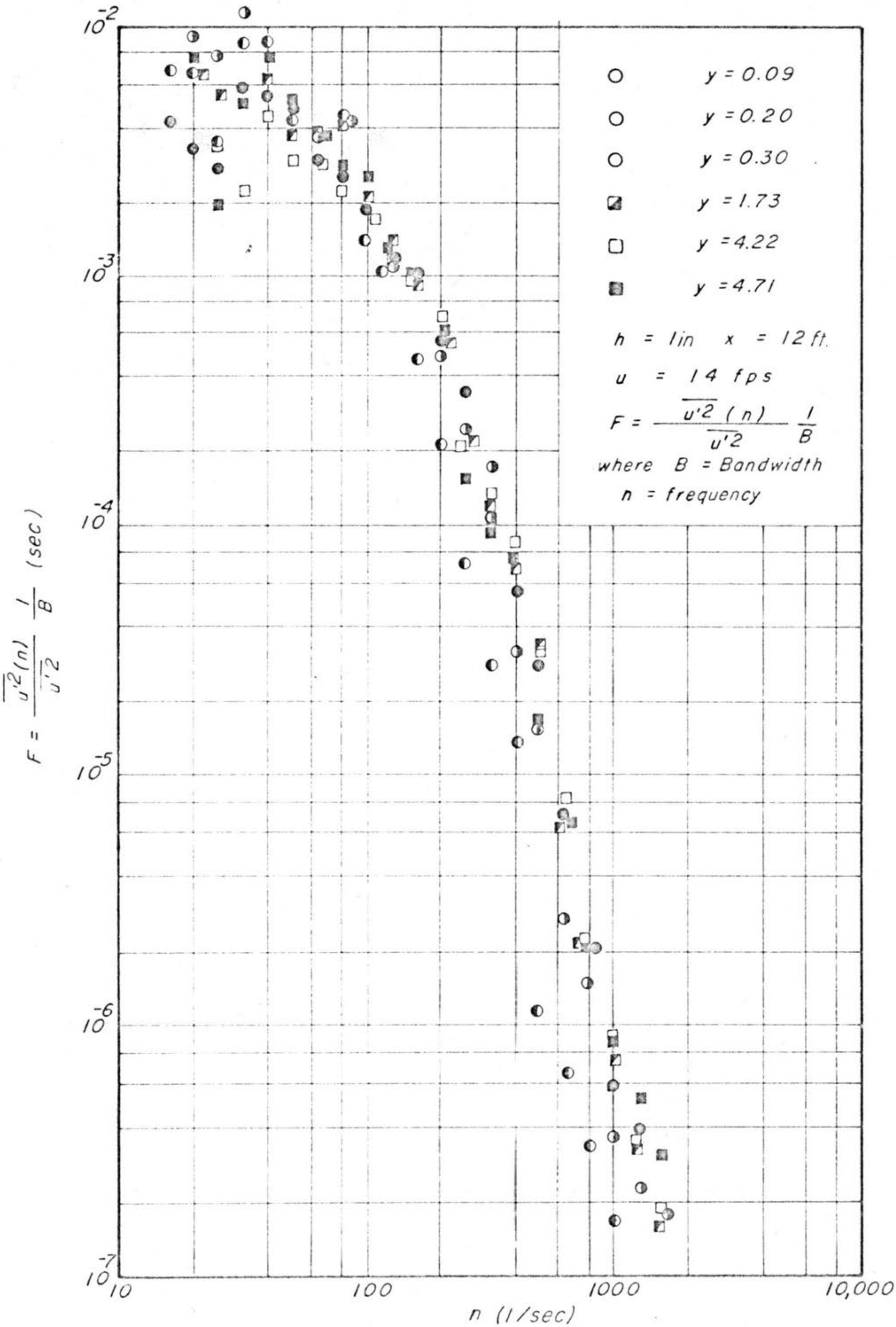

FIG. 6 – 17 TYPICAL INTENSITY SPECTRA

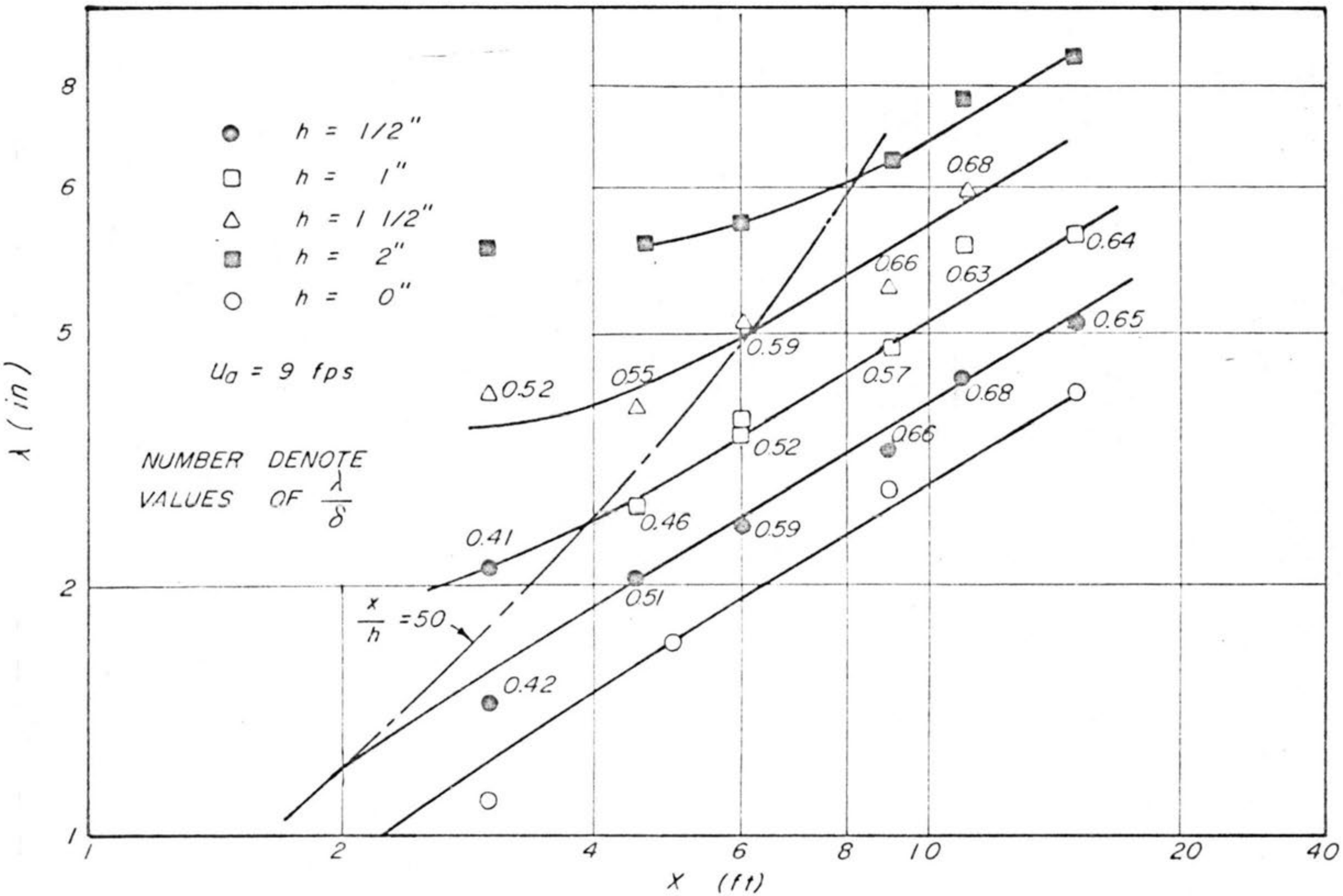

FIG. 6 – 18 PLUME WIDTH λ AS FUNCTION OF x

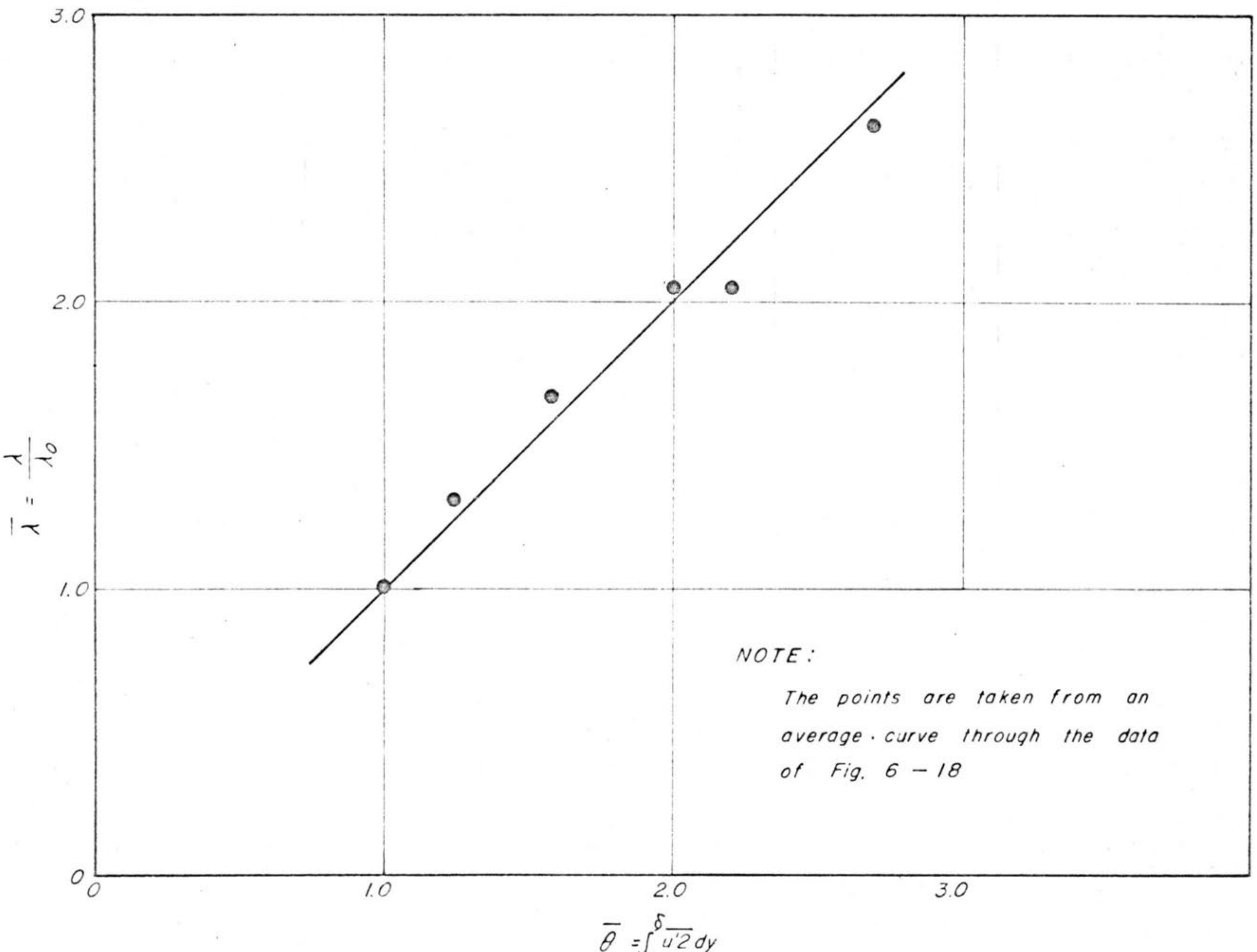

FIG. 6–19 DEPENDENCY OF RELATIVE PLUME SPREAD ON TURBULENCE

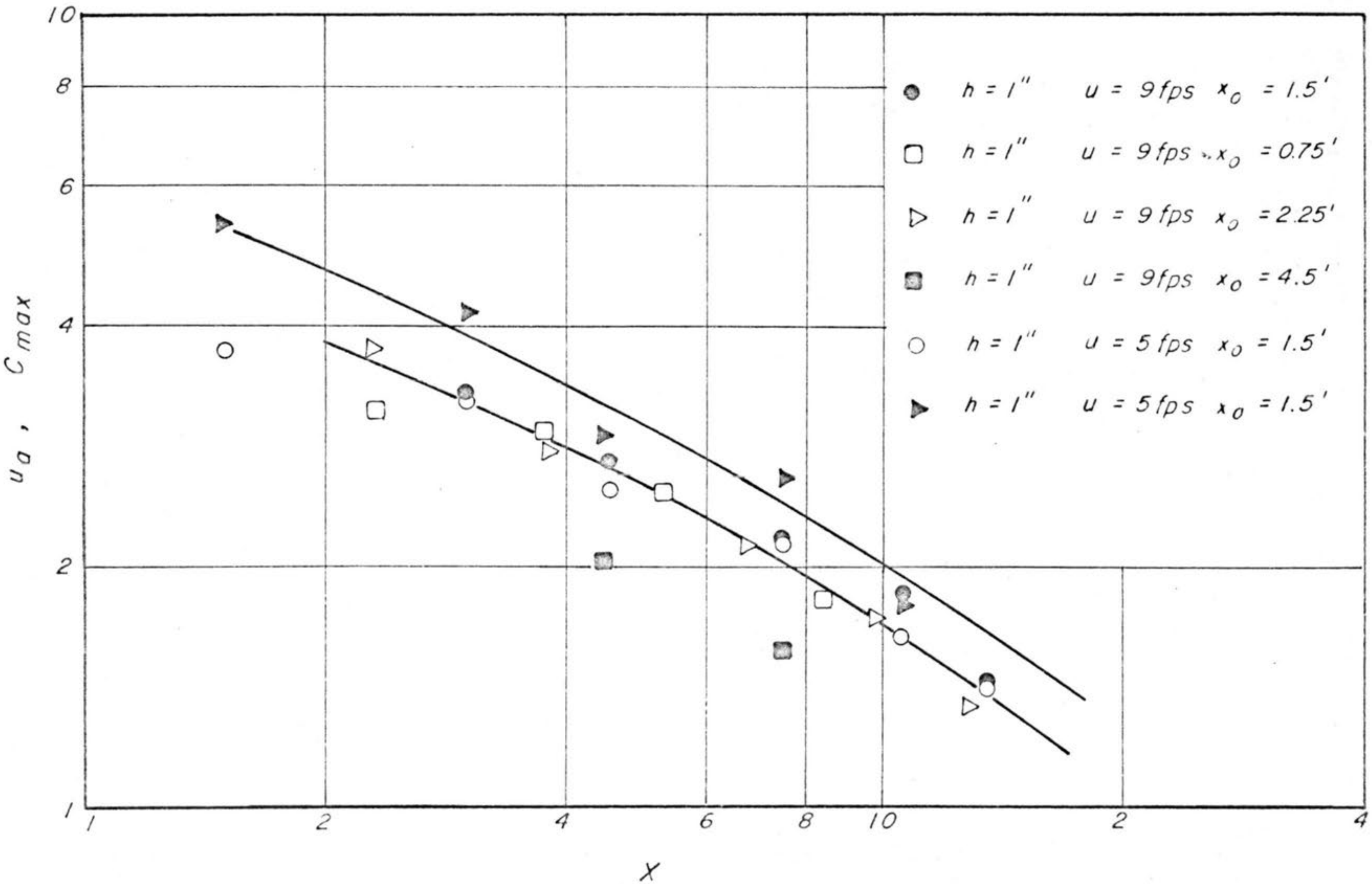

FIG. 6 – 20 MAXIMUM CONCENTRATION AS FUNCTION OF x

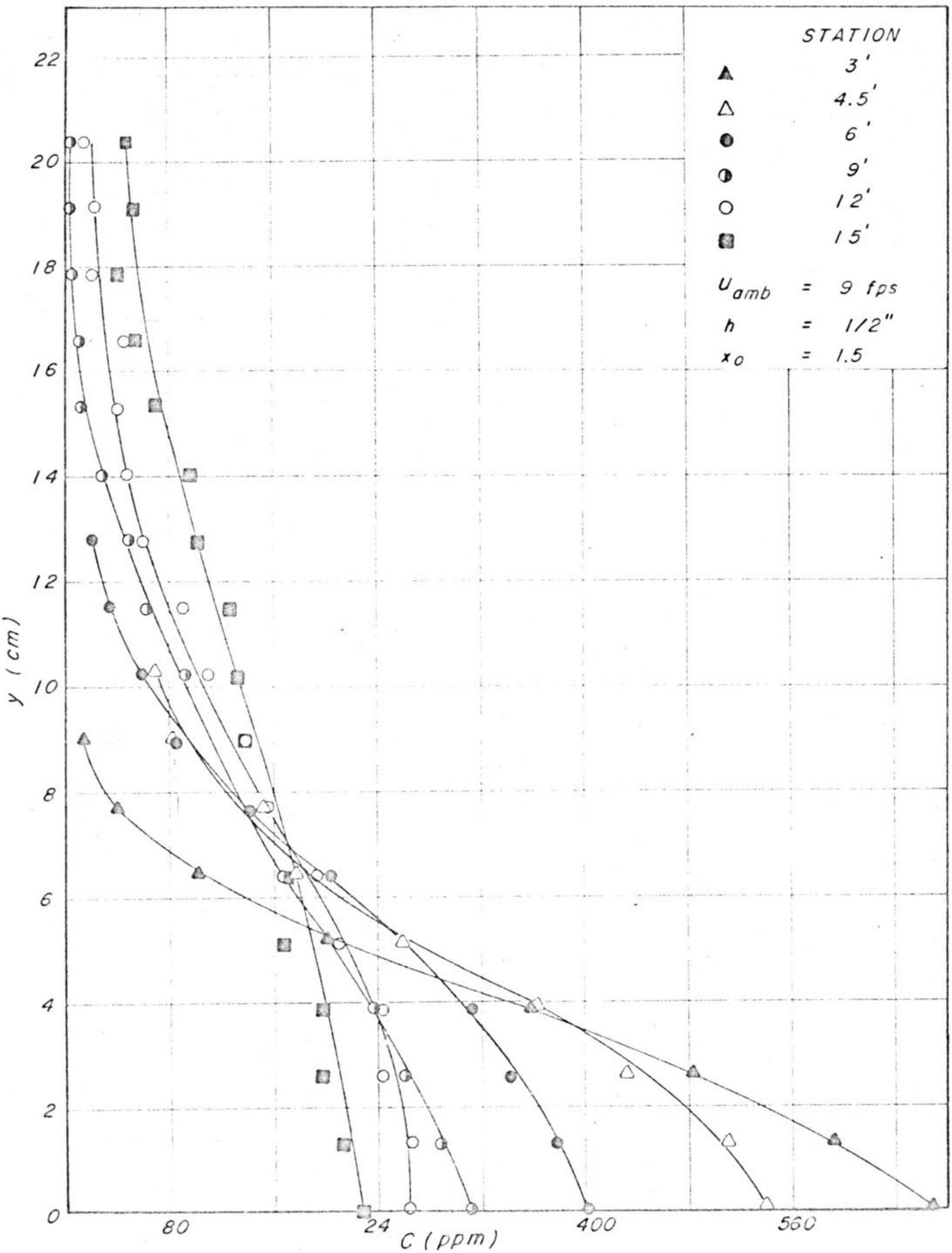

FIG. 6-21 CONCENTRATION PROFILES

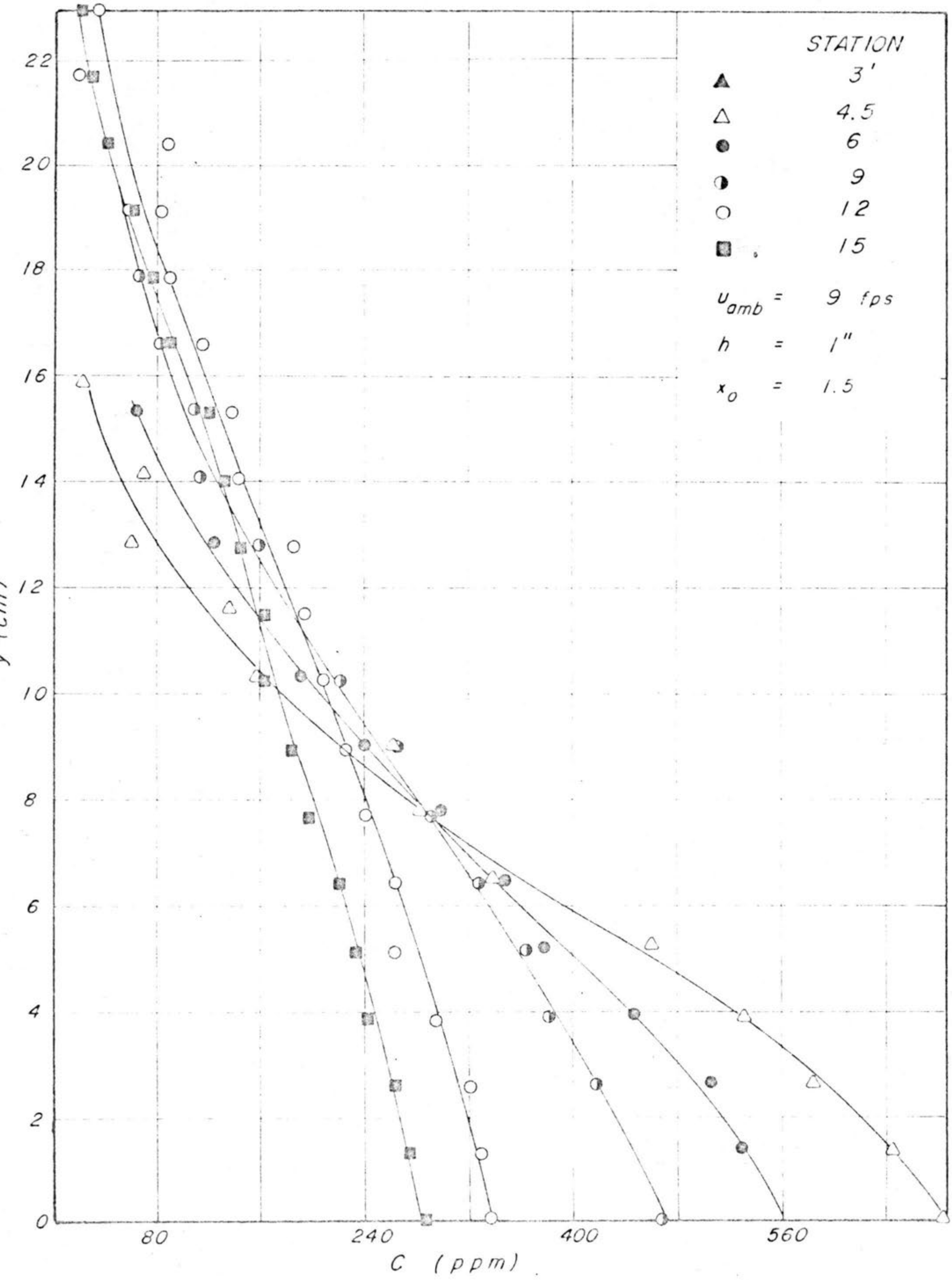

FIG. 6-22 CONCENTRATION PROFILES

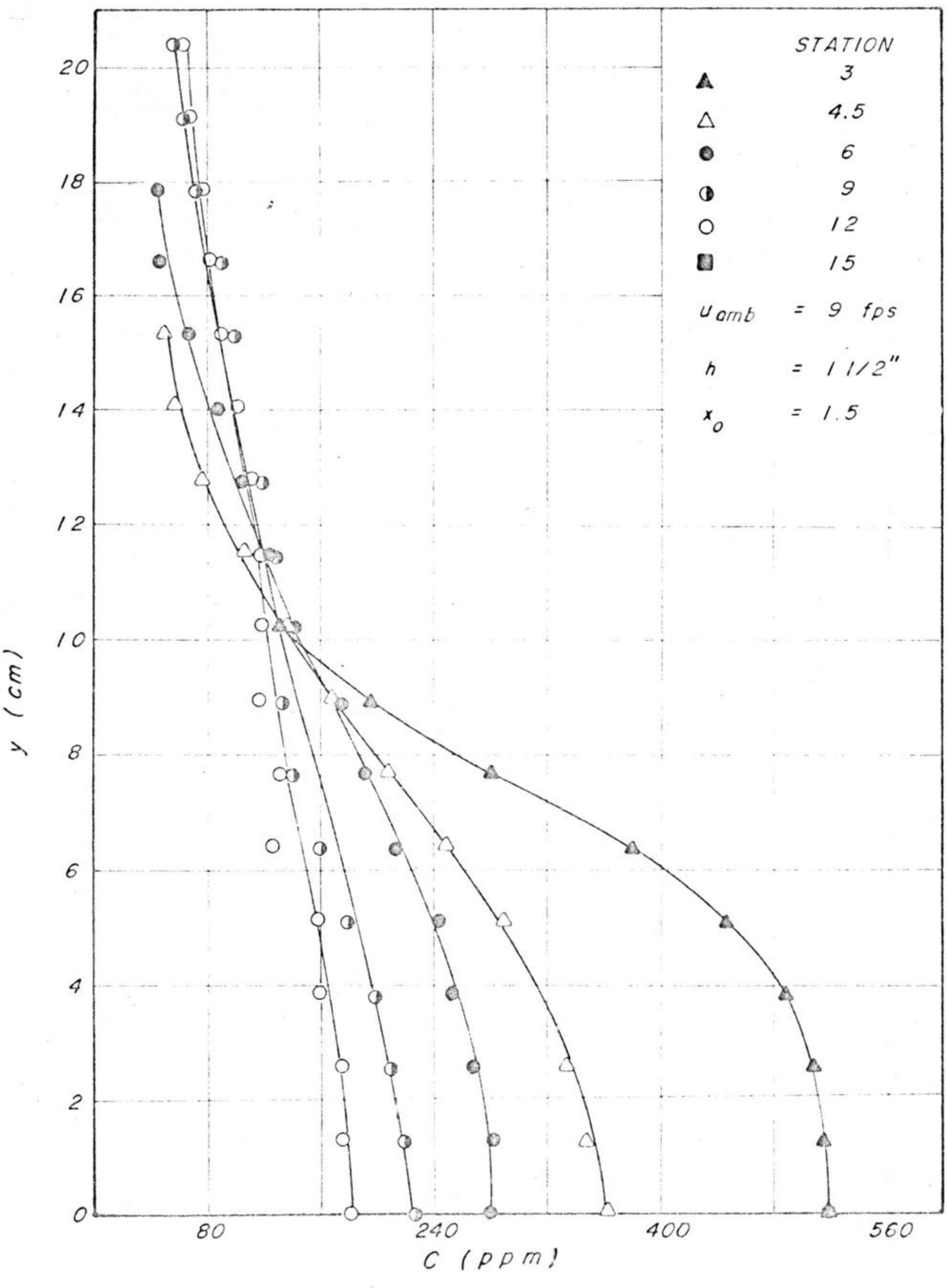

FIG. 6 - 23 CONCENTRATION PROFILES

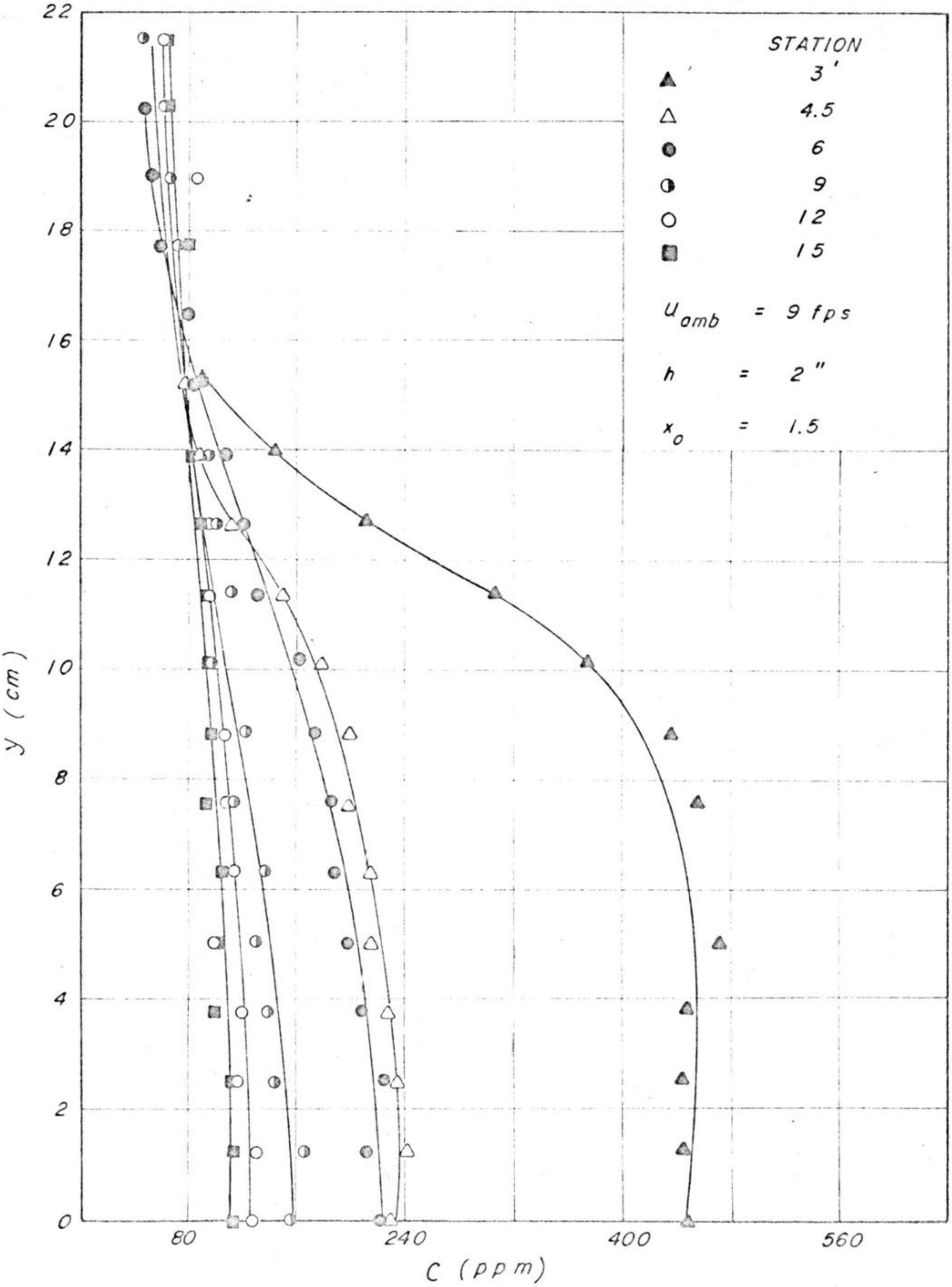

FIG. 6-24 CONCENTRATION PROFILES

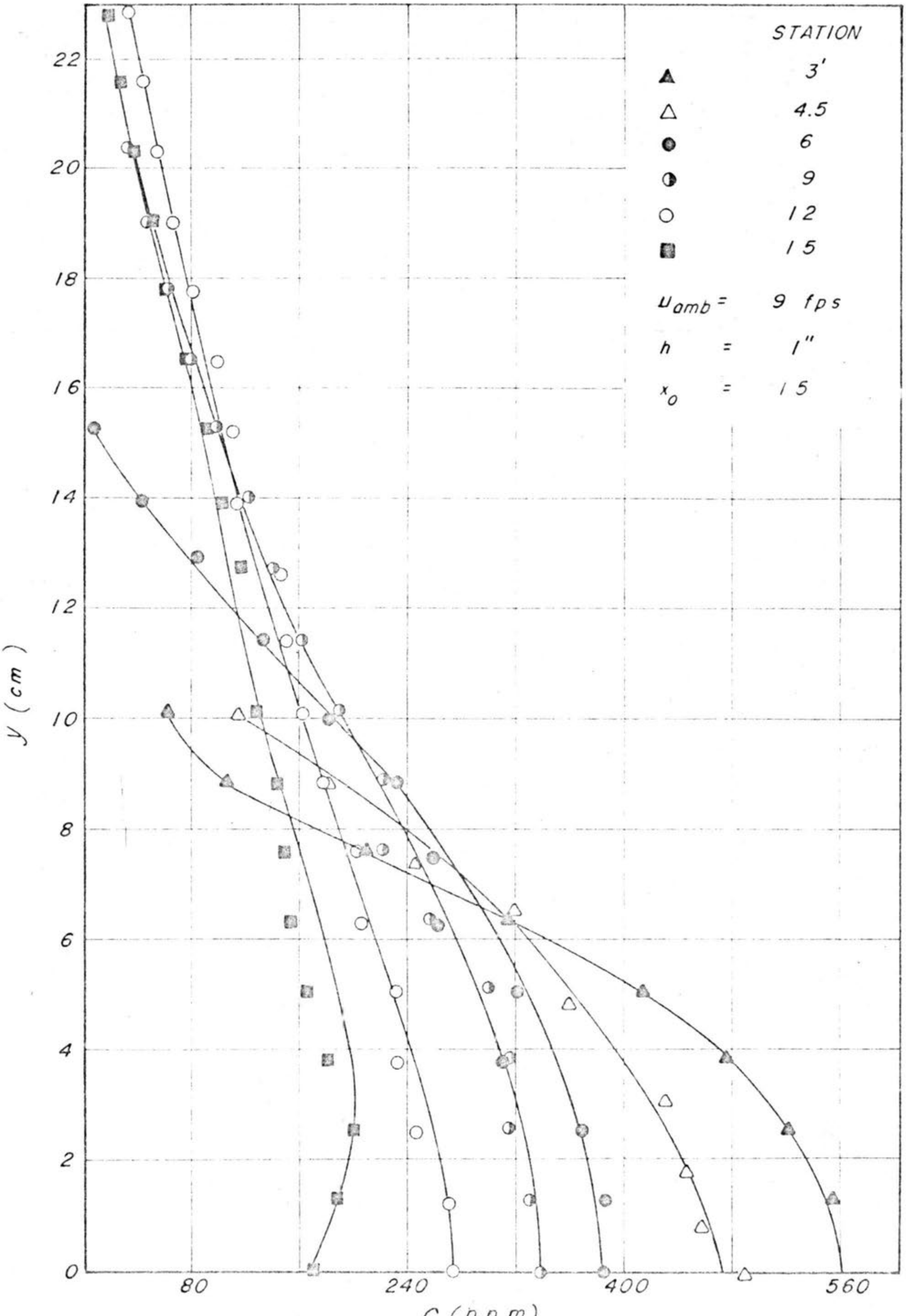

FIG. 6-25 CONCENTRATION PROFILES

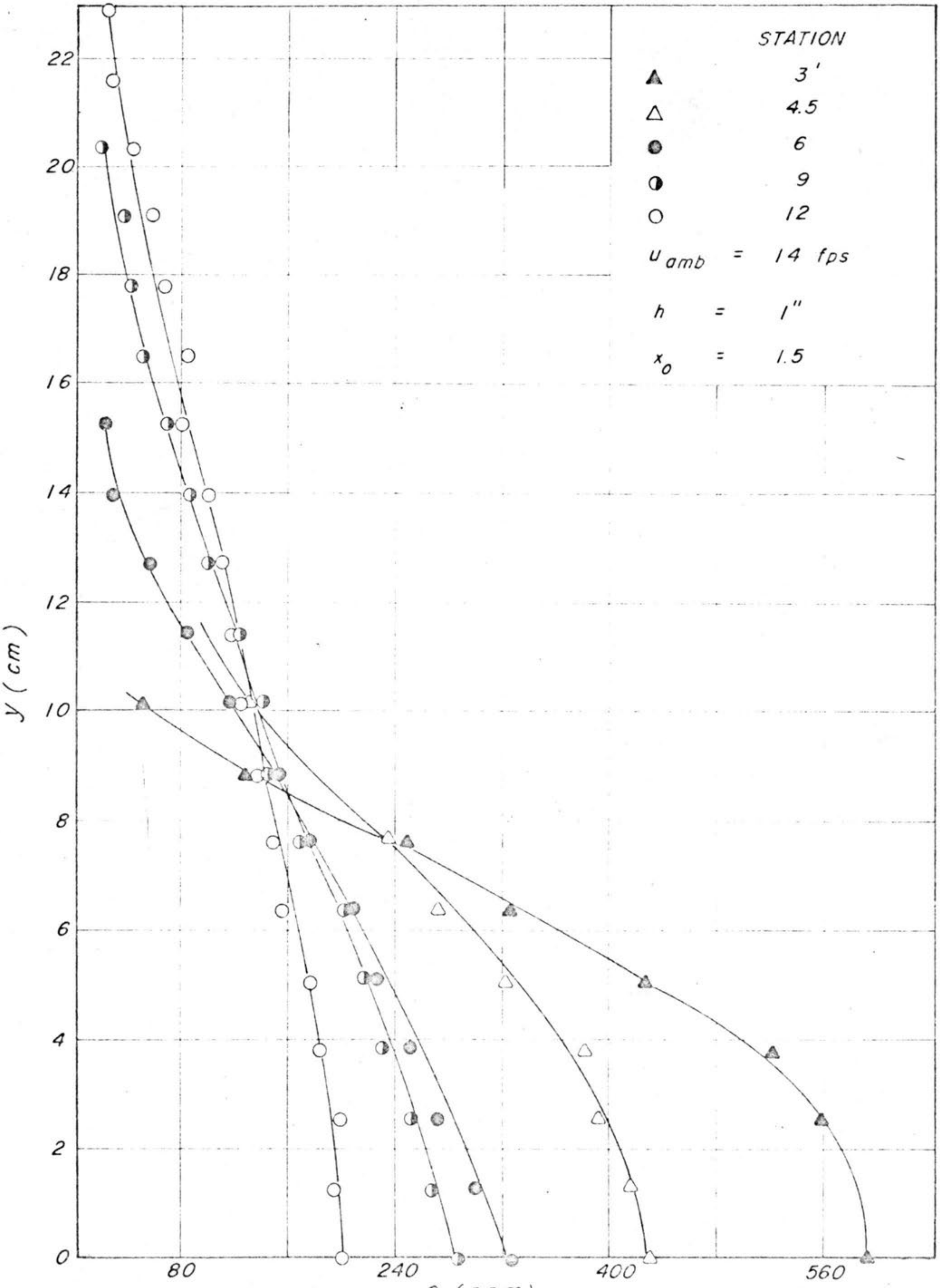

FIG. 6 – 26 CONCENTRATION PROFILES

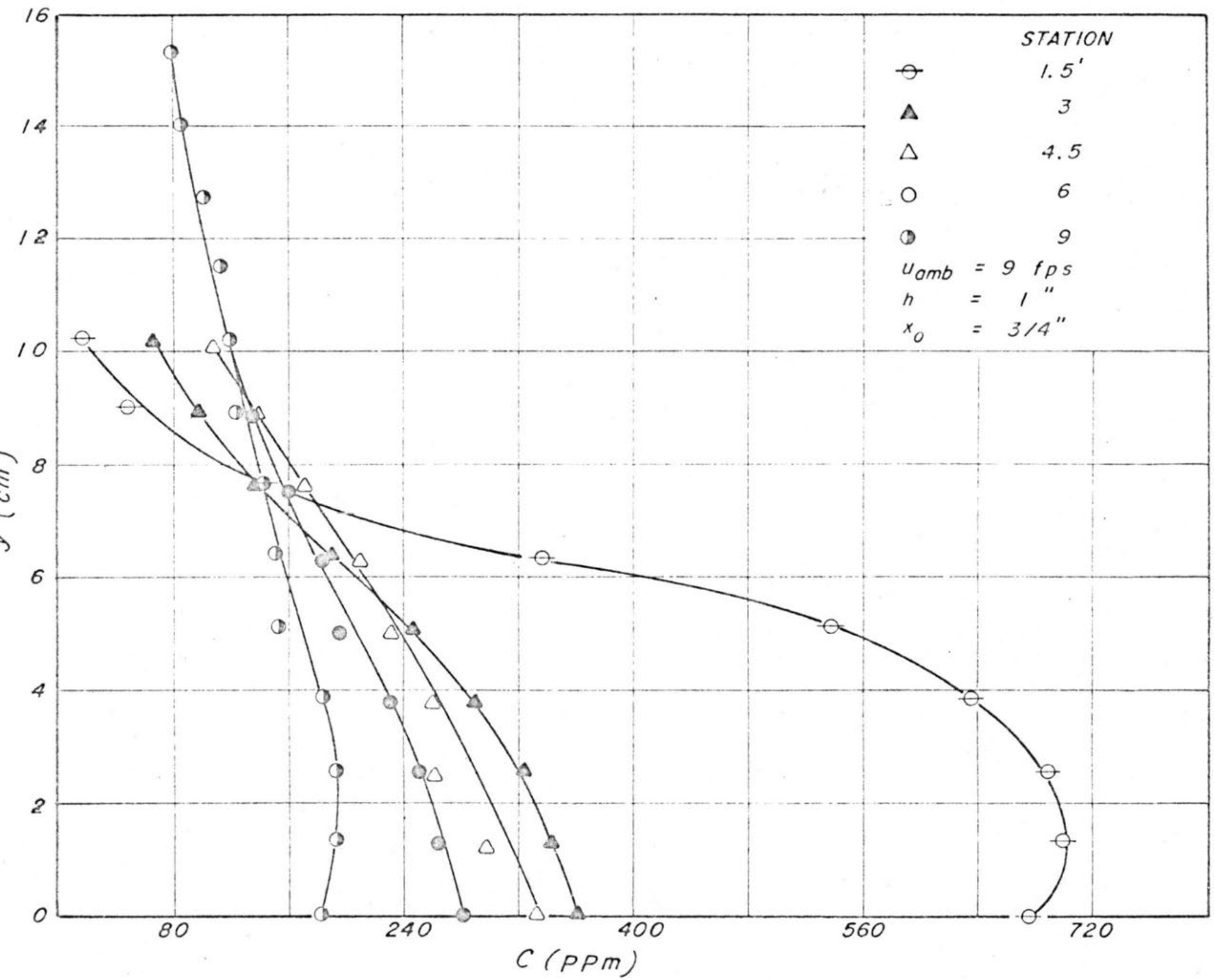

FIG. 6-27 CONCENTRATION PROFILES

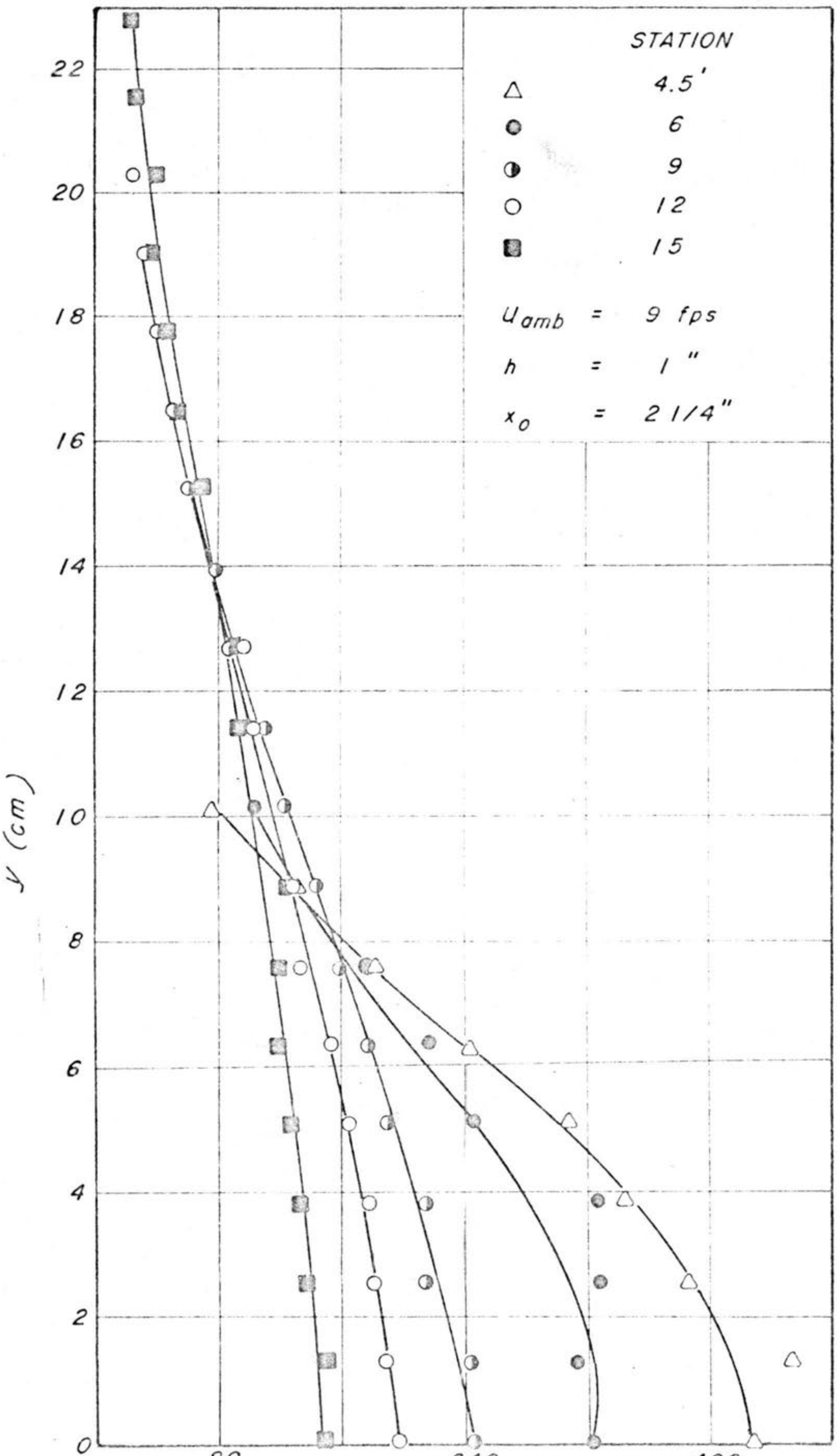

FIG. 6 – 28 CONCENTRATION PROFILE

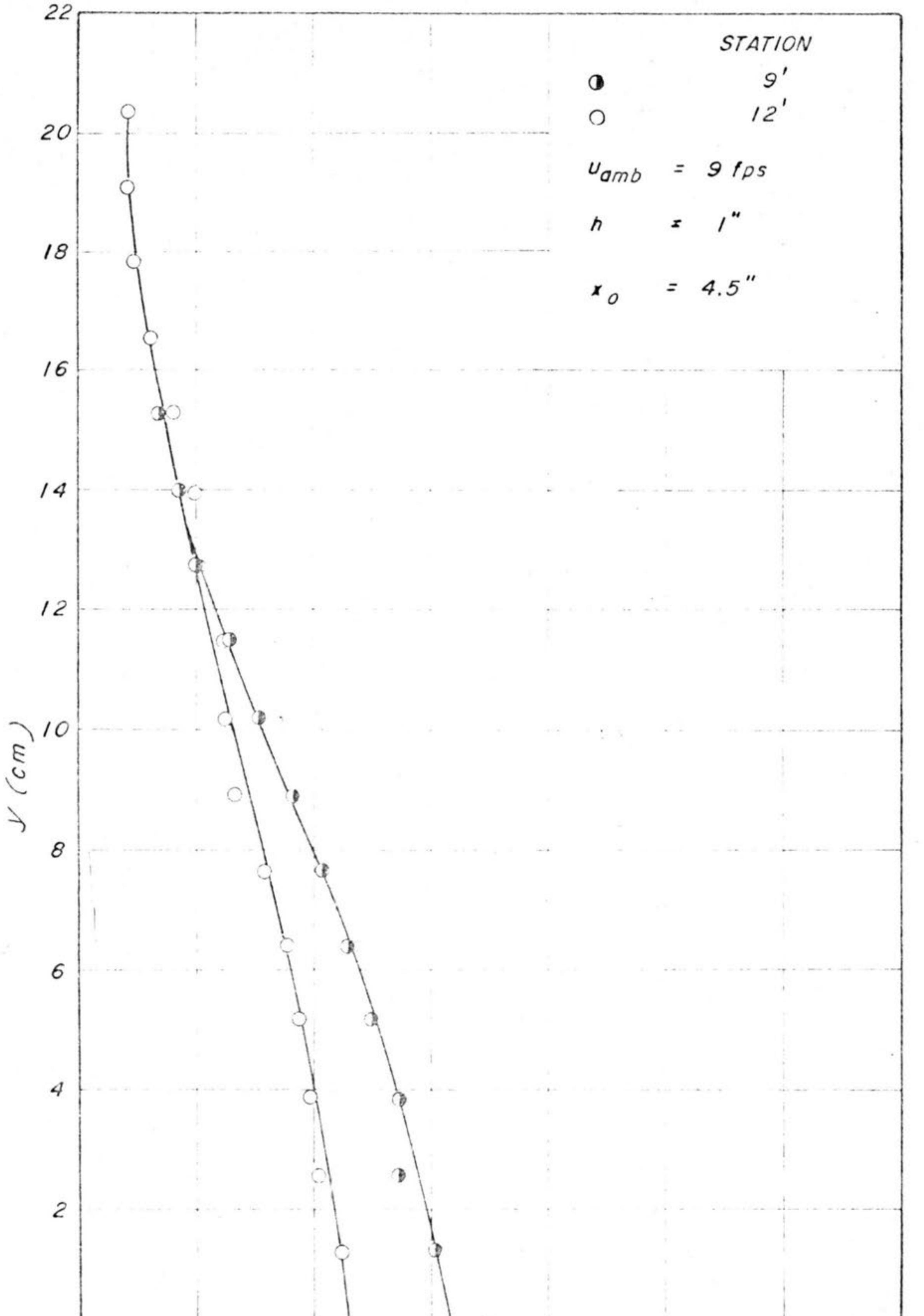

FIG. 6 – 29 CONCENTRATION PROFILES

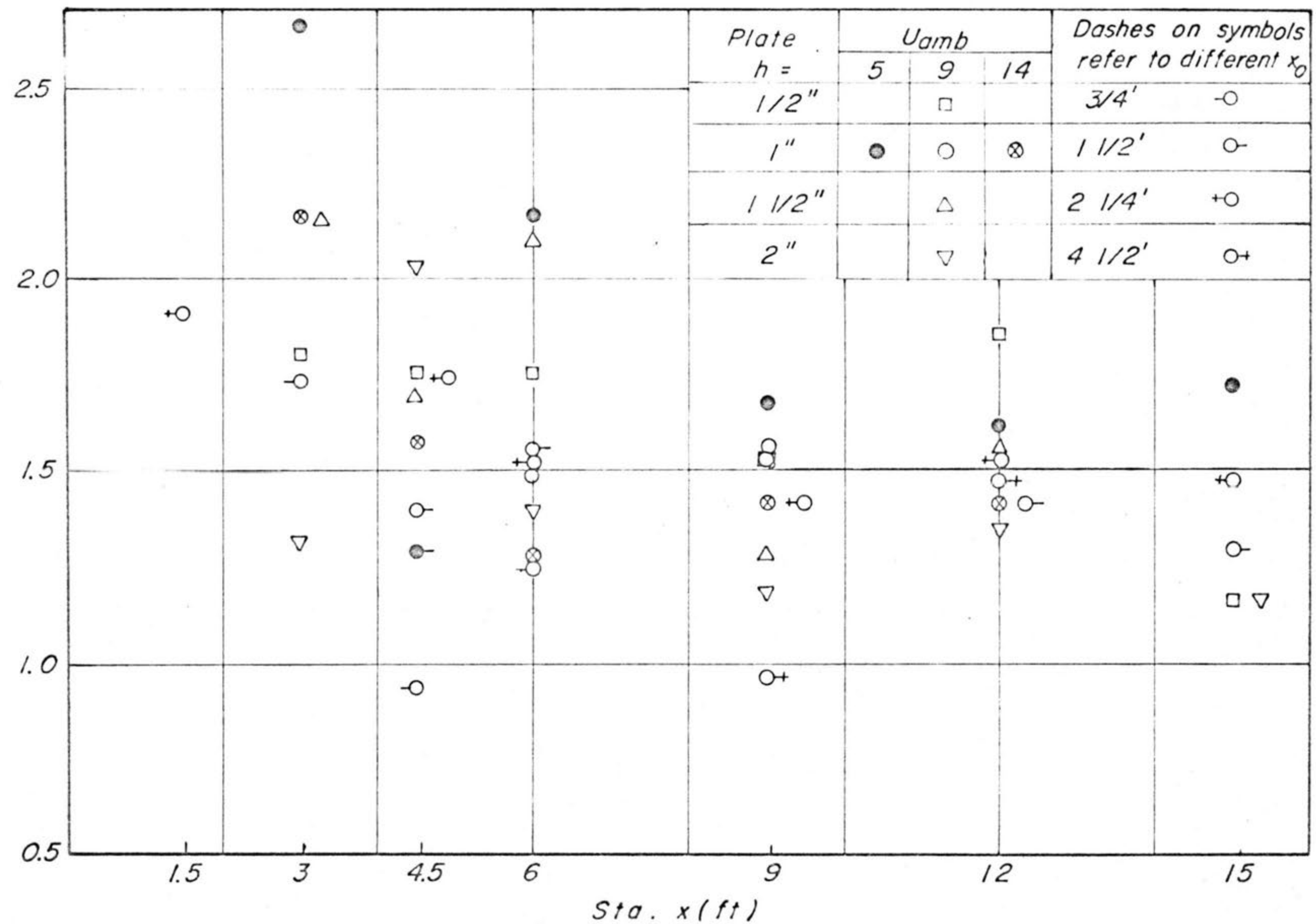

FIG. 6-30 EXPONENT a AS A FUNCTION OF X

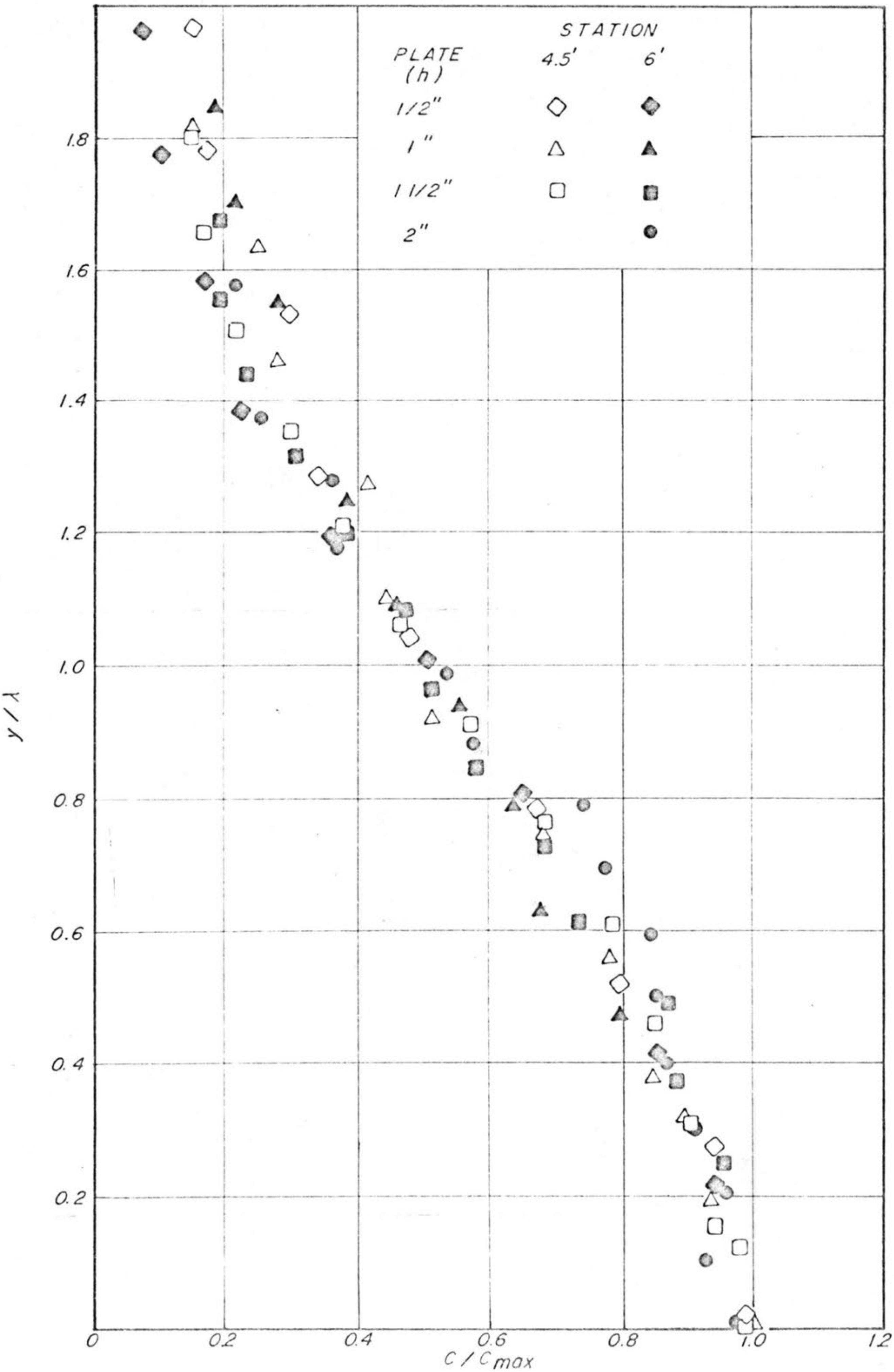

FIG 6-31 CONCENTRATION PROFILES: INTERMEDIATE ZONE

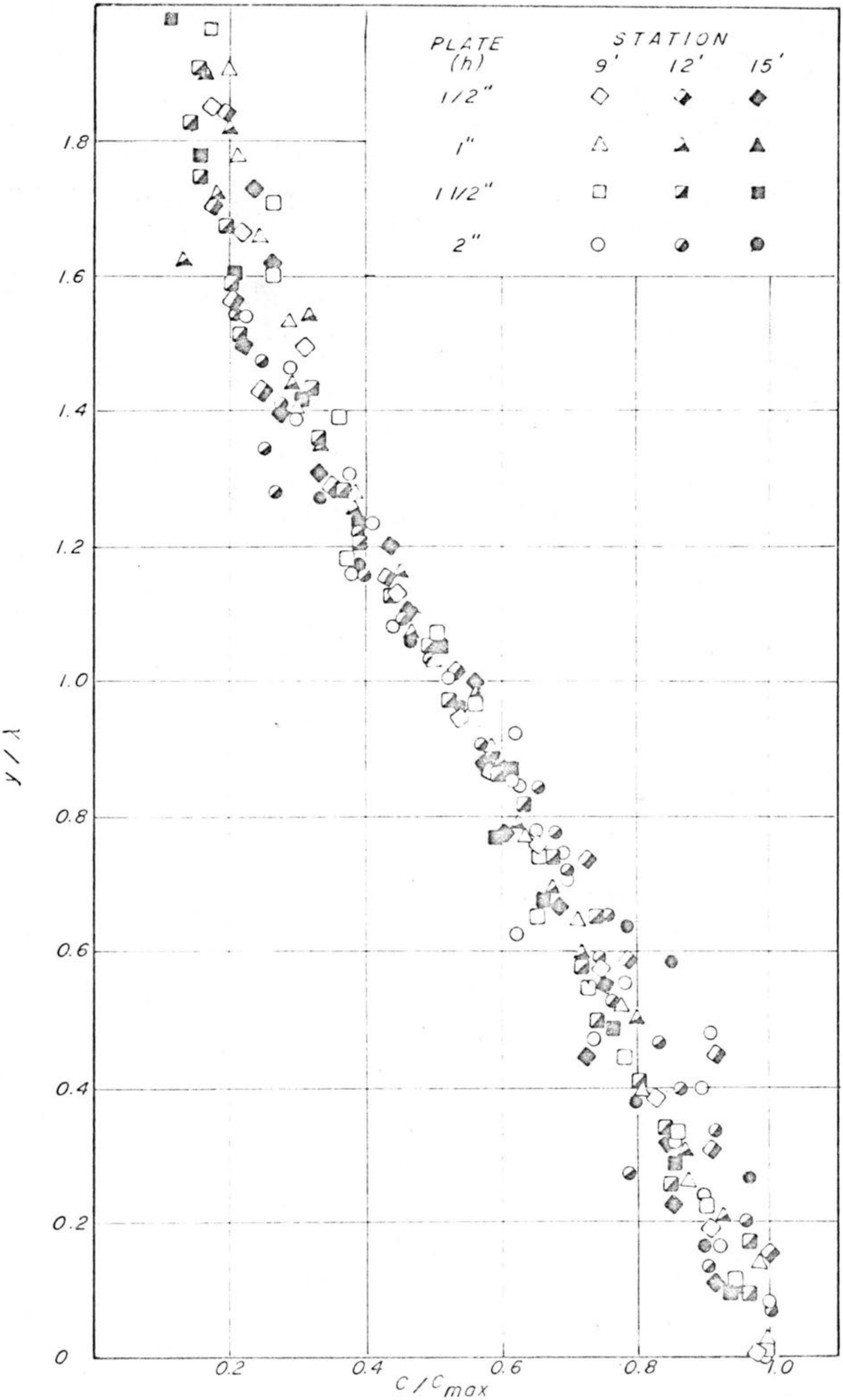

FIG. 6-32 CONCENTRATION PROFILES: FINAL ZONE

APPENDIX C : REFERENCES

REFERENCES

Chapter 3

3-1 TAYLOR, G. I., Diffusion by Continuous Movements. Proceedings, London Mathematical Society, 20:196-212 (1920).

3-2 SCHLICHTING, H., Boundary Layer Theory. Pergamon Press, New York (1955).

3-3 BATCHELOR, G. K., Diffusion in a Field of Homogeneous Turbulence. Australian Journal of Science and Research A, 2:437-450 (Dec. 1949).

3-4 LIN, C. S., MOULTON, R. W., and PUTNAM, G. L., Mass Transfer Between Solid Wall and Fluid Streams. Industrial and Engineering Chemistry, 45:636-646 (1953).

3-5 POREH, M., Diffusion from a Line Source in a Turbulent Boundary Layer. Ph.D. Dissertation, Colorado State University, Fort Collins, Colorado (1961).

3-6 WIEGHARDT, K., Über Ausbreitungsvorgänge in Turbulenten Reibungsschichten. Z. Angew. Math. and Mech. (ZAMM), 27:346-355, No. 11-12 (Nov.-Dec. 1948).

3-7 FRENKIEL, F. N., Turbulent Diffusion: Mean Concentration Distribution in a Flow Field of Homogeneous Turbulence. Advances in Applied Mechanics, 3:61-107 (1953).

3-8 FAVRE, A. J., GALVIGLIO, J. J. and DUMAS, R. J., Further Space-Time Correlation of Velocity in a Turbulent Boundary Layer. Journal of Fluid Mechanics, 3:344-356 (Jan. 1958).

3-9 BALDWIN, L. V. and MICKELSEN, W. R., Turbulent Diffusion and Anemometer Measurements. A.S.C.E. Proceedings, Journal of the Engineering Mechanics Division, 88:37-69 (April 1962).

3-10 TOWNSEND, A. A., The Structure of Turbulent Shear Flow. University Press, Cambridge (1956).

3-11 YIH, C. S., Diffusion from a Line Source in Laminar Flow over a Wedge and in Blasius Flow. Proceedings of the First U. S. National Congress of Applied Mechanics (published by A.S.M.E.), p. 797-800 (June 1951).

3-12 CORRSIN, S. and KISTLER, A. L., The Free Stream Boundaries of Turbulent Flow. N.A.S.A. TN 3133, (1954).

3-13 POREH, M. and CERMAK, J. E., Study of Diffusion from a Line Source in a Turbulent Boundary Layer. To be published in International Journal of Heat and Mass Transfer in Fall 1963.

REFERENCES

Chapter 4

4-1 BARAD, M. L. (editor) 1958 Project Prairie Grass, a field program in diffusion (vols. I and II). Geophysical Research Paper No. 59, Geophysics Research Directorate, Bedford, Mass.

4-2 BATCHELOR, G. K. Diffusion in Free Turbulent Shear Flows, J. Fluid Mech. 3, 67, (1957).

4-3 BATCHELOR, G. K. Some Reflections on the Theoretical Problems Raised at the Symposium (Proc. of Symp. on Atmospheric Diffusion and Air Pollution). Advances in Geophysics 6, 449-52, London: Academic Press Inc., (1959a).

4-4 BATCHELOR, G. K., Note on the Diffusion from Sources in a Turbulent Boundary Layer. Unpublished. (1959b).

4-5 CALDER, K. L., Some Recent British Work on the Problem of Diffusion in the Lower Atmosphere. Proc. U. S. Tech. Conf. on Air Pollution. New York: McGraw-Hill Book Co., (1952).

4-6 CERMAK, J. E., Lagrangian Similarity Hypothesis Applied to Diffusion in Turbulent Shear Flow. J. Fluid Mech. 15, (1), 49-64 (1963).

4-7 CRAMER, H. E., A Practical Method for Estimating the Dispersal of Atmospheric Contaminants. Proc. of the 1st Nat. Conf. on Appl. Met. Hartford, Connecticut (1957).

4-8 DAVAR, K. S., Diffusion from a Point Source within a Turbulent Boundary Layer. Ph.D. Dissertation, Colorado State University, (1961).

4-9 ELLISON, T. H. Turbulent Diffusion. Science Progress 47, 495-506. (1959).

4-10 GIFFORD, F. A., Diffusion in the Diabatic Surface Layer. Proc. Internat. Colloquium on the Mech. of Turbulence, (A. Favre, ed.). No. 108, C.N.R.S., Paris, (1962).

4-11 INOUE, E., The Effects of Thermal Stratification on Turbulent Diffusion in the Atmospheric Surface Layer. Advances in Geophysics 6, 319-30. London: Academic Press Inc. (1959).

4-12 MALHOTRA, R. C., Diffusion from a Point Source in a Turbulent Boundary Layer with Unstable Density Stratification. Ph. D. Dissertation, Colorado State University. (1962).

4-13 MONIN, A. S. and OBUKHOV, A., The Basic Laws of Turbulent Transport in the Ground Layer of the Atmosphere. Trans. (Trudy) Geophys. Inst. Acad. Sci. USSR 151, (1954).

4-14 MONIN, A. S., Smoke Propagation in the Surface Layer of the Atmosphere. Advances in Geophysics 6, 331-43. London: Academic Press Inc., (1959).

4-15 PASQUILL, F., Atmospheric Diffusion. London: D. van Nostrand Co. Ltd. (1962).

4-16 POREH, M., Diffusion from a Line Source in a Turbulent Boundary Layer. Ph.D. Dissertation, Colorado State University, (1961).

4-17 SWINBANK, W. C., Wind Profile in Thermally Stratified Flow. Nature 186 (4723), 463-4. (1960).

4-18 WIEGHARDT, K., Über Ausbreitungsvergänge in turbulenten Reibungsschichten. ZAMM 28, 346-55. (1948).

REFERENCES

Chapter 5

5-1 GEIGER, R., The Climate Near the Ground, Harvard University Press, Cambridge, Mass., (1957).

5-2 LEMON, E., Photosynthesis Under Field Conditions II: An Aerodynamic Method for Determining the Turbulent Carbon Dioxide Exchange Between the Atmosphere and a Corn Field. Agronomy Journal, Vol. 52, pp. 697-703, (1960).

5-3 TAN, H. S. and LING, S. C., A Study of Atmospheric Turbulence and Canopy Flow. Therm Advanced Research Report 611, Ithaca, New York, (Feb. 1961).

5-4 LEMON, E., Energy and Water Balance in Plant Communities. Research Report No. 359, North East Brazch, Soil and Water Conservation Research Division, Agric. Res. Service, U. S. Dept. of Agriculture, (Oct. 1962).

REFERENCES

Chapter 6

6-1 Arie, M. and Rouse, H., Experiments on Two-dimensional Flow Over a Normal Wall, Journal of Fluid Mechanics, 1:129-141, 1956.

6-2 Nagabhushanaiah, Halevoor S., Separation Flow Downstream of a Plate Set Normal to a Plane Boundary, Ph.D. Dissertation, Colorado State University, Fort Collins, Colorado, November 1961.

6-3 Schlichting, H., Grenzschicht Theorie, Verlag G. Braun, Karlsruhe, 1958.

6-4 Sandborn, V. A., An Equation for the Mean Velocity of Boundary Layers, National Aeronautics and Space Agency, Memorandum 2-5-59E, 1959.

6-5 Sandborn, V. A. and Kline, S. J., Flow Models in Boundary Layer Stall Inception, American Society of Mechanical Engineers, Paper No. 60-WA 149, 1960.

6-6 Hama, F. R., Boundary Layer Characteristics for Smooth and Rough Surfaces, Transactions, Society of Naval Architects and Marine Engineers, U. S. A., Vol. 62 S. 333-358.

6-7 Clauser, F. H., The Turbulent Boundary Layer Advances in Applied Mechanics, Bd. 4, 1956.

6-8 Townsend, A. A., The Structure of Turbulent Shear Flow, Cambridge University Press, Cambridge, 1956.